UNIVERSITY OF CALIFORNIA, SAN DIEGO

SAN DIEGO STATE UNIVERSITY

The Electrochemistry of Quinones in Aprotic Solvents

A dissertation submitted in partial satisfaction of the requirements for the degree of Doctor of Philosophy

in

Chemistry

by

Patrick Andrew Staley

Committee in charge:

University of California, San Diego

Professor John Crowell

Professor Michael Sailor

San Diego State University

Professor Diane Kimball Smith, Chair

Professor Christopher R. Harrison

Professor Samuel Kassegne

2016

The Dissertation of Patrick Andrew Staley is approved, and it is acceptable in quality and form for publication in microfilm and electronically:

_____

_____

_____

_____

_____

Chair

University of California, San Diego

San Diego State University

2016

Dedication

I dedicate this work to the people who raised me and the people who supported me through the years: my mother, Nancy Ligutti; my father, Patrick Staley; my step-father, Tony Ligutti; my step mother, Patricia Staley; and my thesis advisor and mentor, Diane Kimball Smith. In particular I would like to thank my loving wife, Nan Mu, who has happily supported me and put up with the late hours without complaint for all these years.

Table of Contents

List of Charts

List of Figures

List of Schemes

List of Equations

List of Tables

Aknowledgements

I would like to thank Eric Mitchel Lopez for the CV's with Vitamin K and CH3I that he gethered which appear in chapter 2.

I would like to thank Lauri Clare for her initial discovery of the irreversibility and nearly ideal cathodic peak height of Vitamin K in CH2Cl2 which lead to chapter 2 and part of chapter 3. Although her CV's do not appear here.

I would like to thank Christina Newell for performing the CV's of duroquinone using Au and Pt electrodes.

I would like to thank Prof. David Pullman for lending me one of his high vacuum chambers, with the associated pumps, and for helping me troubleshoot the chamber for the electrode hydrogenation experiment in chapter 3.

I would like to thank Malory Hicks, a former student of David Pullman, for showing me how to operate the high vecuum chamber used in chapter 3.

I would like to thank Prof. Andrew Cooksy for his help in performing the COSMOtherm calculations that appear in chapter 4.

Vita

EDUCATION

Post-Doc	Robert Bosch LLC	Bioligical-ASIC	07/2016-07/2018
Visiting Scholar	Stanford University	Mechanical Engineering, MEMS	07/2016-07/2017
PhD	University of California, San Diego and San Diego State University	Chemistry	09/2011-12/2016
MA	San Diego State University	Analytical Chemistry	09/2009-05/2015
	San Diego State University	Completed Chemistry BS requirements	03/2008-05/2009
BA	UC Irvine	History	09/2003-09/2007

WORK EXPERIENCE

Project Lead on Corrosion Resistance Coating	Led project team that evaluated metal samples with corrosion resistance coating; a joint project between San Diego State University and Luminit LLC.	09/2014-03/2015
Graduate Research on Electrochemistry: UC San Diego/San Diego State University	Used electrochemical methods, NMR, MS, SERS, and UHV techniques to determine the causes of abnormal behavior observed in electrochemical reactions.	09/2011-08/2016
Graduate Research on Quinones: San Diego State University	Used electroanalytical chemistry and computational chemistry to prove that the “wedge scheme” is required to explain quinone electrochemistry.	01/2014-05/2015

Graduate Research on Viologens: San Diego State University	Synthesized viologen oligomers (small organic molecules) and used spectroscopic methods and electrochemical techniques to measure their dimerization.	10/2012- 12/2013
Teaching Associate: San Diego State University	Responsibilities include teaching laboratory sections, tutoring students, and performing research in analytical chemistry, electrochemistry, and spectroelectrochemistry.	09/2011- 08/2016
Intern: Hewlett-Packard Company	Experimented with different pigments, ink formulas, and different paper types.	06/2010- 09/2010

SELECTED TECHNICAL SKILLS

- NMR Spectroscopy, ^{1}H, ^{13}C, ^{11}B
- UV-Visible Spectroscopy
- Organic Synthesis
- Various Electrochemical Methods (Chronocoulometry, Cyclic Voltammetry, Electrolysis, Differential Pulse Voltammetry, Toeffel Plot, etc.)
- MS
- HPLC
- FTIR
- Electrophoresis
- SEM
- UHV
- MEMS
- SERS

COMPUTER AND STATISTICAL SKILLS

- SciFinder
- Gaussian09
- Microsoft Excel for statistical and graphical analysis
- Linux
- DigiSim 3.03
- Introductory Python
- Introductory Fortran 9

PUBLICATIONS

- Patrick A. Staley, Eric M. Lopez, Laurie A. Clare, and Diane K. Smith. “Kinetic Stabilization of Quinone Dianions via Hydrogen Bonding by Water in Aprotic Solvents”. Journal of Physical Chemistry C, 2015, 119 (35), 20319-20327.
- Patrick A. Staley, Christina M. Newell, David P. Pullman, and Diane K. Smith. “The Effect of Glassy Carbon Surface Oxides in Non-Aqueous Voltammetry: The Case of Quinones in Acetonitrile”. Analytical Chemistry, 2014, 86 (21), pp 10917-10924.

SYMPOSIUM PRESENTATIONS

- 2016 Electrochemical Society Spring "Limits of Acetonitrile Dryness Via Molecular Sieve Method". Patrick A. Staley, Eric M. Lopez, Joy Metzger, and Diane K. Smith.
- 2015 Electrochemical Society Fall “Micron Scale Cathodically Coated Graphene Impedes Corrosion on Ti, CuBe, and Stainless Steel”. Patrick A. Staley, Joy Metzger, Danielle Griffo, Emily Simmons, Chris Griffo, Mark Bennahmias, Russel Kurtz, and Diane K. Smith.
- 2015 Electrochemical Society Fall “Application of the Wedge Scheme to Explain Quinone-Phenol Electrochemical Systems”. Patrick A. Staley and Diane K. Smith.
- 2014 Electrochemical Society Spring “Heterogeneous Proton Transfer as an Explanation for the Unusually Thick Cyclic Voltammograms and Unusually Small Second Redox Wave of Para-Quinones in Aprotic Solvents”. Patrick A. Staley and Diane K. Smith.
- 2014 SDSU SRS “1st Order Decay Reaction Between Vitamin K and Supposedly Inactive Dichloromethane”. Patrick A. Staley, Eric Lopez, and Diane K. Smith.
- 2013 Electrochemical Society Fall “A New Supramolecular Chemistry Motif: Horizontally Linked Viologen Radical Dimers”. Joquel Marie Vasquez, Patrick A. Staley, Shaminee Upeka Keenawinna, and Diane K. Smith.
- 2013 Electrochemical Society Fall “Quinone Electrochemical Mysteries: Thick Cyclic Voltammograms and Tiny Redox Waves”. Patrick A. Staley, Laurie A. Clare, Eric M. Lopez, and Diane K. Smith.
- 2012 SDSU SRS “Unintentional Prot on Coupled Electron Transfer as an Explanation for the Odd Cyclic Voltammetry Behavior of Quinones at Glassy Carbon Electrodes in Organic Solvents”. Patrick A. Staley and Diane K. Smith.
- 2011 American Chemical Society Spring "Concentration and spectroelectrochemical study to test quinone reduction mechanism". Patrick A. Staley, Christina Newell, and Diane K. Smith.
- 2010 Electrochemical Society Fall “Concentration and Computational Studies on Quinones and Tethered Diquinones to Determine the Effect of Dimerization on the Mechanism of Quinone Reduction in Aprotic Solvents”. Patrick A. Staley and Diane K. Smith.

COMMUNICATION SKILLS

- Mentored a high school student for the Greater San Diego Science and Engineering Fair where he won 15 awards and was accepted by Stanford.
- Conversational Spanish.

AWARDS

- Two time Recipient of Awarded Membership from the Electrochemical Society
- Two time Travel Grant Recipient from the Electrochemical Society.
- Recipient of VFW scholarships at UC Irvine.
- Three time recipient of the Governor's Scholarship.

PROFESSIONAL AFFILIATIONS

- Full Member of Sigma Xi Society
- Founding Member/Secretary of Chemistry Graduate Student Association at SDSU
- Member of American Chemical Society
- Member of Electrochemical Society
- Former Member of Student Affiliates of the ACS

Abstract of the Dissertation

The Electrochemistry of Quinones in Aprotic Solvents

by

Patrick Andrew Staley

Doctor of Philosophy in Chemistry

University of California, San Diego 2016

San Diego State University 2016

Professor Diane Kimball Smith, Chair

Quinones are electroactive organic molecules that are used by biological systems as electron shuttles, are used by humans as dyes, pharmaceuticals, reactants, and catalysts, and are being investigated for use in energy transduction and organic electronics, all of which have to do with their electrochemistry. Studies of them have contributed to understanding not only their applications, but also certain aspects of physical organic chemistry in general such as the intersection between hydrogen bonding and electron transfer, the square scheme theoretical concept, and proton coupled electron transfer (PCET).

Quinones are extremely reactive in their fully reduced form to the point that they will undergo SN2 reactions with supposedly stable solvents such as dichloromethane in the absence of water to H-bond with and stabilize the quinone dianions. This stabilization is both kinetic and thermodynamic in nature—meaning

that it comes both from water molecules drawing electron density away from the quinones through their hydrogen bonds, thus making the SN2 reaction less favorable, and from the water molecules themselves getting in between the quinone dianion and its electrophilic target, thus making the reaction slower due to sterics.

Cyclic voltammograms (CV's) of quinones never undergo a set of two ideal redox waves because the presence of oxygenated, protonated functional groups on the surface of the analytical electrodes used to study them causes them to form hydrogen bonds and undergo proton transfer at the surface even if there is nothing in solution that can be a hydrogen bonding or proton transfer guest. The only apparent way to get rid of these groups is a long process of ablation with high temperature hydrogen atoms. The presence of water in solution appears to enhance the non-ideality.

In order to accurately describe the quinone-phenol system, which is the subject of a great deal of the active research in this area, it is necessary to consider hydrogen bonding, electron transfer, and proton transfer reactions, not just two of the three. This is easy to do using the “wedge” scheme, which is a theoretical model to organize mechanisms that require three types of reactions done over and over again. Wedge schemes are shown to give good qualitative approximations of the CV’s of duroquinone and 2-naphthol, with the best including proton transfer from a naphthol-naphthol hydrogen bonded complex that forms slowly in solution.

Chapter 1: Introduction to the Electrochemistry of Quinones in Aprotic Solvents

Abstract

Quinones are electroactive organic molecules that have a history going back more than 100 years wherein their uses have always been dependent upon their electrochemistry. Through the years, this electrochemistry has been used to advance studies in the relationship between electron transfer reactions, proton transfer reactions, and hydrogen bonding. Out of such studies have emerged the theoretical model of the “square” scheme which makes it much easier to organize mechanisms that include large sets of related reactions that can form thermodynamic cycles. While studies of quinones usually revolve around their proton and electron transfer reactions or their hydrogen bonding and electron transfer reactions, it is proposed here that hydrogen bonding should be considered in the same mechanisms with proton transfer and electron transfer reactions. It is further proposed that the “wedge” scheme be borrowed from recent urea electrochemical studies in order to organize the three reaction pathways.

Introduction

Quinones (Q) are organic molecules that can undergo reversible oxidation and reduction (redox or e-transfer) reactions alongside acid-base (protonation or H^+-transfer) reactions. In their reduced form they are most stable as hydroquinones (QH2) where they consist of two hydroxyl groups bound to an aromatic, six carbon ring in resonance with each other as shown in chart 1.1. In their oxidized form, quinones have

two ketone groups on a six carbon ring where the carbons are unsaturated and the oxygens are in resonance with each other; the reactions between those states are shown in schemes 1.1 and 1.2. Because quinones have lone electron pairs on oxygens in their Q and QH2 states, they can accept H-bonds from protic molecules, and because they have protic hydrogens in their QH2 form, they can accept H-bonds from molecules with accessible electron lone pairs. Such H-bonds have been shown to effect e-transfer reactions in the past, but until now no one has proposed a theoretical structure to systematically combine all three reaction types in the case of quinones.[1]

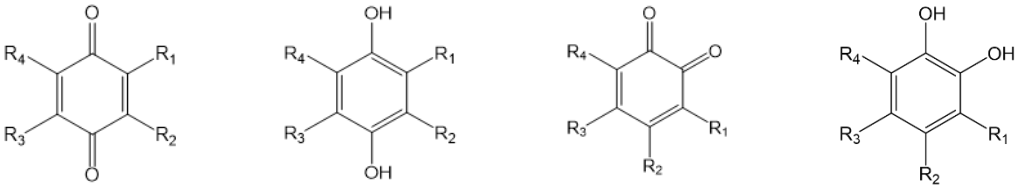

para-quinone para-hydroquinone ortho-quinone ortho-hydroquinone

Chart 1.1. Structures of the quinones.

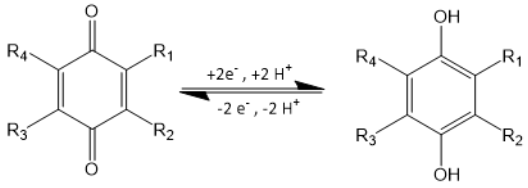

Scheme 1.1. Reduction of para-quinone.

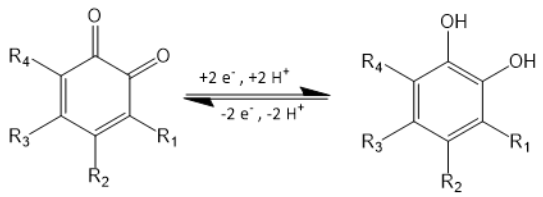

Scheme 1.2. Reduction of ortho-quinone.

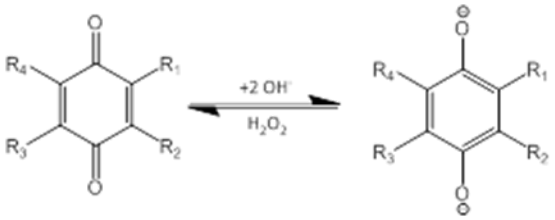

Scheme 1.3. Reduction of para-quinone in alkaline solution.

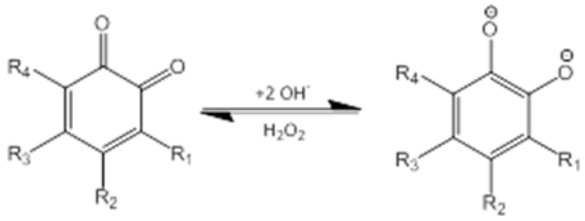

Scheme 1.4. Reduction of ortho-quinone in alkaline solution.

The first discovered quinones came from the quinoa tree in South America, hence the name, and were used as dyes which dissolve and become colorless in basic solution before regaining their color and turning water fast once they dry and are exposed to air. This turned out to be because in basic solution, the reduction of the normally hydrophobic quinone to the somewhat soluble hydroquinone is favored and then followed by the deprotonation of the hydroquinone to form an extremely soluble, colorless anion; once the water is evaporated, oxygen in the air can reoxidize the quinone back to its original, colored, hydrophobic form, shown in schemes 1.3 and

1.4. The H^+ and $2e^-$ or $2H^+$ and $2e^-$ oxidation or reduction reaction occurs commonly in organic chemistry and biochemistry, ranging from organic oxidation series such as those shown in schemes 1.5-1.7 to the biochemical processes of synthesizing acetate or nitrogen fixation shown in schemes 1.8 and 1.9.

Research on quinones over the last 50 years has had two main applications in mind: medicine or biology[2-8] and electronics.[2, 9-11] Basic medical research often deals with the electron transfer pathways such as those associated with cell signaling, which is occasionally performed by the quinone vitamin K, and cellular respiration, which is mediated by ubiquinone.[12] The latter of these two is so common in biological samples that its name comes from "ubiquitous." In order to understand the roles these molecules play in biochemistry, many studies have been performed to determine their reactivity in water[13-15]—the universal solvent of biology—and in aprotic media which are meant to mimic the fatty tissue where these species likely spend most of their time, based upon the greasy side chains that both of them have.[16-18] Examples of more direct medical applications are the anti-tumor drug daunomycinone[19] and the antibacterial drug javanicine.[20] Out of the quinone-based drugs that have been studied, it is thought that the mechanism of action involves the quinone intercalating the target cell's DNA.[21] It should be mentioned that an unrelated set of drugs, nitroimidazoles, have been shown to target bacterial cells rather than mammalian cells due to the difference in the ambient redox potential, were it is the very reducing environment of the bacterial cytosol that activates the antibiotic;[22] this shows that bacterial cells are often

more reducing than mammalian cells and could hypothetically contribute to the selectivity of quinone-based antibiotics as well.

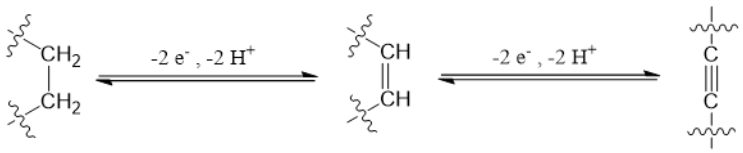

Scheme 1.5. Oxidation of ethylene group.

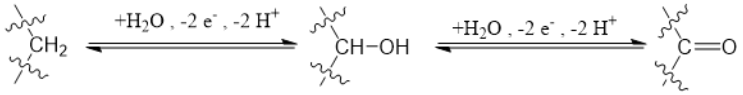

Scheme 1.6. Oxidation of methylene with oxygen.

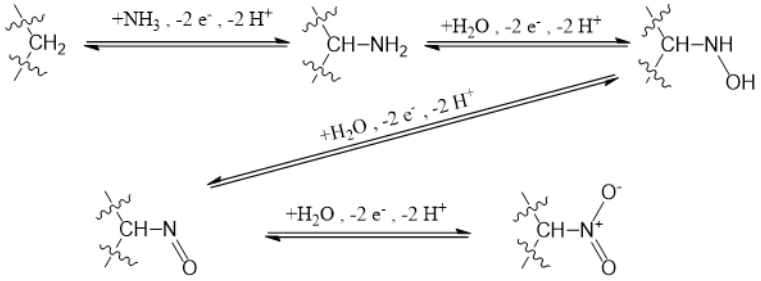

Scheme 1.7. Oxidation of methylene group with nitrogen, then with oxygen.

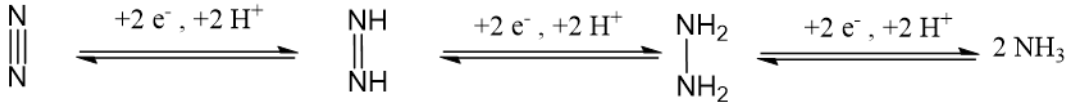

Scheme 1.8. Reduction of nitrogen gas.

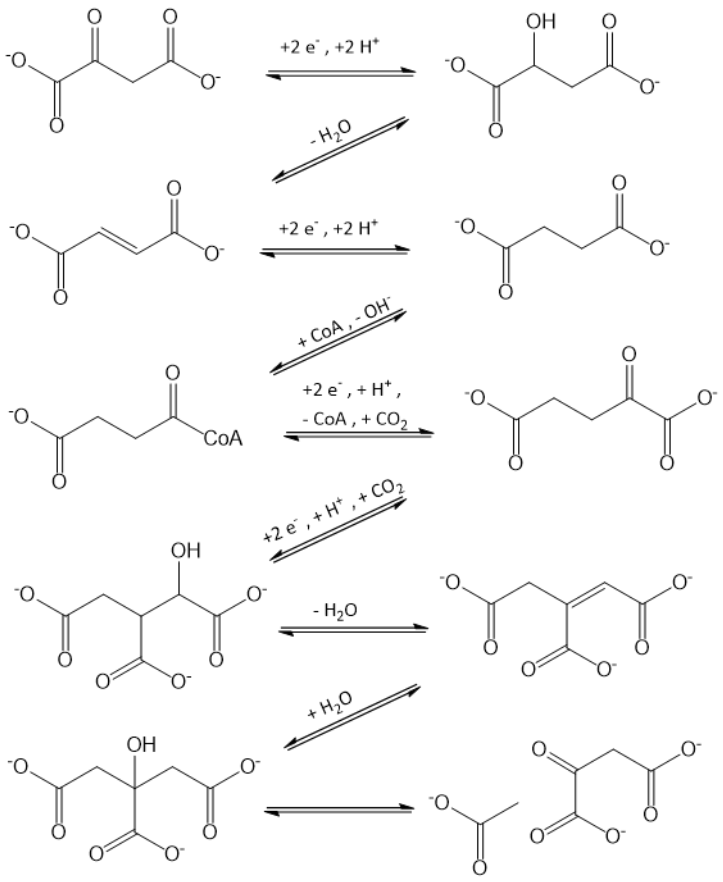

Scheme 1.9. Acetate synthesis reaction.[23]

Electronics research regarding quinones can largely be divided into the areas of nano-scale computation and energy transduction. In the case of computation, quinones have been used in experiments to find nanoscale transistors and memory bits.[24, 25] In the case of energy transduction, research into quinone chemistry has involved studies on its role in photosynthesis in an effort to produce artificial photosynthesis. In this case, the ubiquinone is used as an electron shuttle to remove electrons irreversibly at the end of an electron transport chain in photosystem II, and carry them to photosystem I. Each protein docks with ubiquinone by H-bonding to the oxygens of Q or the hydrogens of QH2.[26] In another application of quinone energy transduction,

several laboratories have tried to use quinones as a stable redox couple for flow cells or fuel cells.[27-29] One of the latest applications of quinones is a combination of computation and medicine where the interface between the redox and acid-base chemistry of duroquinone, which will be discussed in detail later, is used to modulate in real time the pH of a buffered solution intended for use in clinical assays.[30]

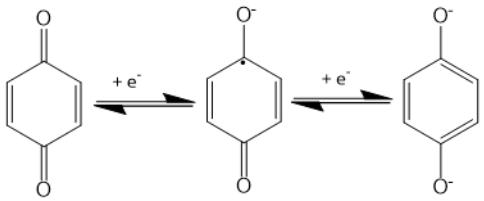

Scheme 1.10. Reduction of benzoquinone in aprotic solvent.

Quinone redox reactions involve two electron transfers with could occur sequentially or together, depending upon the environment in which the reactions take place. When quinones are oxidized or reduced in aprotic conditions, the electron transfers are sequential as shown in scheme 1.10 because adding an electron to a molecule that already has a negative charge requires more potential energy than adding it to the same molecule with no charge since the energy barrier due to coulombic repulsion must be overcome. These studies are often intended to mimic the environment in fatty tissues, where the molecules are surrounded by hydrophobic groups. Quinones being reduced or oxidized in an aqueous buffer accept two protons and two electrons together. This mechanism is shown in scheme 1.11; it consists of a one electron reduction followed by a protonation by the buffer, followed by another reduction and a final protonation. The reason this happens in one kinetic step is that

the protonation of the radical anion results in a neutral radical, which does not have a coulombic repulsion energy barrier against electron acceptance, but does have a half empty orbital which allows electron pairing. This is a general relationship between redox reactions and acid-base reactions: because the potential needed to reduce or oxidize a molecule is partly dependent upon the charge of the molecule itself, H^+-transfer reactions dramatically change the redox potential with the addition of a proton moving the redox potential positive—making reduction easier and oxidation harder—and the loss of a proton moving the redox potential negative—making reduction harder and oxidation easier.

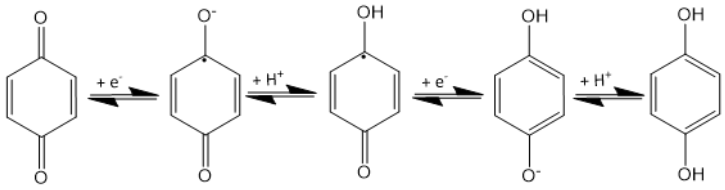

Scheme 1.11. Reduction of quinone in protic solvent; steps separated.

The relationship between H-bonding and H^+-transfer is well known since both involve a hydrogen atom sigma bound to an electronegative atom being attracted to another atom that has a full or partial negative charge,with the difference being that in the case of H^+-transfer, the attraction is enough to cause the H^+ nucleus to trade its sigma bond with the starting atom for a sigma bond with the other atom. This close relationship has led physical chemists who study it to simulate proton transfer as a transition between two H-bonded states.[31-33] This makes sense because the hydrogen nucleus, proton, deuteron, or trition, is too massive to tunnel more than an angstrom or

so, which means that "pure" H^+-transfer that does not involve H-bond activated complexes do not occur under normal conditions and that any reaction system that is modeled with H^+-transfer but without H-bonding carries with it the implicit assumption that the formation and dissociation of the H-bonding complex is fast on the time scale of the experiment on both the reactant and product sides. This assumption is valid with a large enough driving force, but if the driving force is within a few orders of magnitude of the strength of the H-bond complex, it is possible that the H-bonded state will have to be considered in its own right in order to accurately explain the proton transfer system.

Just as with H^+-transfer reactions, H-bonding reactions are chemical steps that can change the equilibrium potential of a redox couple, the difference being that H^+-transfer changes the redox potential of a couple by transferring a positive charge either to or from the redox active species, H-bonding changes the redox potential of a species by transferring a partial positive charge either onto or off of the redox active species because the attraction between the hydrogen and the other partner involves the injection of electron density into the hydrogen's orbitals. In the case where the hydrogen is on the redox active species (H-donor) a hydrogen bond will shift the redox potential negative, making oxidation easier and reduction harder. In the case where the redox active species does not have the hydrogen involved in the H-bond (H-acceptor) the H-bond will shift the wave positive, making the oxidation harder and the reduction easier. As a corollary to this, if the redox active species is the H-donor then the oxidized state of the species will have a stronger H-bond complex than the reduced

state because oxidizing the species will decrease the electron density that is available to the bonded hydrogen, thus making it more susceptible to attraction to another molecule; if the redox active species is the H-acceptor, the oxidized state will have a weaker H-bond complex than the reduced state because the redox species will have more electron density to donate to the bonding hydrogen in its reduced state than in its oxidized state.

Because H-bonding only involves a partial positive charge rather than a full positive charge, the effect that H-bonding has on the redox potential of a system is less than full H^+-transfer, but in cases where a large number of hydrogen bonds can all occur in the same system H-bonding can result in significant shifts. Quinones, which can accept up to 4 H-bonds in their oxidized state and up to 6 in their fully reduced state, are redox systems that can be affected quite strongly with multiple H-bonding partners.[2, 17, 18, 34] In the case of reduction in aprotic solvents, the potentials of the separate redox waves are affected by trace water in the solution to such an extent that they have been used to measure the water concentration of organic solvents.[18] Because adding the second electron causes so much intramolecular repulsion, the increase in charge localization between the radical anion and the dianion is greater than between the neutral and radical anion, so anything that can accept the electron density, such as H-bonds, will affect the second reduction step more than the first reduction. This means that the redox potentials for the Q/Q^- and Q^-/Q^{2-} transitions will move closer together with increasing H-bond strength and number. It has been shown that this happens to such a large extent that when the solvent is water, thus allowing the

maximum number of H-bonds in every state, the two redox potentials become experimentally indistinguishable. This is true even in the absence of added acid capable of protonating the radical anion intermediate, or when the pH is such that the hydroquinone is completely deprotonated.[15]

The most common ways to study e-transfer reactions experimentally are flash photolysis for e-transfer followed by analysis by ultrafast spectroscopy, or any of a variety of voltammetry techniques where e-transfer between the analyte and an electrode serve both as the means of e-transfer and analysis. The majority of of studies of e-transfer in quinones, and the majority of experiments discussed in this document, have used the latter experimental method because it is the easiest to setup and arguably the most versatile. Voltammetry techniques, such as cyclic voltammetry (CV), focus on changing the electric potential of an electrode, the working electrode, and measuring the resulting change in current. In order to change the potential of the working electrode, it is necessary to have a second electrode, the counter electrode, in the solution as well. The counter electrode must either be made from a material that is more active than the working electrode, or must have a greater surface area, or both to ensure that the limiting current comes from the chemistry happening at the working electrode. A third electrode must also be used to put the potential of the working electrode in perspective; this is the reference electrode and it is usually made from multiple parts so that it has its own redox couple—such as Hg/HgCl or Ag/AgCl—under stable conditions to which the potential of the working electrode can be compared. For this document, the reference electrode was a Ag wire, which changes

potential between experiments but not during experiment, and the CV's were then re-referenced to ferrocene/ferrocenium (Fc/Fc^+) which was added to the electrochemical cell at the end of the experiment. The result is a graph with peaks that correspond to electron transfer reactions, and analysis of them typically focuses on the potential at which they occur, the current associated with their maximums, and their shape.

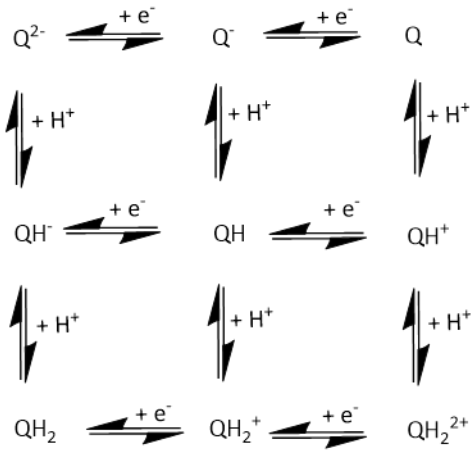

Scheme 1.12. Quinone H^+-transfer and e-transfer square scheme.

Analysis of CV's involves trying to come up with mechanisms that will explain the data and determining the thermodynamic and kinetic reaction constants and miscellaneous parameters such as diffusion coefficients, solution resistance, and concentration. Because mechanisms can become very complex, some shorthand mechanisms have been invented to make the concepts simpler and more manageable. For systems that involve electron transfer and one other type of reaction that is possible for both oxidation states, the simplifying device is the "square scheme": one dimension, usually the horizontal, is reserved for e-transfer reactions and the other type of reaction is on the other axis. Scheme 1.12 is a rewriting of scheme 1.11 using

the square scheme. By writing out all of the possible reaction steps, it is possible to introduce any generic acid to this mechanism; by writing all the reaction steps as reversible, the possibility of equilibria is opened up; by writing out the e-transfer and H^+-transfer reactions consistently along parallel lines, the existence and location of each of the thermodynamic cycles becomes much easier to see. A similar, but much larger scheme, scheme 1.13, is written out for the H-bonding and electron transfer mechanism; while this scheme seems complex, imagine trying to rewrite it as one long chain of reactions and then figuring out how many H-bonds happen at each time, and then having to rewrite the chain every time the relative concentrations of quinone and water are changed; alternatively, imagine reading scheme 1.13 with some of the e-transfers on the vertical axis and with some of the H-bond reactions on the horizontal axis. With the square scheme, complex mechanisms are complex due to the large number of reactions, not because the method of showing them gets in the way.

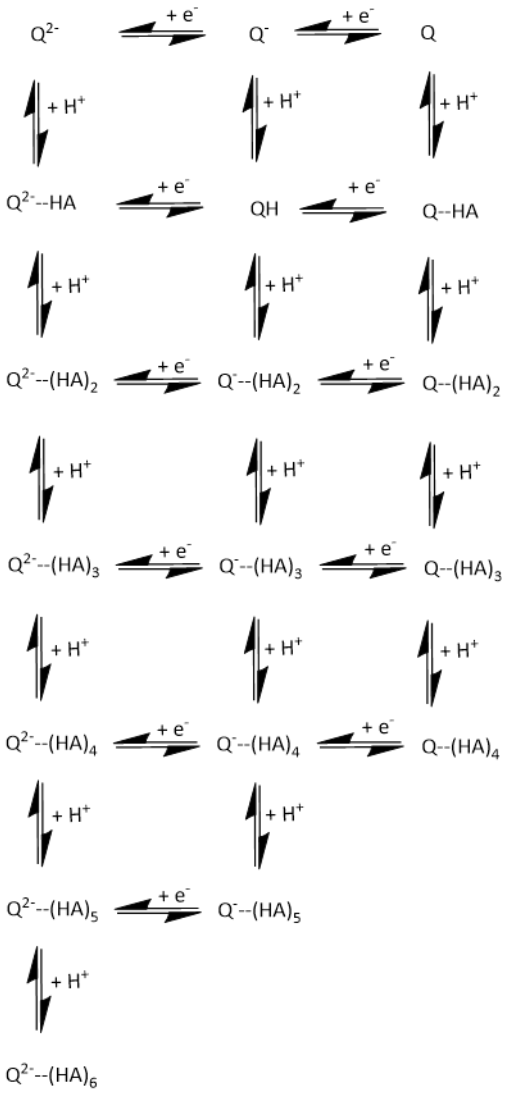

Scheme 1.13. Quinone H-bond and e-transfer square scheme.

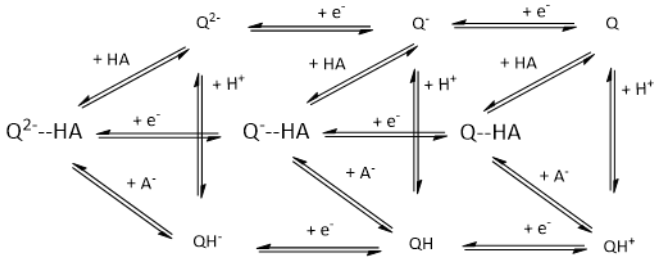

Scheme 1.14. Quinone wedge scheme.

In the circumstances where there are two types of reactions in addition to e-transfer—or with any three reaction types—it is possible to simplify it into three reaction dimensions in a "cube" scheme, or to simplify that even further into a "wedge" scheme as shown in scheme 1.14.[35] This has been used to analyze systems that have H-bonding and H^+-transfer in addition to e-transfer by starting with the cube scheme and then removing proton transfer within the H-bonding complex because that would not affect concentration or scanrate dependence studies since it is a unimolecular process and also will be extremely fast compared to all other reactions in the mechanism. Due to the close relationship between H-bonding and H^+-transfer, chemical systems which can be accurately modeled by neglecting either H-bonding or H^+-transfer should be regarded as the exceptions which only occur when H^+-transfer is much more favorable than H-bonding, or vice versa. The question of whether or not a three dimensional reaction scheme should be used to model an organic redox couple in the presence of a H-bonding or H^+-transfer guest has to do with the choice of the H-bonding or H^+-transfer guest.

Aside from where portions of this thesis have already been published,[36, 37] there has been no attempt in the literature to use a three dimensional reaction scheme to explain quinone electrochemistry. That is the ultimate goal of this thesis and will be addressed in Chapter 4 with consideration of multiple possible wedge schemes as well as H-bonding effects between the H-donor guest molecules. As-yet unexplained features of quinone electrochemistry include the reason why the CV redox wave for the reduction of the radical anion is smaller than for the reduction of the fully oxidized

species in aprotic solution, and the reason why low concentration quinone CV's or CV's in the presence of weak acids contain a new redox wave at a potential intermediate of the normal waves. These are serious problems for any analysis using CV's, and they will be addressed in Chapter 3 with reference to the functional groups that exist naturally on the surface of analytical electrodes and the effect that trace water may play in altering the shape of the CV beyond changing the potential of the redox waves. In the past few years, there have been a few publications that noted the speed of H^+-transfer reactions with water[38, 39] and the concentration of water in organic solvents,[18, 40, 41] and it has turned out that the concentration of trace water in aprotic organic solvents has a large effect on the reactivity of quinones such that in the absence of water the quinone dianion becomes a strong nucleophile;[36] this will be discussed in Chapter 2.

References

1. Weinberg, D. R.; Gagliardi, C. J.; Hull, J. F.; Murphy, C. F.; Kent, C. A.; Westlake, B. C.; Paul, A.; Ess, D. H.; McCafferty, D. G.; Meyer, T. J. *Chemical Reviews* **2012**, *112*, 7, 4016-4093.

2. Astudillo, P. D.; Valencia, D. P.; Gonzalez-Fuentes, M. A.; Diaz-Sanchez, B. R.; Frontana, C.; Gonzalez, F. J. *Electrochimica Acta* **2012**, *81*, 197-204.

3. Cross, A. R.; Segal, A. W. *Biochimica et Biophysica Acta (BBA) - Bioenergetics* **2004**, *1657*, 1, 1-22.

4. Esposti, M. D. *Biochimica et Biophysica Acta (BBA) - Bioenergetics* **1998**, *1364*, 2, 222-235.

5. Liu, H.; Ramnarayanan, R.; Logan, B. E. *Environmental Science and Technology* **2004**, *38*, 7, 2281-2285.

6. Nakai, K.; Takagi, Y.; Tsuchiya, T. *Carbohydrate Research* **1999**, *316*, 47-57.

7. Protti, A.; Singer, M. *Critical Care* **2006**, *10*, 228-234.

8. Shearer, M. J. *The Lancet* **1995**, *345*, 8944, 229-234.

9. Jurchescu, O. D.; Popinciuc, M.; Wees, B. J. v.; Palstra, T. T. M. *Advanced Materials* **2007**, *19*, 5, 688-692.

10. Mamada, M.; Kumaki, D.; Nishida, J.-i.; Tokito, S.; Yamashita, Y. *ACS Applied Materials and Interfaces* **2010**, *2*, 5, 1303-1307.

11. McCreery, R. L. *Analytical Chemistry* **2006**, *78*, 11, 3490-3497.

12. Alberts, B.; Johnson, A.; Lewis, J. In *Molecular Biology of the Cell*, 4th ed., 2002.

13. Bailey, S. I.; Ritchie, I. M. *Electrochimica Acta* **1985**, *30*, 1, 3-12.

14. Petrova, S. A.; Kolodyazhny, M. V.; Ksenzhek, O. S. *Journal of Electroanalytical Chemistry and Interfacial Electrochemistry* **1990**, *277*, 189-196.

15. Quan, M.; Sanchez, D.; Wasylkiw, M. F.; Smith, D. K. *Journal of the American Chemical Society* **2007**, *129*, 42, 12847-12856.

16. Guin, P. S.; Das, S.; Mandal, P. C. *International Journal of Electrochemistry* **2011**, *2011*, 816202, 22.

17. Gupta, N.; Linschitz, H. *Journal of the American Chemical Society* **1997**, *119*, 27, 6384-6391.

18. Hui, Y.; Chng, E. L. K.; Chng, C. Y. L.; Poh, H. L.; Webster, R. D. *Journal of the American Chemical Society* **2009**, *131*, 4, 1523-1534.

19. Arcamone, F.; Franceschi, G.; Orezzi, P.; Cassinelli, G.; Varvieri, W.; Mondelli, R. *Journal of the American Chemical Society* **1964**, *86*, 23, 5334-5335.

20. Wolfbeis, O. S.; Furlinger, E. *Mikrochimica Acta* **1983**, *3*, 385-398.

21. Lown, J. W. *Molecular and Cellular Biochemistry* **1983**, *55*, 1, 17-40.

22. Valdez, C. A.; Tripp, J. C.; Miyamoto, Y.; Kalisiak, J.; Hruz, P.; Andersen, Y. S.; Brown, S. E.; Kangas, K.; Arzu, L. V.; Davids, B. J.; Gillin, F. D.; Upcroft,

J. A.; Upcroft, P.; Fokin, V. V.; Smith, D. K.; Sharpless, K. B.; Echmann, L. *Journal of Medicinal Chemistry* **2009**, *52*, 13, 4038-4053.

23. Ljungdahl, L. G.; Wood, H. G. *Annual Review of Microbiology* **1969**, *23*, 515-538.

24. Bandhopadhyay, A.; Pal, A. J. *Journal of Physical Chemistry B* **2003**, *107*, 11, 2531-2536.

25. Peng, H.; Liu, Z. *Coordination Chemistry Reviews* **2010**, *254*, 1151-1168.

26. Guskov, A.; Kern, J.; Gabdulkhakov, A.; Broser, M.; Zouni, A.; Saeger, W. *Nature Structural and Molecular Biology* **2009**, *16*, 334-342.

27. Ferguia, S.; Masuda, A.; Tsujimura, S.; Kano, K. *Bioelectrochemistry* **2009**, *76*, 14-18.

28. Srinivasan, S.; Ticianelli, E. A.; Derouin, C. R.; Redondo, A. *Journal of Power Sources* **1988**, *22*, 359-375.

29. Willner, I.; Arad, G.; Katz, E. *Bioelectrochemistry and Bioenergetics* **1998**, *44*, 2, 209-214.

30. Fomina, N.; Johnson, C. A.; Maruniak, A.; Bahrampour, S.; Lang, C.; Davis, R. W.; Kavusi, S.; Ahmad, H. *Lab on a Chip* **2016**, *16*, 2236-2244.

31. Gu, J.; Leszczynski, J. *Journal of Physical Chemistry A* **1999**, *103*, 15, 2744-2750.

32. Johannissen, L. O.; Irebo, T.; Sjodin, M.; Johansson, O.; MHammarstrom, L. *Journal of Physical Chemistry B* **2009**, *113*, 50, 16214-16225.

33. Li, X.; Cai, Z.; Sevilla, M. D. *Journal of Physical Chemistry B* **2001**, *105*, 41, 10115-10123.

34. Gamboa-Valero, N.; Astudillo, P. D.; Gonzalez-Fuentes, G. A.; Leyva, M. A.; Rosales-Hoz, M. d. J.; Gonzalez, F. J. *Electrochimica Acta* **2016**, *188*, 602-610.

35. Clare, L. A.; Pham, A. T.; Magdaleno, F.; Acosta, J.; Woods, J. E.; Cooksy, A. L.; Smith, D. K. *Journal of the American Chemical Society* **2013**, *135*, 50, 18930-18941.

36. Staley, P. A.; Lopez, E. M.; Clare, L. A.; Smith, D. K. *Journal of Physical Chemistry C* **2015**, *119*, 35, 20319-20327.

37. Staley, P. A.; Newell, C. M.; Pullman, D. P.; Smith, D. K. *Analytical Chemistry* **2014**, *86*, 21, 10917-10924.

38. Bonin, J.; Costentin, C.; Louault, C.; Robert, M.; Saveant, J.-M. *Journal of the American Chemical Society* **2011**, *133*, 17, 6668-6674.

39. Fa, K.; Tulock, J. J.; Sweedler, J. V.; Bohn, P. W. *Journal of the American Chemical Society* **2005**, *127*, 40, 13928-13933.

40. Hui, Y.; Webster, R. D. *Analytical Chemistry* **2011**, *83*, 3, 976-981.

41. Ooyama, Y.; Sumomogi, M.; Nagano, T.; Kushimoto, K.; Komaguchi, K.; Imae, I.; Harima, Y. *Organic and Biomolecular Chemistry* **2011**, *9*, 1314-1316.

Chapter 2: Kinetic Stabilization of Quinone Dianions via Hydrogen Bonding by Water in Aprotic Solvents

Abstract

It is well-established that very weak acids such as water and alcohols strongly H-bond to quinone dianions, Q^{2-}, in aprotic solvents. This results in thermodynamic stabilization of Q^{2-} and a shift of the formal potential of the $Q^{-/2-}$ couple to less negative values. This study shows that the strong H-bonding of water also results in a type of kinetic stabilization of Q^{2-}. CVs of the naturally occurring naphthoquinone Vitamin K1 in very dry 0.1 M NBu_4PF_6/CH_2Cl_2 show a reversible $Q^{0/-}$ wave but a chemically irreversible $Q^{-/2-}$ wave. Similar behavior is seen with anthraquinone and duroquinone. Evidence suggests that this is due to nucleophilic attack of Q^{2-} on CH_2Cl_2 to give ether products. Addition of water results not only in the expected positive shift in potential of the second wave but also an increase in the chemical reversibility. This indicates that the H-bonding of water to Q^{2-} blocks the irreversible reaction with CH_2Cl_2 by significantly decreasing the rate of that reaction. Further experiments show that the kinetic stabilization by water is great enough that it can slow the reaction of Q^{2-} with iodomethane, a very reactive electrophile, in MeCN.

Introduction

The role of H-bonding in electron transfer reactions continues to be an important area of investigation in organic electrochemistry both for fundamental and practical reasons. One very important role for H-bonding can be to facilitate proton-coupled electron transfer (PCET) reactions.[1-5] This is essential to biological electron

transfer, but also important, for example, in electrochemical-based fuel producing and consuming reactions. In general, for reactions in which proton transfer accompanies electron transfer, electron transfer through the H-bond complex formed between the electroactive species and the acid or base giving or taking the proton can provide a lower energy pathway that is faster than the non-H-bonded pathways. A degree of rate enhancement can be expected if the electron and proton transfer occur in a stepwise manner within the H-bond complex,[6] but this can be enhanced even further by the occurrence of a concerted process in which both the proton and electron move in the same kinetic step and therefore avoid highly charged intermediates.[1-5,7-8] Another way in which H-bonding can affect the kinetics of PCET reactions is through the formation of H-bond networks that can rapidly transfer protons to and from the electron transfer site.[9] In a related manner, large H-bond networks, such as those found in water, can increase the rate of concerted PCET reactions by decreasing the associated reorganization energy through delocalization of the charge produced by proton transfer.[9,10]

From the above discussion it is clear that H-bonding can play a significant role when proton transfer accompanies electron transfer. However, even without full proton transfer, H-bonding can often facilitate electron transfer by preferentially stabilizing the products of reversible electron transfer reactions. This makes the electron transfer thermodynamically easier, and results in a shift in the apparent formal potentials to less extreme values. The fact that intra-molecular H-bonding and inter-molecular H-bonding to solvent can facilitate electron transfer has been appreciated

for some time.[11] More recently, this realization has been extended to intermolecular H-bonding with added guests. Numerous studies on this subject have appeared over the last 20 years. Redox couples utilized include quinones,[12-18] flavins,[19,20] nitroaromatics,[21-23] and phenylenediamines.[24,25]

The reason that H-bonding can have such a significant effect on electron transfer is that electron transfer generally results in very large changes in the acid/base strength of organic redox couples. As outlined in Scheme 2.1, for a reversible or quasi-reversible organic redox couple, reduction will typically increase the electron density on electronegative atoms which leads to a large increase in the basicity, and therefore H donors (acids) will H-bond more strongly to the reduced forms. The standard potential for the overall reaction at 25 °C is given by eq 2.1, which shows that it is shifted positive from the electron-transfer-only reaction by an amount proportional to the logarithm of K_{HB}. Along the same lines, oxidation will typically decrease the electron density on electronegative atoms, greatly increasing the acidity of H's attached to those atoms. In this case the standard potential for the overall reaction at 25 °C is shifted negative, eq 2.2.

$$E^{\circ\prime}_{app} = E1^{\circ} + 0.0592V \times logK_{HB} \quad (2.1)$$

$$E^{\circ\prime}_{app} = E1^{\circ} - 0.0592V \times logK_{HB} \quad (2.2)$$

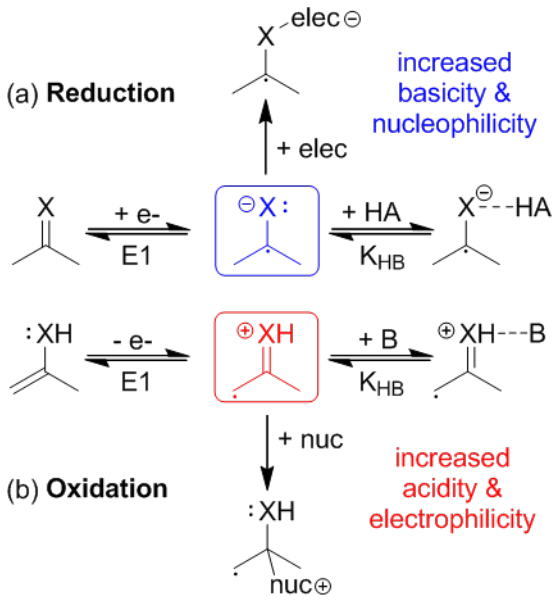

Scheme 2.1. Effects of reduction and oxidation on the reactivity of organic redox couples.

In addition to the above roles for H-bonded intermediates, there is also another role that has not been widely discussed in the literature. Strong H-bonding to the products of the electron transfer reaction, not only affects the apparent potential of the electron transfer, but also can affect the lifetime of the electron transfer products by interfering with other reactions that might otherwise take place. Referring back to Scheme 2.1, reduction not only increases the basicity of the heteroatom, but also the nucleophilicity, which could lead to nucleophilic attack on any electrophiles present, vertical reaction in Scheme 2.1a. The lifetime of the reduced state would be decreased by an amount related to the rate constant of the nucleophilic reaction and the concentration of electrophile. However, H-bonding to the reduced state should block or at least interfere with the nucleophilic reaction. In the simple scenario outlined in Scheme 2.1a, the nucleophilic reaction only occurs in the non-H-bonded state. H-

bonding reactions are fast and reversible, whereas the nucleophilic reaction is likely slower but irreversible. This means that it would be unlikely that the H-bonding reaction could completely prevent the nucleophilic reaction, but if the value of K_{HB} and the concentration of HA are such that the equilibrium position strongly favors the H-bond complex, then the nucleophilic reaction would be greatly slowed because the nucleophile would only be present at a very low concentration. Similar arguments can be made for an oxidation, Scheme 2.1b, except it is the electrophilicity that is increasing so the lifetime of the oxidized product could be decreased by the presence of nucleophiles in solution.

In contrast to the shifting of the observed potential of a redox couple in the presence of a H-bonding guest, the effect discussed above is essentially kinetic in nature. While this type of effect is not inherently surprising, it has not been widely discussed in the context of H-bonding and electron transfer. A notable exception is a series of papers by Evans and co-workers on the electrochemistry of t-butyl-substituted *o*-benzoquinones in acetonitrile.[26-30] As outlined in Scheme 2.2, quinones are expected to undergo two reversible reactions in aprotic solvents, first to the radical anion and then to the dianion. In the case of the *o*-quinones, the dianion contains two negatively-charged O atoms immediately adjacent to each other. Not surprisingly, this species is very reactive. What has been observed is that under very dry conditions the second cyclic voltammetric (CV) wave for the *o*-benzoquinones, corresponding to the second reduction to the dianion, is not only totally irreversible, but also extremely broad and very small compared to the first CV wave. Addition of water shifts this

wave to more positive potentials, as expected, due to the stronger H-bonding of water to the dianion than the radical anion. However, it also greatly increases the size of the second wave leading eventually to it obtaining a full one electron height, although it is still irreversible due to proton transfer. In their most recent report,[30] after having ruled out more obvious possibilities, Evans and Rene suggest that the small wave could be due to reaction of this extremely reactive dianion with the radical anion, initiating an oligomerization process which consumes radical anion, with the result that there is less radical anion to be reduced. They hypothesize that H-bonding of water prevents this reaction, resulting in the growth in size of the second wave as water is added.

Scheme 2.2. General electrochemical reduction mechanism for quinones in aprotic solvents.

The electrochemistry observed for the t-butyl-*o*-benzoquinones is unique, but kinetic stabilization of quinone dianions by H-bonding is not. In this work, it is demonstrated that kinetic stabilization of the quinone dianions by H-bonding to water also occurs with the much more commonly studied and much less reactive *p*-quinones. In particular, in very dry CH_2Cl_2, the second reduction of *p*-quinones is of full one electron height, but totally irreversible. Evidence is presented that this is due to nucleophilic attack of the quinone dianion on the solvent, resulting in a chloromethylether. However, as water is titrated in, not only does the second wave shift to more positive potential, the chemical reversibility also increases until eventually the wave becomes fully reversible at typical scan rates, indicating that

water is able to block the reaction with the solvent. It is also shown that the kinetic stabilization by water is great enough that it can block the reaction with iodomethane, a very reactive electrophile, in MeCN.

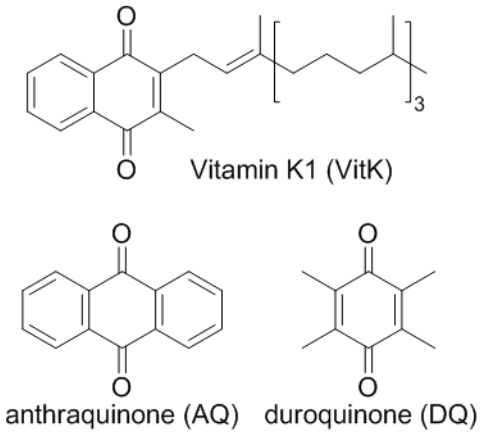

Chart 2.1. Quinones used in this study

Most of the studies in this work have been done with Vitamin K1, VitK, Chart 1. VitK is a naturally occurring naphthoquinone that is necessary for proper blood clotting and the growth and maintenance of bones.[31] Webster and co-workers have extensively studied the electrochemistry of VitK in organic solvents.[32-35] Among the outcomes of this work, they developed a simple method to estimate the water content of organic solvents typically used for electrochemistry based on the $E_{1/2}$ separation between the two CV waves for VitK in different solvents. It should be noted, however, that the effects we observe in very dry CH_2Cl_2 are not limited to VitK. Very similar results are seen both with anthraquinone, AQ, and duroquinone, DQ, Chart 1, indicating that this is a general phenomenon with *p*-quinones.

Experimental

Chemicals. Vitamin K1, VitK, (Alpha Aesar) was used as received. Duroquinone (97%, Acros) and 9,10-anthraquinone were both purified by sublimation. Methyliodide (99 %, Alpha Aesar, stabilized by Cu or Ag) was purified by simple distillation to remove an electroactive impurity. The water titrations were done using 18 MΩ water produced from a Millipore-type cartridge filtration system. Tetrabutylammonium hexafluorophosphate (NBu_4PF_6) was purified by recrystallization three times from 95/5 ethanol/water and then dried overnight, under vacuum, at 100 °C. HPLC-grade CH_2Cl_2 and MeCN were dried by refluxing overnight with calcium hydride, followed by passing through a column of activated alumina. The dried solvent was then immediately added to pre-weighed NBu_4PF_6 in an amber bottle, under Ar, to make a 0.1 M solution, and taken into a N_2 atmosphere dry box. The electrolyte solution was used as is for the "wet" experiments. For the "very dry" experiments, activated 3A molecular sieves were added and the electrolyte solution allowed to sit for at least 48 hours before use. The molecular sieves were activated by heating at 250 °C under vacuum overnight.

Voltammetry. Cyclic voltammograms (CVs) were taken at room temperature, inside a N_2 atmosphere drybox, using a CH Instruments Model 760d digital potentiostat. A three electrode setup was used with a glassy carbon (GC) working electrode, Pt counter electrode, and Ag wire quasi-reference electrode. The latter was housed in a separate, vycor-tipped glass tube containing blank electrolyte. The difference between the $E_{1/2}$ for ferrocene (Fc) and that for the first quinone reduction

was used to re-reference the CVs afterwards. Before use, the GC electrode was polished using 0.25 µm diamond polishing paste (Metadi II, Buehler), thoroughly rinsed with water and acetone, then polished with 0.05 µm alumina polishing paste (Masterprep Suspension, Buehler), followed by rinsing with water, acetone, isopropanol and acetone. After the cell was set up, the GC working electrode was cycled 2000-4000 times at a scan rate of 20V/s through the potential window to attain a stable background prior to data collection for each experiment. After backgrounds were taken, the quinone was added to the cell from a 20-50 mM stock solution using a microliter syringe to give a 1 mM quinone concentration. Additions of water and CH_3I were made from the neat liquids using microliter syringes.

Digital Simulations. Digital simulations of cyclic voltammograms were performed using DigiSim 3.03. The uncompensated resistance in the cell was determined by fitting the peak-to-peak separation of the first quinone reduction assuming it is completely electrochemically reversible at the scan rates used.

Results and Discussion

Typical voltammetry of *p*-quinones in aprotic solvents. *p*-Quinones, represented in this study by vitamin K1 (VitK), 9,10-anthraquinone (AQ), and duroquinone (DQ), Chart 2.1, are known to undergo two reversible one-electron reductions in aprotic solvents, first to the radical anion and then to the dianion, and an associated comproportionation/disproportionation reaction, as shown in Scheme 2.2. Typical experimental cyclic voltammograms (CVs) of quinones are represented by

those of VitK, shown as the black scans in Figures 2.1 and 2.2, in which VitK is reduced and re-oxidized in 0.1 M NBu_4PF_6/CH_2Cl_2 and 0.1 M NBu_4PF_6/MeCN, respectively. The solvents used in these experiments have been prepared using standard drying techniques (the "wet" electrolyte conditions described in the Experimental section).[36] The peaks in Figures 2.1 and 2.2 that are labelled Ic and Ia are the reversible reduction and re-oxidation reaction between the neutral quinone and the radical anion shown as the first electron transfer step in Scheme 2.2, and the peaks labelled IIc and IIa are the reversible reduction and re-oxidation reaction between the radical anion and the dianion shown as the second electron transfer step in Scheme 2.2. Although the CVs qualitatively look like they are well described by the mechanism in Scheme 2.2, careful inspection of quinone CVs in organic solvents typically reveals deviations.[14,27] In Figures 2.1 and 2.2 overlaid digital simulations of the voltammograms (red scans) show what the CVs should look like if Scheme 2.2 offered a complete description of quinoidal electrochemistry. As can be seen, the second wave, IIc/IIa, is smaller in the experimental CVs than in the simulated ones, and there is more current between the waves in the experimental CVs than in the simulated CV's. Deviations from Scheme 2.2 to explain these discrepancies have been discussed by Macias-Ruvalcaba et al.[37] and us[38] and will also be discussed in Chapter 3.

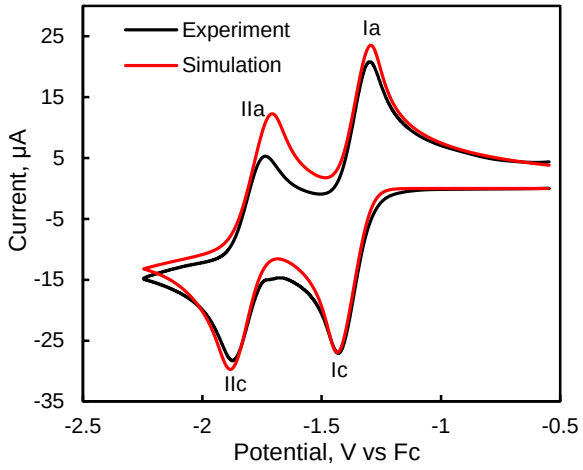

Figure 2.1. Background-subtracted CV (0.2 V/s) of 1.0 mM VitK in 0.1M NBu_4PF_6/CH_2Cl_2 ("wet conditions" – see Experimental Section). Black: Experimental CV; Red: Simulated CV using Scheme 2.2b,2.2c mechanism. Simulation parameters: $E°(Q/Q^{-}) = -1.351$ V; $k°(Q/Q^{-}) = 0.30$ cm/s; $E°(Q^{-}/Q^{2-}) = -1.779$ V; $k°(Q^{-}/Q^{2-}) = 0.0047$ cm/s; $K_{comp/disp} = 1.7e7$ (thermodynamically redundant); $k_{f,\,comp/disp} = 7.32$ e7 $M^{-1}s^{-1}$; $D_Q = 1.19e{-}5$ cm^2/s; $D_{Q-} = 5.37e{-}6$ cm^2/s; $D_{Q2-} = 5.37e{-}6$ cm^2/s; $R_u =$ 1275Ω.

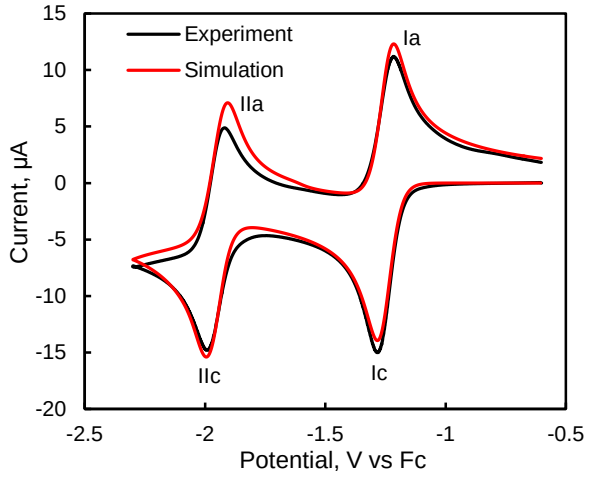

Figure 2.2. Background-subtracted CV (0.2 V/s) of 1.0 mM VitK in 0.1M NBu_4PF_6/MeCN ("wet" conditions). Black: experimental CV; Red: simulated CV using Scheme 2b,2c mechanism. Simulation parameters: $E°(Q/Q^{-}) = -1.242V$; $k°(Q/Q^{-}) = 3.0e6$ cm/s; $E°(Q^{-}/Q^{2-}) = -1.947$ V; $k°(Q^{-}/Q^{2-}) = 0.0066$ cm/s; $K_{comp/disp}$ = 8.3e11 (thermodynamically redundant); $k_{f,\ comp/disp} = 1.7e6\ M^{-1}s^{-1}$; $D_Q = 2.76e{-}6$ cm^2/s; $D_{Q-} = 1.59e{-}6\ cm^2/s$; $D_{Q2-} = 1.59e{-}6\ cm^2/s$; $R_u = 350\Omega$.

In comparing the CV's of VitK in the two solvents, a point of interest is that the second redox wave is much closer in potential to the first in CH_2Cl_2 than in MeCN. Like the too small second CV wave and the extra current between waves, this is another observation that cannot be explained solely by the reactions in Scheme 2.2. Since CH_2Cl_2 is considerably less polar than MeCN, it should be harder, not easier, to form the dianion in this solvent since CH_2Cl_2 will solvate the dianion less effectively than MeCN. However, the explanation for this discrepancy, unlike the others, is straightforward. Because CH_2Cl_2 is solvating the dianion less effectively than MeCN,

electrostatic interactions with the dianion will be stronger in CH_2Cl_2 than MeCN. These interactions would include ion-pairing with the electrolyte cation, NBu_4^+ in this case, as well as H-bonding with water, which, without extreme measures, will be present at higher concentrations than the quinone even in nominally "dry" organic solvents. Both ion-pairing and H-bonding will stabilize the dianion much more so than the radical anion leading to a shift in the $E_{1/2}$ of the second reduction towards the first.

Voltammetry of quinones in very dry CH_2Cl_2; evidence for the high reactivity of the quinone dianion. As noted above, and discussed in many other reports in the literature,[14-18,39] the presence of water and other very weak acids can alter the redox potentials of quinones through thermodynamic stabilization of the charged states via hydrogen bonds. The point we wish to make in this report is that this H-bonding also creates a type of kinetic stabilization in that it can interfere with other reactions that the dianion, in particular, would otherwise undergo. This is dramatically illustrated by the data in Figure 2.3 which shows experimental and simulated CVs of VitK in an exceptionally well-dried electrolyte solution of 0.1 M NBu_4PF_6/CH_2Cl_2 ("very dry" conditions described in the Experimental). Figures 2.6 and 2.7 show the results of similar experiments done with AQ or DQ in place of VitK. In all cases, with no added water, peak IIa is almost completely absent and a new peak, labelled IIIa, has appeared. The absence of peak IIa indicates that the product of IIc, the dianion, has reacted and become non-electroactive at its normal redox potential. The appearance of peak IIIa means that something in the solution has been created which is oxidizable, but is much more stable in its reduced form than either the

quinone dianion or radical anion. We can assume that whatever reaction the dianion went through involved the oxygen atoms, since they would have most of the excess negative charge. The reaction that comes to mind most easily is a nucleophilic attack of the quinone dianion on an electrophile, which results in an ether, Scheme 2.3. The ether would be electroactive, but only at a very positive potential because it is now singly charged rather than doubly charged and one of the oxygens cannot go back to being a carbonyl.

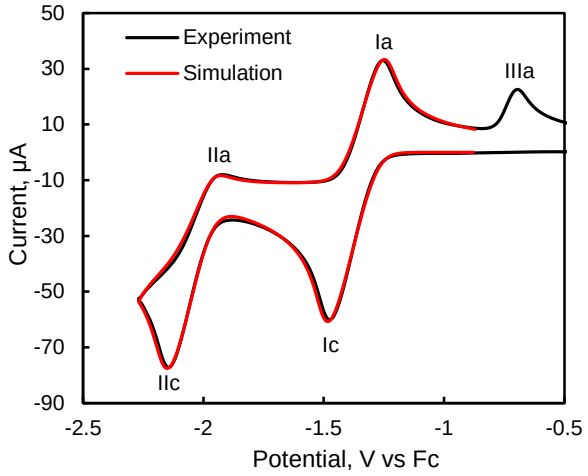

Figure 2.3. Background subtracted CV (1.0 V/s) of 1.0 mM VitK in 0.1M NBu_4PF_6/CH_2Cl_2 ("very dry" conditions). Black: Experimental CV; Red: Simulated CV using Scheme 2.2b,2.2c + Scheme 2.3 mechanism.

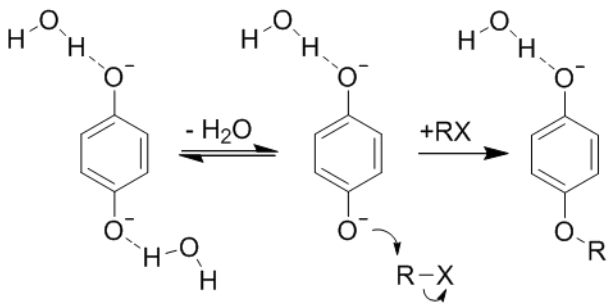

Scheme 2.3. Reaction of Q^{2-} with an electrophile, where *p*-benzoquinone dianion represents the three quinones studied here.

Further information on the reaction of the quinone dianion in the very dry CH_2Cl_2 is provided by the data shown in Figure 2.4, which displays the results of an experiment in which CH_3I was titrated into a solution of VitK in very dry CH_2Cl_2. The CV's start out just like in previous experiments, with a lack of peak IIa and a large peak IIIa, but as the CH_3I concentration increases, peak IVa grows in and IIIa decreases in height. Given that CH_3I is a well-known methylating agent, the methyl ether is the likely product of a reaction between CH_3I and the quinone dianion and the most likely source of the new peak IVa. Since peak IIIa is very close in potential to peak IVa, this provides support for the identification of peak IIIa as being due to oxidation of an ether formed by reaction of the dianion with an electrophile. Furthermore, since CH_3I is a very reactive electrophile, the electrophile that results in peak IIIa must be present at a very large excess in order to still out compete CH_3I even when the VitK:CH_3I ratio is 1:40. The only two compounds that are present at such a high concentration are the electrolyte, NBu_4PF_6, and the solvent, CH_2Cl_2. Since the

only reasonable leaving group for an SN_2 attack of the quinone dianion on NBu_4^+ is a neutral amine, the product ether would be an alkyl ether if NBu_4^+ was the electrophile. This is more electron-donating than the methyl ether resulting from an attack on CH_3I and would therefore give a peak IIIa that is at a potential equal to or negative of peak IVa, not positive of it as observed. Thus the most likely electrophile is the solvent, CH_2Cl_2. This is consistent with the relative peak potentials, since the resulting ether would be a chloromethyl ether, which is electron-withdrawing compared to the methyl ether resulting from reaction with CH_3I, and would result in peak IIIa being positive of peak IVa. It also should be noted that this reaction is not observed in very dry MeCN containing NBu_4^+ (vide infra), further supporting the conclusion that NBu_4^+ is not the electrophile.

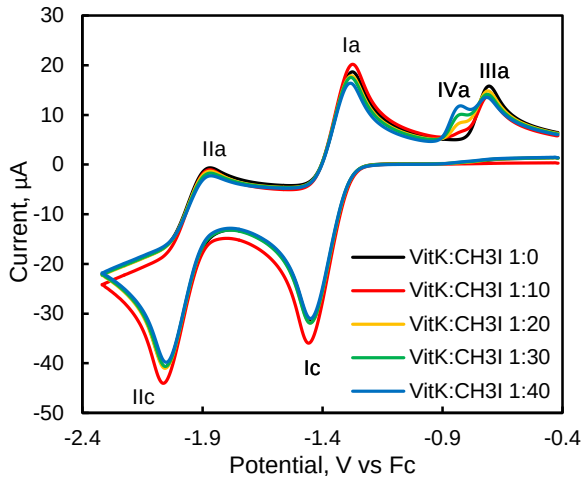

Figure 2.4. Background-subtracted CVs (0.50 V/s) of 1.0 mM VitK in 0.1M NBu_4PF_6/CH_2Cl_2 ("very dry" conditions) with increasing amounts of CH_3I.

Kinetic stabilization of quinone dianion by H-bonding with water.

Comparison of the CVs of VitK taken in very dry CH_2Cl_2 electrolyte, Figure 2.3, to

those taken in standard CH_2Cl_2 electrolyte, Figure 2.1, indicate a greatly reduced reactivity of the quinone dianion under the standard conditions. That this is due to the presence of water can be confirmed by titrating water into the very dry electrolyte as shown in Figure 2.5. Again, very similar behavior is observed for both AQ and DQ as shown by Figures 2.6 and 2.7. In all cases incremental addition of water leads not only to a shift in wave II to more positive potentials, due to the thermodynamic stabilization of the quinone dianion, but also to a gradual increase in the chemical reversibility of the wave, with peak IIa growing in and peak IIIa decreasing as the water content increases. These effects clearly show that the addition of water decreases the reactivity of the quinone dianion, which in the absence of water is evidently a reactive enough nucleophile to attack CH_2Cl_2, a very poor electrophile.

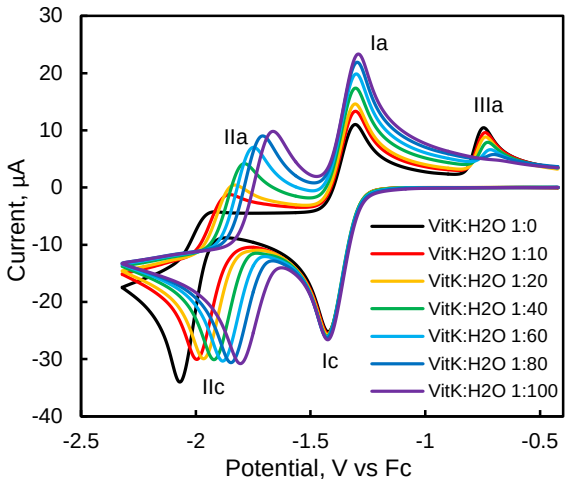

Figure 2.5. Background-subtracted CVs (0.20 V/s) of 1.0 mM VitK in 0.1M NBu_4PF_6/CH_2Cl_2 ("very dry" conditions) with increasing amounts of H_2O.

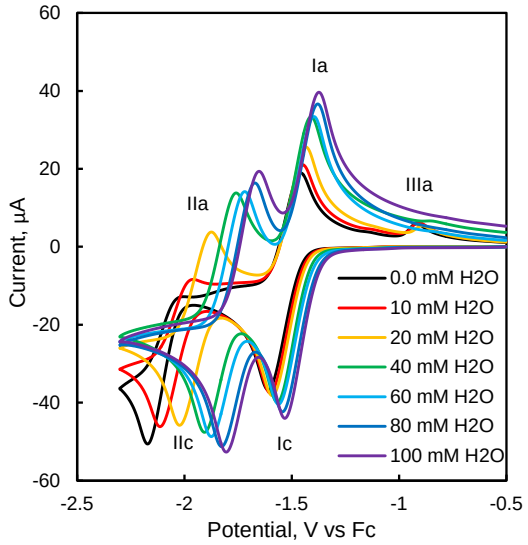

Figure 2.6. Background-subtracted CVs (0.10 V/s) of 1.3 mM 9,10-anthraquinone in 0.1M NBu_4PF_6/CH_2Cl_2 (initially "very dry" conditions) with increasing amounts of H_2O.

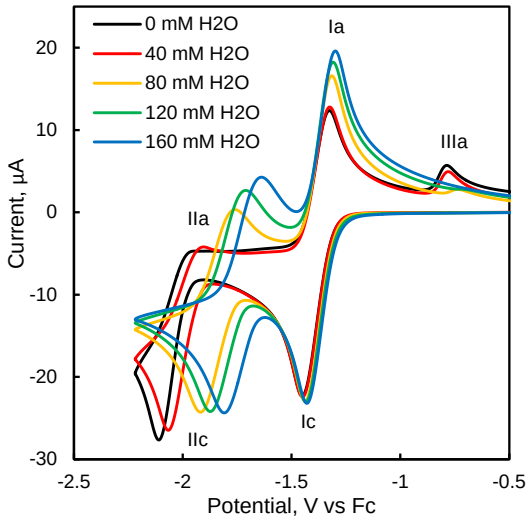

Figure 2.7. Background-subtracted CVs (0.10 V/s) of 1.0 mM duroquinone in 0.1M NBu_4PF_6/CH_2Cl_2 (initially "very dry" conditions) with increasing amounts of H_2O.

Evidence for the kinetic nature of the stabilization can be seen more directly by comparing the scan rate dependence of VitK in the very dry CH_2Cl_2 before and after addition of 40 mM water, Figure 2.8. The CV's have been normalized for scan rate to make easier comparisons. Note that there is an increase in the peak-to-peak separation of the CV waves and a decrease in the cathodic peak currents as the scan rate increases. This is largely due to the presence of uncompensated resistance, R_u, in the cell and the resulting IR_u drop.[40] If only electron transfer was occurring, the anodic peak currents would follow the same trend as the cathodic peak currents, but because of the chemical reaction, the currents for peaks IIa and Ia show the opposite behavior, increasing as the scan rate increases. This indicates that the chemical reaction between the quinone dianion and the solvent is starting to be outrun by going to the faster scan rates, which means there is more dianion and radical anion to be oxidized on the return scan. Peak IIIa, which is due to the ether product, shows the opposite trend, decreasing as the scan rate increases since less ether has been produced at the faster scan rates. Comparing the scan rate dependences under the two conditions, the scan rate effect on peak IIIa is much more significant with 40 mM water present. At 0.2 V/s peak IIIa is clearly present with 40 mM water, but at 2 V/s it is almost gone. In contrast, there is very little relative change in the size of peak IIIa in the absence of water, other than that resulting from the IR drop. The fact that peak IIIa is present in 40 mM water indicates that the reaction between the quinone dianion is still occurring, but the

greater relative decrease in its size in 40 mM water compared to no water indicates it is much slower with the water present.

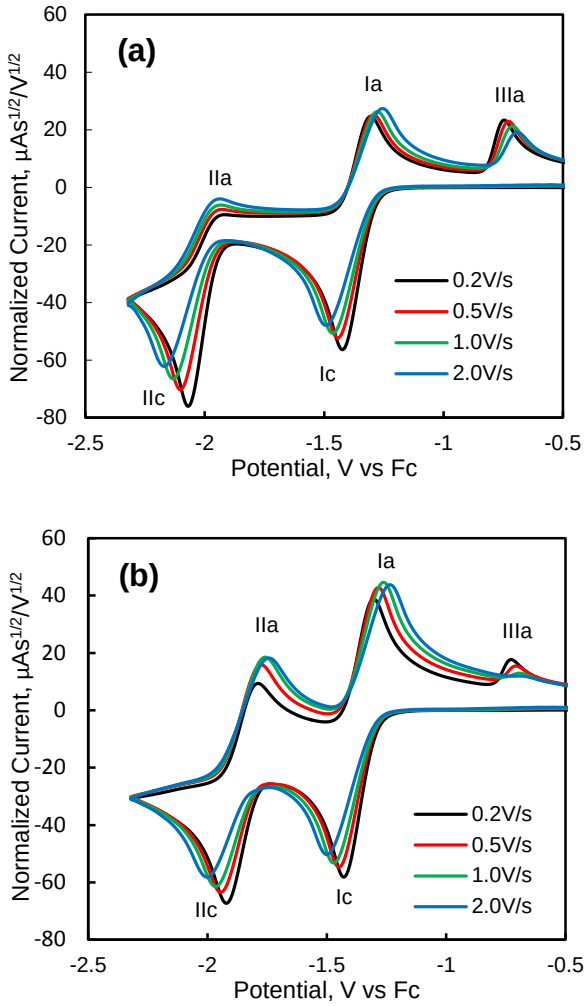

Figure 2.8. Background-subtracted CVs of 1.0 mM VitK in 0.1M NBu_4PF_6/CH_2Cl_2 at different scan rates with (a) 0 mM added H_2O and (b) 40mM added H_2O. The currents have been normalized by dividing by the square root of the scan rate.

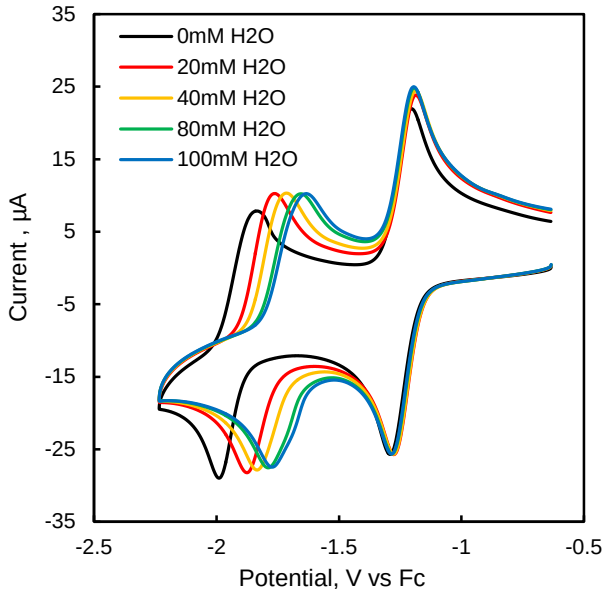

Figure 2.9. CVs (0.10 V/s) of 1.0 mM Vitamin K1 in 0.1M NBu_4PF_6/MeCN (initially "very dry" conditions) with increasing amounts of H_2O. Note that these CV's are not background-subtracted.

In contrast to CH_2Cl_2, the kinetic stabilization of the quinone dianion by water is not as obvious in MeCN. As shown in Figure 2.9, addition of water to very dry MeCN causes the $E_{1/2}$ of wave II to shift positive as expected, but there is no significant change in the size or chemical reversibility as water is added. This may reflect the fact that MeCN is more polar and therefore does a better job solvating the dianion by itself than CH_2Cl_2 does. However, it is likely more important that MeCN is an even poorer electrophile than CH_2Cl_2 and so a direct reaction with the quinone dianion and MeCN is not possible. However, by adding a reactive electrophile such as CH_3I, it can be seen that water also exerts a kinetic stabilization effect in MeCN as well. This is shown in Figure 2.10, as an overlay of CV's obtained as water is titrated

into a 1:1 solution of CH_3I and VitK in MeCN. The initial CV, black scan, is that of VitK by itself in MeCN dried over molecular sieves. After addition of 1 equivalent of MeI, red scan, the current of peak IIa greatly decreases and peak IVa positive of peak Ia appears. This is consistent with reaction of CH_3I with the quinone dianion to form the methyl ether as observed in CH_2Cl_2. As water is titrated in, wave II shifts positive in potential as expected. With 10 mM water, there is little change in the height of peak IIa or IVa, but with 40 and then 80 mM water a clear increase in peak IIa, accompanied by a decrease in the height of peak IVa, is observed. Control experiments, Figure 2.11, indicate that the CH_3I does not react with water under these conditions, therefore the increased reversibility cannot be attributed to a loss of CH_3I. Thus it appears that H-bonding of water responsible for the shift in peak potentials of wave II is also responsible for the slower reaction with CH_3I in MeCN.

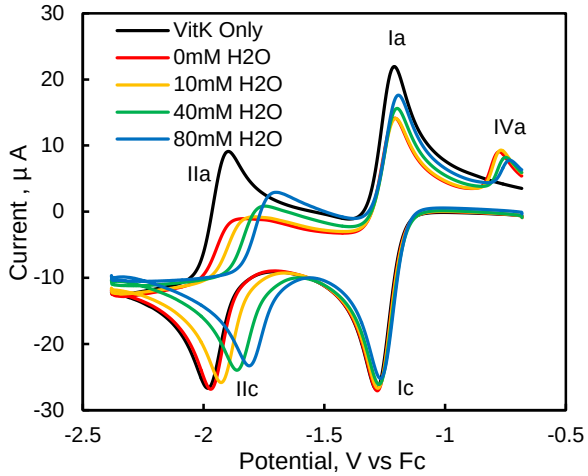

Figure 2.10 Background-subtracted CVs (0.20 V/s) of 1.0 mM VitK in 0.1M NBu_4PF_6/MeCN (initially "very dry" conditions). Black: VitK by itself; Red: + 1 mM CH_3I; Yellow, green and blue: increasing concentrations of H_2O.

Control Experiments for the Effect of Water on the Reaction of CH_3I with $VitK^{2-}$ in MeCN. Figure 2.11 shows the results of an experiment very similar to that illustrated in Figure 2.10 in which water is added to a 1:1 mixture of CH_3I and VitK initially in very dry MeCN. The difference is that in these CVs, the potential is initially scanned positive from ~ −0.5 V vs Fc out to ~ +1 V vs Fc, then back negative through the VitK reduction peaks Ic and IIc to −2.4 V vs Fc. The scan direction is then switched again, going back positive through the VitK and product oxidation peaks back out to +1 V vs Fc. This is followed by another switch in scan direction, ending at about −0.5 V vs Fc. The black CV is VitK by itself. Note that there are no peaks observed in the positive potential region, consistent with the chemical reversibility of the two quinone CV waves Ic/Ia and IIc/IIa under these conditions. Addition of 1 equivalent of CH_3I, red CV, has little effect on the quinone reduction peaks, but peak IIa is drastically reduced in height and peak Ia is smaller as well. This, as noted earlier, is consistent with CH_3I reacting with the quinone dianion, a conclusion support by the appearance of new oxidation peaks IVa through VIIIa. Peak IVa, discussed in the main text is believed to be due to oxidation of the monomethylated ether product. Peaks Va to VIIIa, which were not present on the initial positive scan, have to be due to additional products of the reaction between the quinone dianion and CH_3I. One of these products should be iodide, which would be oxidized in the positive potential region. This claim is supported by a CV of KI in 0.1 M NBu_4PF_6/MeCN, green dashed line, which shows two oxidation peaks (presumably

to I_3^- and I_2) in the same vicinity as peaks Va and VIa, albeit at slightly more negative potentials. The additional oxidation peaks are presumably due to other ether products, for example, the dimethylated ether.

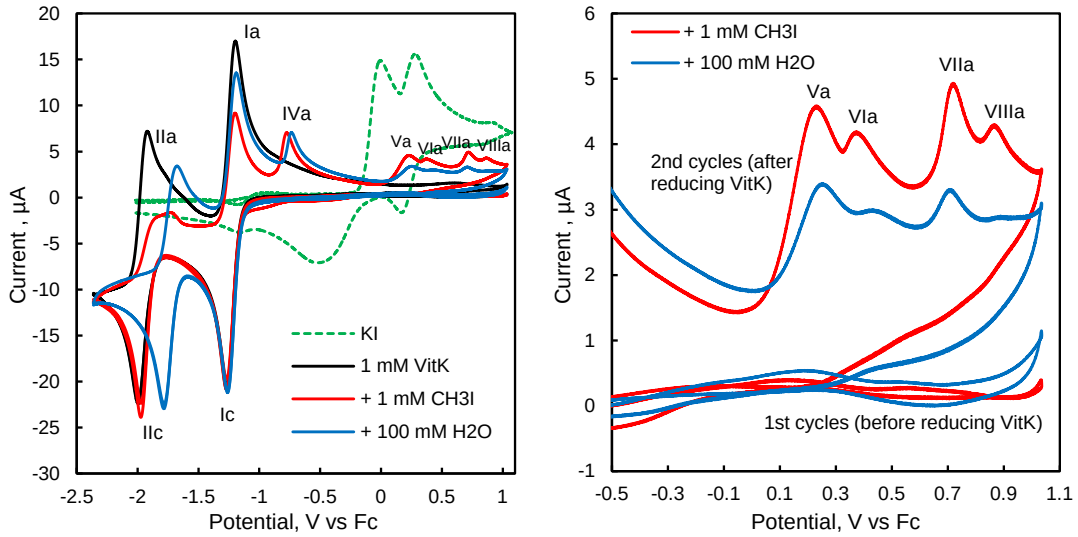

Figure 2.11. Background-subtracted CVs (0.10 V/s) in 0.1M NBu_4PF_6/MeCN (initially "very dry" conditions). Black: 1 mM VitK; Red: + 1 mM CH_3I; Blue: + 100 mM H_2O. Black, red and blue scans start at 0 V, go to +1 V, then -2.4 V, then back to +1 V, and end at 0 V. Green dashed line: KI by itself. Figure on right expands the positive voltage region for the VitK + CH_3I CV (red) and VitK + CH_3I + H_2O CV (blue).

As observed earlier, addition of water, blue CV in Figure 2.10, causes a positive shift in the second quinone reduction, but also an increase in the quinone oxidation peaks IIa and Ia, along with a decrease in the size of the product oxidation peaks, IVa through VIIIa. As noted earlier, this is consistent with the strong H-

bonding of water to the quinone dianion slowing the reaction with CH_3I. An alternative explanation, that the water has reacted with the CH_3I causing a decrease in the amount of CH_3I, is not supported by the data in Figure 2.11. This is because reaction of water with CH_3I would also produce iodide, so, if this reaction was happening in the bulk solution, then, on the first positive going scan in the presence of water, oxidation peaks for iodide should be present. But, as the expanded Figure 2.10 (on the right) shows, there are no peaks in this region on the first cycle, they only appear after the potential is scanned through the VitK reduction.

Another way to confirm that water does not react significantly with CH_3I under the conditions and timescale of the CV experiments, would be to look directly at the reduction peak of CH_3I, which occurs several 100 mV more negative than the second VitK reduction. Unfortunately, reduction of water overlaps with the CH_3I reduction so it was not possible to use this more direct means to monitor the CH_3I concentration with water present.

CONCLUSIONS

In this work it has been shown that strong H-bonding by water to several different p-quinone dianions can greatly slow down the reaction of the dianions with electrophiles. Thus H-bonding provides a type of kinetic stabilization to the dianion, increasing the lifetime of what otherwise is a very reactive species, and, therefore, also increasing the chemical reversibility of the electron transfer. This effect is certainly

not unique to quinone dianions and water, but, if looked for, will likely be found for many organic redox couples in the presence of suitable H-bonding partners. It also adds another facet to the important role that H-bonding can play in electron transfer.

REFERENCES

1. Weinberg, D. R.; Gagliardi, C. J.; Hull, J. F.; Murphy, C. F.; Kent, C. A.; Westlake, B. C.; Paul, A.; Ess, D. H.; McCafferty, D. G.; Meyer, T. J., Proton-Coupled Electron Transfer. *Chem. Rev.* **2012,** *112*, 4016-4093.

2. Huynh, M. H. V.; Meyer, T. J., Proton-Coupled Electron Transfer. *Chem. Rev.* **2007,** *107*, 5004-5064.

3. Costentin, C.; Robert, M.; Saveant, J.-M., Update 1 of: Electrochemical Approach to the Mechanistic Study of Proton-Coupled Electron Transfer. *Chem. Rev.* **2010,** *110*, PR1-PR40.

4. Hammes-Schiffer, S., Proton-Coupled Electron Transfer: Moving Together and Charging Forward. *J. Am. Chem. Soc.* **2015,** *137*, 8860-71.

5. Migliore, A.; Polizzi, N. F.; Therien, M. J.; Beratan, D. N., Biochemistry and Theory of Proton-Coupled Electron Transfer. *Chem. Rev.* **2014,** *114*, 3381-3465.

6. Clare, L. A.; Pham, A. T.; Magdaleno, F.; Acosta, J.; Woods, J. E.; Cooksy, A. L.; Smith, D. K., Electrochemical Evidence for Intermolecular Proton-Coupled Electron Transfer through a Hydrogen Bond Complex in a p-Phenylenediamine-Based Urea. Introduction of the "Wedge Scheme" as a Useful Means To Describe Reactions of This Type. *J. Am. Chem. Soc.* **2013,** *135*, 18930-18941.

7. Costentin, C.; Robert, M.; Saveant, J. M., Concerted Proton-Electron Transfers: Electrochemical and Related Approaches. *Acc. Chem. Res.* **2010,** *43*, 1019-1029.

8. Saveant, J.-M., Concerted Proton-Electron Transfers: Fundamentals and Recent Developments. *Annual Review of Analytical Chemistry, Vol 7* **2014,** *7*, 537-560.

9. Bonin, J.; Costentin, C.; Robert, M.; Saveant, J. M.; Tard, C., Hydrogen-Bond Relays in Concerted Proton-Electron Transfers. *Acc. Chem. Res.* **2012,** *45*, 372-381.

10. Bonin, J.; Costentin, C.; Louault, C.; Robert, M.; Saveant, J. M., Water (in Water) as an Intrinsically Efficient Proton Acceptor in Concerted Proton Electron Transfers. *J. Am. Chem. Soc.* **2011,** *133*, 6668-6674.

11. Peover, M. E., A Polarographic Investigation into the Oxidation-Reduction Behavior of Quinones: The Roles of Electron Affinity and Solvent. *J. Chem. Soc.* **1962**, 4540-9.

12. Ge, Y.; Lilienthal, R. R.; Smith, D. K., Electrochemically-Controlled Hydrogen Bonding. Selective Recognition of Urea and Amide Derivatives by Simple Redox-Dependent Receptors. *J. Am. Chem. Soc.* **1996,** *118*, 3976-7.

13. Ge, Y.; Miller, L.; Ouimet, T.; Smith, D. K., Electrochemically Controlled Hydrogen Bonding. o-Quinones as Simple Redox-Dependent Receptors for Arylureas. *J. Org. Chem.* **2000,** *65*, 8831-8838.

14. Gupta, N.; Linschitz, H., Hydrogen-Bonding and Protonation Effects in Electrochemistry of Quinones in Aprotic Solvents. *J. Am. Chem. Soc.* **1997,** *119*, 6384-6391.

15. Gomez, M.; Gonzalez, F. J.; Gonzalez, I., A Model for Characterization of Successive Hydrogen Bonding Interactions with Electrochemically Generated Charged Species. The Quinone Electroreduction in the Presence of Donor Protons. *Electroanalysis* **2003,** *15*, 635-645.

16. Gomez, M.; Gomez-Castro, C. Z.; Padilla-Martinez, I. I.; Martinez-Martinez, F. J.; Gonzalez, F. J., Hydrogen Bonding Effects on the Association Processes between Chloranil and a Series of Amides. *J. Electroanal. Chem.* **2004,** *567*, 269-276.

17. Macias-Ruvalcaba, N. A.; Gonzalez, I.; Aguilar-Martinez, M., Evolution from Hydrogen Bond to Proton Transfer Pathways in the Electroreduction of a-NH-Quinones in Acetonitrile. *J. Electrochem. Soc.* **2004,** *151*, E110-E118.

18. Tessensohn, M. E.; Hirao, H.; Webster, R. D., Electrochemical Properties of Phenols and Quinones in Organic Solvents are Strongly Influenced by Hydrogen-Bonding with Water. *J. Phys. Chem. C* **2013,** *117*, 1081-1090.

19. Breinlinger, E.; Niemz, A.; Rotello, V. M., Model Systems for Flavoenzyme Activity. Stabilization of the Flavin Radical Anion through Specific Hydrogen Bond Interactions. *J. Am. Chem. Soc.* **1995,** *117*, 5379-80.

20. Kajiki, T.; Moriya, H.; Hoshino, K.; Kuroi, T.; Kondo, S. i.; Nabeshima, T.; Yano, Y., Functionalized Flavin Receptors. Regulation of Redox Properties of 6-Azaflavin via Hydrogen Bondings with Melamine Derivatives Bearing Guanidinium Ion(s) in Organic Solvents. *J. Org. Chem.* **1999,** *64*, 9679-9689.

21. Bu, J.; Lilienthal, N. D.; Woods, J. E.; Nohrden, C. E.; Hoang, K. T.; Truong, D.; Smith, D. K., Electrochemically Controlled Hydrogen Bonding. Nitrobenzenes as Simple Redox-Dependent Receptors for Arylureas. *J. Am. Chem. Soc.* **2005,** *127*, 6423-6429.

22. Martinez-Gonzalez, E.; Frontana, C., Employment of Electrodonating Capacity as an Index of Reactive Modulation by Substituent Effects: Application for Electron-Transfer-Controlled Hydrogen Bonding. *J. Org. Chem.* **2014,** *79*, 1131-1137.

23. Martinez-Gonzalez, E.; Armendariz-Vidales, G.; Ascenso, J. R.; Marcos, P. M.; Frontana, C., Site-Specific Description of the Enhanced Recognition Between Electrogenerated Nitrobenzene Anions and Dihomooxacalix[4]arene Bidentate Ureas. *J. Org. Chem.* **2015,** *80*, 4581-4589.

24. Woods, J. E.; Ge, Y.; Smith, D. K., Electrochemically Controlled Hydrogen Bonding. Electrolyte Effects in an Oxidation-Based Arylurea-Amide System. *J. Am. Chem. Soc.* **2008,** *130*, 10070-10071.

25. Clare, J. P.; Statnikov, A.; Lynch, V.; Sargent, A. L.; Sibert, J. W., Wurster-Type Ureas as Redox-Active Receptors for Anions. *J. Org. Chem.* **2009,** *74*, 6637-6646.

26. Lehmann, M. W.; Evans, D. H., Mechanism of the Electrochemical reduction of 3,5-Di-tert-butyl-1,2-benzoquinone. Evidence for a Concerted Electron and Proton Transfer Reaction Involving a Hydrogen-Bonded Complex as Reactant. *J. Phys. Chem. B* **2001,** *105*, 8877-8884.

27. Lehmann, M. W.; Evans, D. H., Anomalous Behavior in the Two-Step Reduction of Quinones in Acetonitrile. *J. Electroanal. Chem.* **2001,** *500*, 12-20.

28. Macias-Ruvalcaba, N. A.; Okumura, N.; Evans, D. H., Change in Reaction Pathway in the Reduction of 3,5-Di-tert-butyl-1,2-benzoquinone with Increasing Concentrations of 2,2,2-Trifluoroethanol. *J. Phys. Chem. B* **2006,** *110*, 22043-22047.

29. Evans, D. H.; Rene, A., Reinvestigation of a Former Concerted Proton-Electron Transfer (CPET), the Reduction of a Hydrogen-Bonded Complex Between a Proton Donor and the Anion Radical of 3,5-Di-tert-butyl-1,2-benzoquinone. *Phys. Chem. Chem. Phys.* **2012,** *14*, 4844-4848.

30. Rene, A.; Evans, D. H., Electrochemical Reduction of Some o-Quinone Anion Radicals: Why Is the Current Intensity so Small? *J. Phys. Chem. C* **2012,** *116*, 14454-14460.

31. Shearer, M. J., Vitamin-K. *Lancet* **1995,** *345*, 229-234.

32. Hui, Y.; Chng, E. L. K.; Chng, C. Y. L.; Poh, H. L.; Webster, R. D., Hydrogen-Bonding Interactions Between Water and the One- and Two-Electron-Reduced Forms of Vitamin K1: Applying Quinone Electrochemistry to Determine the Moisture Content of Non-Aqueous Solvents. *J. Am. Chem. Soc.* **2009,** *131*, 1523-1534.

33. Hui, Y. L.; Chng, E. L. K.; Chua, L. P. L.; Liu, W. Z.; Webster, R. D., Voltammetric Method for Determining the Trace Moisture Content of Organic Solvents Based on Hydrogen-Bonding Interactions with Quinones. *Anal. Chem.* **2010,** *82*, 1928-1934.

34. Webster, R. D., Voltammetry of the Liposoluble Vitamins (A, D, E and K) in Organic Solvents. *Chem. Rec.* **2012,** *12*, 188-200.

35. Lim, Z. H.; Chng, E. L. K.; Hui, Y. L.; Webster, R. D., The Hydrogen-Bonded Dianion of Vitamin K-1 Produced in Aqueous-Organic Solutions Exists in Equilibrium with Its Hydrogen-Bonded Semiquinone Anion Radical. *J. Phys. Chem. B* **2013,** *117*, 2396-2402.

36. Note that as it turns out the MeCN used for the CV in Figure 2.2 was quite dry. Further drying by sitting over activated molecular sieves has little effect as shown by comparing the $\Delta E_{1/2}$ of the two quinone waves to that seen for the CV in Figure S3 with no added water. Apparently drying HPLC-grade MeCN solely by distilling over CaH_2 can be quite effective if one immediately takes it into the dry box as was done in this case. If the CV had been done outside the dry box, it is likely that the solution would have been quite wet due to rapid pickup of water from the environment. In contrast, the CH_2Cl_2 used for the CV in Figure1 was quite wet, with an estimated [H_2O] of 70 mM by comparison to Figure 2.5. However, this is likely just incidental - one cannot conclude that the CaH_2 drying is less effective for CH_2Cl_2 than MeCN without further investigation.

37. Macias-Ruvalcaba, N. A.; Felton, G. A. N.; Evans, D. H., Contrasting Behavior in the Reduction of 1,2-Acenaphthylenedione and 1,2-Aceanthrylenedione. Two Types of Reversible Dimerization of Anion Radicals. *J. Phys. Chem. C* **2009,** *113,* 338-345.

38. Staley, P. A.; Newell, C. M.; Pullman, D. P.; Smith, D. K., The Effect of Glassy Carbon Surface Oxides in Non-Aqueous Voltammetry: The Case of Quinones in Acetonitrile. *Anal. Chem.* **2014,** *86,* 10917-10924.

39. Quan, M.; Sanchez, D.; Wasylkiw, M. F.; Smith, D. K., Voltammetry of Quinones in Unbuffered Aqueous Solution: Reassessing the Roles of Proton Transfer and Hydrogen Bonding in the Aqueous Electrochemistry of Quinones. *J. Am. Chem. Soc.* **2007,** *129,* 12847-12856.

40. "IR drop" refers to the current-dependent voltage drop ("IR" = $I \times R_u = V$) between the reference electrode and the working electrode. In the presence of significant solution resistance, which certainly is the case in CH_2Cl_2, the true voltage of the working electrode lags farther and farther behind the applied potential as the current increases. Since the actual currents are increasing with scan rate, the effect is larger at faster scan rates resulting in broader waves with peak potentials that are shifted to more extreme potentials as the scan rate increases. See Bard, A. J.; Faulkner, L. R., *Electrochemical Methods: Fundamentals and Applications*. 2nd ed.; John Wiley & sons: New York, 2001, p. 233.

Chapter 3. Glassy Carbon Surface Phenolic Functionality and Its Effect on Quinone Electrochemistry

Abstract

Glassy carbon (GC) electrodes are well known to contain oxygenated functional groups such as phenols, carbonyls and carboxylic acids on their surface. The effects of these groups on voltammetry in aqueous solution are well-studied, but there has been little discussion of their possible effects in non-aqueous solution. In this study it is shown that the acidic functional groups, particularly phenols, are likely causes of anomalous features often seen in the voltammetry of quinones in non-aqueous solution. These features, a too small second cyclic voltammetric wave and extra current between the two waves that sometimes appears to be a small, broad third voltammetric wave, have previously been attributed to different types of dimerization. In this work, concentration-dependent voltammetry in acetonitrile rules out dimerization with a series of alkyl-benzoquinones because the anomalous features get larger as the concentration decreases. At low concentrations, solution bimolecular reactions will be relatively less important than reactions with surface groups. Addition of sub-stoichiometric amounts of naphthol at higher quinone concentrations, produces almost identical behavior as seen at low quinone concentrations with no added naphthol. This implicates hydrogen bonding and proton transfer from the surface phenolic groups as the cause of the anomalous features in quinone voltammetry at GC electrodes. This conclusion is supported by the perturbation of surface oxide coverage on GC electrodes through different electrode pre-treatments

Introduction

In chapter 2, part of the argument for the effect of the water H-bonding complex came from comparisons between experimental data and simulations of the mechanism, which is a standard way to show that the mechanism is reasonable. Before an attempt to accurately simulate a new mechnism involving quinones and some guest molecule, such as the wedge scheme, it is essential to be confident that we can accurately simulate the quinone reductions by themselves. That leads to the problem that voltammograms of quinones alone in aprotic solutions have never followed the shape that would be expected of two ideal one-electron transfers. Where both redox waves in quinone CV's are supposed to be the same size, the second redox wave is always smaller than the first in actual experiments. So ubiquitus is this problem that it has become an interesting phenomenon in its own right with explanations mainly involving different types of quinone dimers forming in aprotic solution when the quinones are in their radical anionic form, so that the quinones that go into the second redox wave are not simply the free floating radical anions. Another likely explanation, and one that will be put forward in this chapter, is that the unexpectedly small second wave is due to some of the quinones being reduced and oxidized at a potential in between the two expected redox waves because some of them interact with H-bonding and H^+-transfer partners on the electrode surface such as phenolic functional groups.

Glassy carbon, along with platinum and gold, are the most commonly used solid electrode materials for electroanalytical techniques. The advantages of glassy

carbon are mainly that it is inexpensive and has a large voltage window in aqueous solution. It is also useful for working with compounds with functional groups that strongly adsorb on platinum and gold. The latter quality is often why glassy carbon is used in organic solvents. The case in point is quinones, where glassy carbon is the material of choice in nearly every experiment.[1, 3-8, 10-13, 15, 16, 18-26, 31-33]

Although glassy carbon is thought of as relatively inert and generally promotes outer sphere electron transfer, it is well known that oxygenated functional groups exist on the electrode surface.[8, 9, 21, 22, 25] The oxygenated groups include phenols, carboxylic acids, ketones, ethers, aldehydes, and alcohols.[4, 5, 8, 9, 22, 23] In some cases, it has been shown that these groups can promote electron transfer. “Activation” of glassy carbon electrodes, which consists of oxidizing the surface, has been shown to promote quinone reduction in aqueous solutions.[28] Discussion of oxidative functional groups on glassy carbon has primarily focused upon aqueous electrochemistry, but these groups are also present during experiments with non-aqueous solution and may affect electrochemistry, particularly if acidic or basic analytes are present. This point does not appear to have been discussed in the literature, and quinones are an excellent redox species to explore it.

Quinones are the prototypical organic redox couple. They were the first organic redox couple to be studied successfully through electrochemistry[35] and are important for biology and pharmaceuticals,[1, 14, 17, 29-31] organic computation,[16, 21, 22, 24] and power systems.[10, 11] More specifically for our purposes: substituted para-quinones are well known to primarily undergo electron transfer, pi-dimerization, and proton

transfer reactions; para-quinones change their basicity dramatically between oxidation states;[36] and there are a wide variety of quinones that can simply be bought commercially because they are so widely used. In the case of this study, 2,3,5,6-tetramethylbenzoquinone (duroquinone, DQ) was the main focus due to its non-reactivity; related quinones were used to control for steric hinderance: 2,5-dimethylbenzoquinone (25MBQ); 2,5-di-tert-butylbenzoquinone (25BBQ); 2,6-dimethylbenzoquinone (26MBQ); and 2,6-di-tert-butylbenzoquinone (26BBQ).

Previous authors have notice that the redox wave for the second electron transfer is smaller than for the first electron transfer. Gupta and Lipshitz were the first to publish about it and proposed that it was due to radical dimerization in which the dimer is electroinactive, see Scheme 3.1.[13] Macias-Ruvalcaba and Evans also published a mechanism to explain the unusually small 2nd redox wave which involved an electroactive radical dimer as in Scheme 3.2, they then used digital simulation and temperature dependent spectroscopy to verify that dimerization occurs with 2,3-dichloro-5,6-dicyanobenzoquinone, although they had to go far below room temperature to do so.[19] Astudillo et al. recently published a mechanism whereby reduced quinone dimers can be held together through hydrogen bonding if there are two protons available per dimer, possibly stolen from trace water in the aprotic organic solvent.[1] Distinguishing between these three mechanisms could be challenging, but such a may be unnecessary if this well-known observation is due to hydrogen bonding or proton transfer between the quinones and acidic groups on the surface.

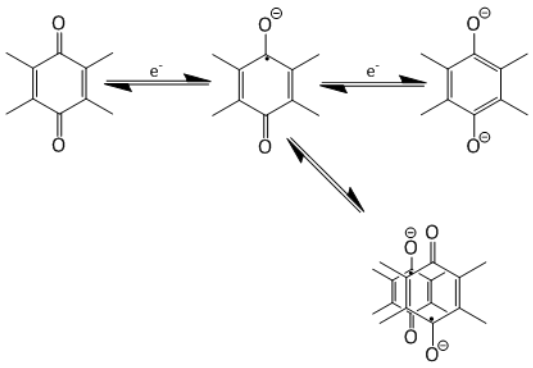

Scheme 3.1. Gupta and Linschitz quinone radical dimerization mechanism.

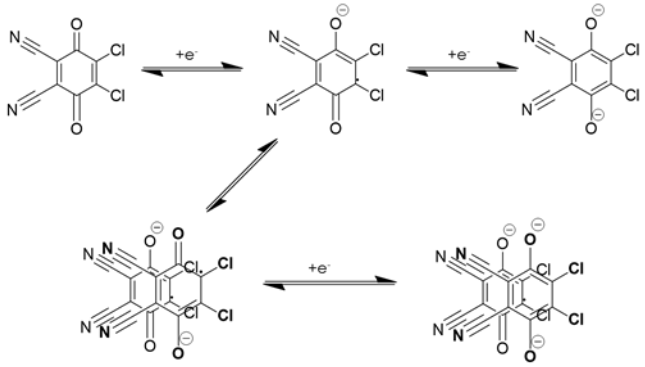

Scheme 3.2. Macias-Ruvalcaba and Evans quinone radical dimer mechansim.

In this work, attempts to find the dimerization constant were unsuccessful because the relative height of the second redox wave shrinks with decreasing concentration. In the case of dimerization, the opposite should happen, but to make matters worse, a third redox wave appears at the lower concentrations which is not predicted by any existing quinone dimerization mechanism. The concentration dependence patterns just described were seen with all of the quinones studied in this paper, showing that steric hinderance, which should play a noticeable role in

dimerization, had little to no effect. What did have an effect was oxidizing or reducing the electrode in order to increase or decrease the protic groups on its surface, indicating that the surface groups which are naturally on all glassy carbon electrodes can affect analytical performance through unintended side reactions.

Experimental

Chemicals. MeCN was HPLC grade and dried by refluxing overnight with CaH_2. Tetrabutylammonium hexafluorophosphate (NBu_4PF_6) was purified by recrystallization from 95% EtOH 3 times followed by drying overnight at 100 °C under vacuum. Vitamin K was used as received with no additional purification. 2-naphthol (NO) and all of the quinones were purified through sublimation.

General Cyclic Voltammetry Procedure. Voltammetry was performed under nitrogen, in a dry box, using a one-compartment cell with three electrodes: 0.0407 cm^2 glassy carbon (GC) working electrode, Pt wire counter electrode, and Ag wire quasi-reference electrode in a separate compartment. The working electrode was polished in atmosphere with 0.25 µM Buehler diamond polishing paste, and then 0.05 µM Buehler alumina slurry before being placed in electrolyte solution. The electrode was then cycled through the potential range until the background stabilized—usually ~2000 cycles.

The electrolyte solution consisted of 0.1 M NBu_4PF_6 in MeCN and was made 40-60 mL at a time by adding the appropriate amount of MeCN to NBu_4PF_6 in a tinted bottle by passing the MeCN through a column of activated alumina and using Ar to both push the MeCN through the column and to fill the tinted bottle to minimize

moisture and minimize loss of MeCN from adsorption to the alumina. Analytes were added from highly concentrated stock solutions using microliter syringes. At the end of experiments, ferrocene (Fc) was added to the cell for use as an internal reference and the CV's were later re-referenced to V vs Fc.

Scan Rate and Concentration Dependence Studies. Cyclic voltammograms were taken at multiple scan rates from 0.1 V/s to 2 V/s. Concentration dependence studies were performed between 0.010 mM and more than 1.0 mM, but most of the lower concentration scans were thrown out due to an unacceptable signal to noise ratio.

Electrode Oxidation and Reduction. "Oxidized" electrodes were prepared by first polishing normally, as described above, and then being placed in 0.1 M aqueous sulfuric acid and cycled 30 times between -0.52 V and 1.83 V vs SCE at 0.15 V/s, followed by water and acetone rinsings.

"Reduced" electrodes were initially prepared by polishing with a 50 nm alumina slurry in deoxygenated cyclohexane. This procedure was reported to bring the oxygen content of the surface from 15% to 4%[18] but was found by us to make the background unstable, presumably due to irreversible reactions with the analyte after the background scans were already completed.

Stability was achieved through hydrogenation under high vacuum through modification of another published procedure.[34] Direct use of the referenced procedure was impossible because our electrodes have Kel-F as insulation, and that would melt under the literature hydrogenation procedure. Furthermore, a more in-depth study of

GC hydrogenation found that to actually etch the electrode surface—so that polishing with the deoxygenated slurry would not be needed—it is necessary that the electrode reach a temperature of approximately 650 K,[2] which would also melt Kel-F.

In light of the above concerns, hydrogenation was performed by modifying a procedure previously used to hydrogenate silicon[34] in an ultrahigh vacuum chamber by pumping down to 5.0E-6 torr and then backfilling with H_2 to a pressure of 6.0E-5 torr, followed by running current through a W filament to heat it to approximately 1900 K while it was approximately 1 cm from the electrode surface. The temperature of the electrode was monitored by thermocouple and the current to the filament was stopped when the electrode reached 50 ^{o}C; the electrode was then allowed to cool before current was started again. The total time that the filament had current flowing through it was 30 min. This procedure is expected to produce a sufficient flux of H atoms at the electrode surface to at least partially remove the oxygenated functional groups.

Digital Simulation. Simulated CV's were made with DigiSim 3.03 using the fitting algorithm. The parameters were fit to the experimental CV using an iterative procedure by fitting the parameters in the following order: E° values, diffusion coefficients, heterogeneous rate constants, and repeat two more times. The transfer coefficient, α, was set to 0.5 for both electron transfers. Values were fit relative to the Ag quasi reference electrode and then re-referenced to Fc. In the end the values attained were: E° = -1.24 V vs Fc and k_s = 39.0 cm/s for the first reduction; E° = -1.93 V vs Fc and k_s = 0.0229 cm/s for the second reduction; D = 6.04E-5 cm^2/s for all species; R = 350 Ω.

DFT Calculations. Density functional theory (DFT) calculations were performed with Gaussian 9 using Gaussview 4.5 as the interface and the cc-pvdz basis set to find the electro-static potential (ESP) for 26MBQ and 26BBQ in order to compare the steric hindrance caused by their substituents.

Results and Discussion

Figure 3.1 shows cyclic voltammograms (CV's) of 1 mM DQ in 0.1 M NBu_4PF_6/MeCN obtained using a gold disk working electrode (red scan) and a Pt disk (blue scan). The first wave (Ic/Ia), corresponding to reduction to the radical anion, is reversible. However, in both cases the second wave (IIc/IIa), presumably corresponding to the reduction of the radical anion to the dianion, is too small and highly distorted. This behavior is typical for quinones with Pt or Au in non-aqueous solvents, which explains why these common electrodes are rarely used for quinones in non-aqueous solvents.

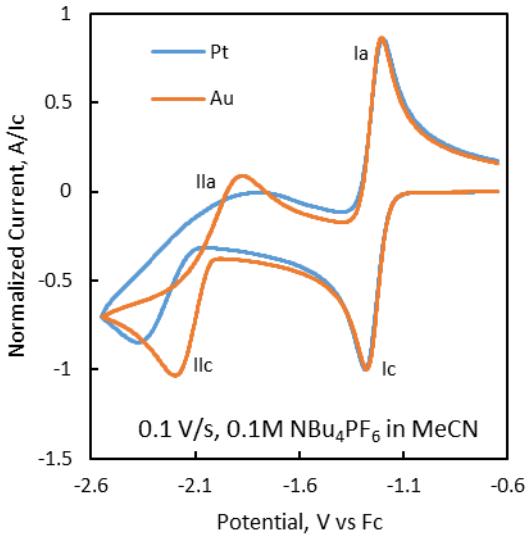

Figure 3.1. CV's of 1 mM DQ in 0.1 M NBu_4PF_6/MeCN at 0.1 V/s. Blue scan: Pt disk working electrode; red scan: Au disk working electrode. Current was normalized by dividing by the Ic peak current.

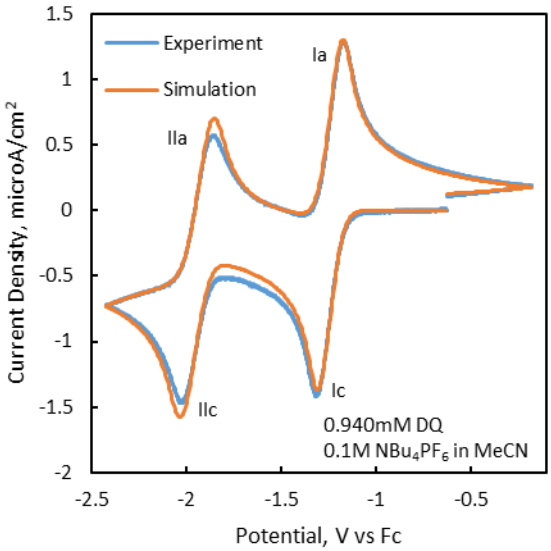

Figure 3.2. CV of 1 mM DQ in 0.1 M NBu_4PF_6/MeCN at 0.1 V/s. Blue scan: Experimental CV using a GC disk working electrode; red scan: simulated CV assuming two sequential electron transfers. Simulation parameters are given in the Experimental section.

In contrast to Pt and Au, use of glassy carbon (GC) working electrodes produces much more ideal CV's with quinones in non-aqueous solvents. This is seen for duroquinone (blue scan) in Figure 3.2. The second wave (IIc/IIa) is clearly much closer to ideal in this CV than those in Figure 3.1, explaining why GC is the electrode of choice for quinones in non-aqueous solvents. However, even in this CV the behavior is actually not completely ideal. The red scan shows the best fit simulated CV that could be obtained assuming a simple two step mechanism, involving

sequential electron transfer steps. Even if one assumes slower kinetics for the second electron transfer (a reasonable assumption) the second wave in the experimental CV is smaller than it should be. The current between the two waves in the experimental CV is also larger than in the simulated CV. As discussed in the Introduction this behavior has been noted by several Authors, and each has offered a slightly different explanation, but all of them involve some form of dimerization. What has not been discussed so far is the role that the GC electrode may be playing in this behavior.

Concentration Dependence of Duroquinone. So far the explanation for the oddly small second wave and the odd thickness between the two normal waves has been some version of dimerization. While dimerization has been verified experimentally in some cases, those cases have all been quinones which have hydroxyl groups, strong electron withdrawing groups, or which form sigma dimers.[19, 20] In order to explain why this unexpected electrochemistry is present in quinones generally, the mechanism also must be present in quinones generally. If dimerization were the case then the CV should be more ideal—the ratio between the peak currents for IIc and Ic should increase as the concentration of DQ decreases—thus favoring the radical monomer over the dimer. Moreover, the presence of large steric groups should also affect the peak current ratio of IIc and Ic because they would favor the monomer rather than the dimer.

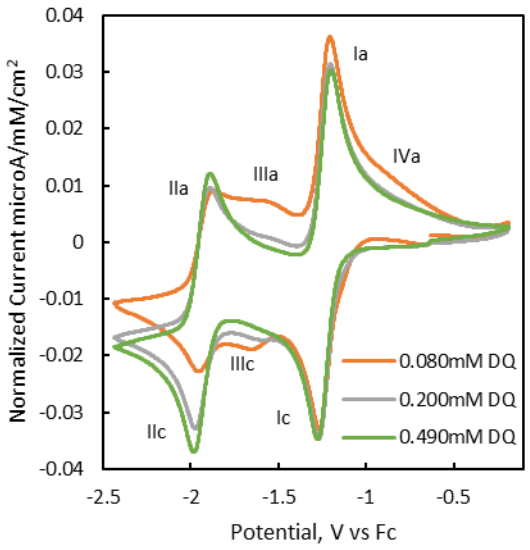

Figure 3.3. Overlaid background-subtracted CV's of different concentrations of DQ performed at 0.1V/s in 0.1M NBu_4PF_6/MeCN. The currents have been normalized by dividing by the DQ concentration and electrode area.

Figure 3.3 shows an overlay of three scans of DQ taken at different concentrations in which the current has been normalized to allow an easy qualitative comparison. What we see here is that the size of the second wave (IIc/IIa) shrinks as compared to the first wave (Ic/Ia) as the concentration decreases; this is the opposite of what should happen if dimerization of any kind were the cause of the unexpectedly small size. Moreover, the odd thickness between the two expected waves resolves into a third wave (IIIc/IIIa) of its own, and another completely unexpected oxidation peak (IVa) also grows in at a potential positive of wave one (Ic/Ia). Rather than dimerization, these results are consistent with something present at low concentration

that is causing some of the DQ to go through redox reactions at potentials that are different from the bulk of the DQ. Hydrogen bonding and proton transfer have both been shown to change the potential of quinone electron transfer reactions, the extent to which this happens depends upon the pK_a of the proton donor and its concentration. This point will be returned to later.

Figure 3.4 shows two quinones that are representative of the steric hinderance experiments. These are electro-static potential surfaces that show how charge is distributed at 95% electron density. From these surfaces, it can be seen that the electron surfaces of the methyl hydrogens are not significantly further out than that of the pi electrons, and therefore do not present a significant hinderance toward radical pi dimerization. On the right hand side of the figure it can be seen that the electron density associated with the tert-butyl groups actually does go significantly beyond the pi electrons, so that they would get in the way and hinder pi dimerization.

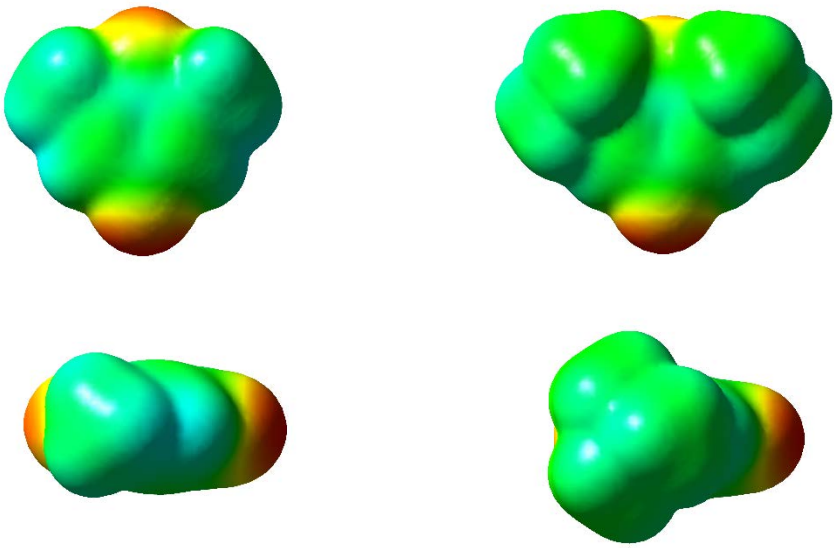

Figure 3.4. Electrostatic potential (ESP) of differently substituted quinones to show the relative steric hinderance of methyl vs tert-butyl groups to pi dimerization. Top left, ESP surface of 2,6-dimethylbenzoquinone viewed from directly above the carbon ring plane; bottom left, ESP surface of 2,6-dimethylbenzoquinone viewed from beside one of the methyl groups; top right, ESP surface of 2,6-di-tert-butylbenzoquinone viewed from directly above the carbon ring plane; bottom right, ESP surface of 2,6-di-tert-butylbenzoquinone viewed from beside one of the tert-butyl groups.

Figure 3.5 shows the results of concentration dependence experiments involving five differently substituted quinones, allowing a comparison between the behaviors of quinones with different amounts of steric hindrance. The horizontal axis is the concentration in mM and the vertical axis is the ratio between the peak potential of the second reduction peak (IIc in Figure 3.3, in the case of DQ) and the first reduction peak (Ic in Figure 3.3, in the case of DQ). A dimer of any kind is less stable

as the total concentration of its constituents decreases because the monomers take longer to find new partners once the dimer breaks up. This should lead the peak ratio to come closer to 1 as the concentration of quinone decreases if dimerization were the reason for the second wave being so small, but what actually happens is the opposite. Figure 3.5 shows quantitatively, and for five differently substituted quinones, that one of the salient features of Figure 3.3—that as the concentration of quinone decreases, the ratio of peak IIc to peak Ic also decreases—is not only present in other quinones, but is apparently unaffected by steric hindrance. Steric hindrance is another thing that should affect dimerization because the more that the reactive groups—in this case the radical that is distributed across the aromatic ring—are kept away from each other, the less stable any dimer would be.

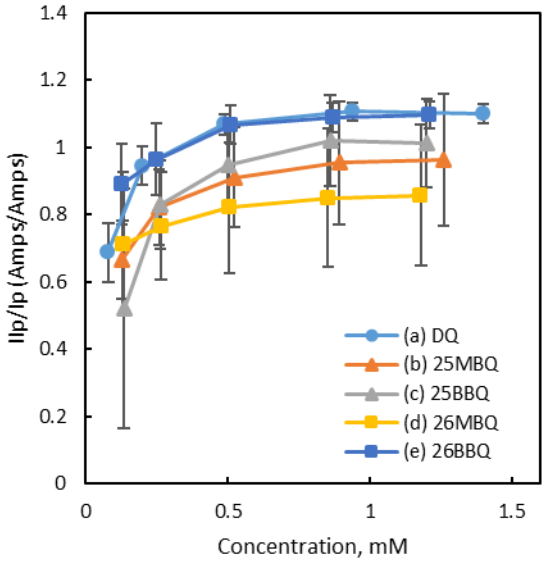

Figure 3.5. Quinone concentration vs the relative heights of their two major reduction peaks, expressed as the height of peak IIc (radical anion reduced to dianion) divided by the height of peak Ic (neutral quinone reduced to radical anion). The peak currents were obtained from CV's performed at 0.1V/s in 0.1M NBu_4PF_6/MeCN.

Put together, figures 3.3, 3.4, and 3.5 rule out dimerization as an explanation for the general trend of the quinone second reduction (IIc/IIa) being smaller than the first (Ic/Ia) and suggest that there is something present at moderately low concentration to cause some of the DQ to be reduced or oxidized at different potentials. That something might be water, but the presence of water generally causes a gradual shift in the potentials which suggests a kinetically fast equilibrium, not a sudden appearance of one more redox wave. An attempt was made to estimate the

water concentration based upon the difference between vitamin K1's $E_{1/2}$ values based upon Webster's method,[15] but the potential difference was outside the linear range of Webster's equation so all we know is that the water concentration is less than 8 mM.

Addition of 2-Naphthol. It is well known that glassy carbon contains oxygenated groups from its manufacture, and that there are oxygenated groups on the surface as a result of polishing in air. With that in mind, proton transfer from the electrode surface to the quinone emerges as a possible explanation for the decreasing size of wave II in Figures 3.3 and 3.5 as the concentration is lowered, as well as the new redox wave (IIIc/IIIa) that grows in at lower concentrations. If this were the case then the position of the third wave (IIIc/IIIa) should depend on the pK_a of the proton donor group and there should be no case in which more than one proton transfer per quinone occurs, since the proton donors would be separated by a large average distance on the surface. Phenolic groups are the most common protic groups on the glassy carbon, so CV's taken with 2-naphthol (NO) titrated into DQ solution were compared to the lower concentration duroquinone CV's.

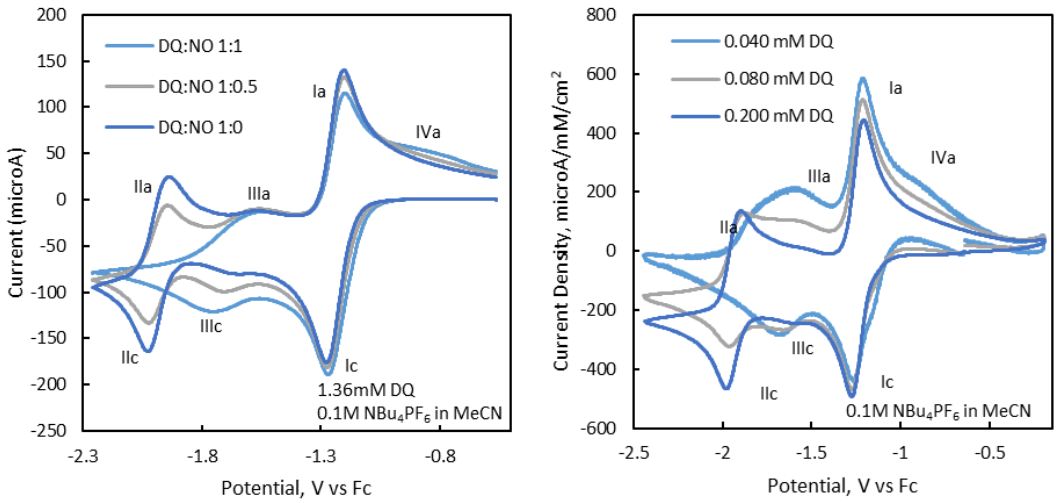

Figure 3.6. Left, background-subtracted CV's for a high concentration of DQ with naphthol titrated in, showing the growth of three new peaks; right, background-subtracted CV's of duroquinone at lower concentrations with no added naphthol showing the growth of three peaks similar to the three in the left overlays as the DQ concentration decreases. The currents were normalized by dividing by the DQ concentration and electrode area. Scans were taken at 0.5 V/s in 0.1M NBu_4PF_6/MeCN.

Figure 3.6 shows, side by side, an overlay of high concentration DQ CV scans with NO titrated in, and an overlay of low concentration DQ CV scans which have been normalized to allow for easy comparison. As has been described above, as the concentration of DQ is decreased a third redox wave (IIIc/IIIa, Figure 3.6, right) grows in, as does a new oxidation peak (IVa, Figure 3.6, right) which are as yet undefined. As NO is titrated into the high concentration DQ solution a new wave

(IIIc/IIIa, Figure 3.6, left) which presumably corresponds to the reduction and oxidation of a strongly hydrogen bonded complex between NO and DQ and occurs at the same potential as peak three (IIIc/IIIa) in the low concentration study, and a new oxidation peak (IVa, Figure 3.6, left) which presumably corresponds to oxidation of the singly protonated, doubly reduced quinone and is at the same potential as the fourth oxidation peak (IVa) in the low concentration study. This behavior is what would be expected if the extra peaks in the low concentration scans were the result of hydrogen bonding and proton transfer between the quinone and phenolic functionalities on the GC surface because NO is also a phenol and would therefore have a similar pK_a and hydrogen bonding characteristics. The lowest concentration DQ scan has the same characteristics as the DQ and NO scan in which NO and DQ are equal in concentration, which is also what we should expect if the new peaks in the low concentration scans come from interactions between DQ and surface phenols because the average distance between surface phenols should be large enough that two surface phenols cannot interact with the same quinone molecule.

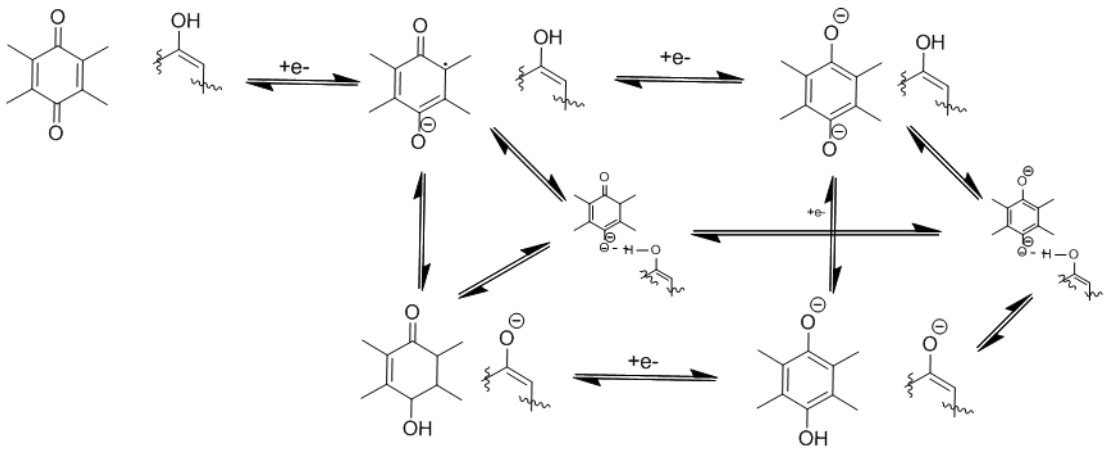

Scheme 3.3. The wedge mechanism for DQ on GC.

A pure proton-electron transfer reaction would have resulted in wave three (IIIc/IIIa, Figures 3.3 and 3.6) being sharp rather than broad, which means that a hydrogen bonding complex must be included and this gives us the wedge type reaction mechanism shown in scheme 3.3. The reason the broadness of wave three (IIIc/IIIa, Figures 3.3 and 3.6) points to a hydrogen bonding complex is that when the complex breaks up the proton could go with the quinone or the phenol which means that some of the radical form is quickly removed, thus broadening the wave in the negative potential direction, and some of the fully reduced form removed by the equillibrium with the free floating, protonated, doubly reduced form, thus broadening the wave in the positive potential direction.

Perturbation of Surface Oxygenated Groups. If oxygenated groups on the electrode surface are the source of the third redox wave (IIIc/IIIa, Figures 3.3 and 3.6) and an explanation for the small size of the second redox wave (IIc/IIa, Figures 3.3 and 3.6) then it should be possible to perturb both waves by reducing or oxidizing the

electrode surface. Specifically what should happen is: at the lower concentrations of duroquinone, where wave two (IIc/IIa) is almost completely gone and wave three (IIIc/IIIa) is much larger, an electrode surface that has been oxidized—and thus has more oxygenated groups—should have wave two (IIc/IIa) disappear altogether and wave three (IIIc/IIIa) grow; an electrode surface that has been reduced—and thus has fewer oxygenated groups—should have a comparably larger wave two (IIc/IIa) and smaller wave three (IIIc/IIIa).

Figure 3.7 shows a comparison of CV's of low concentration DQ in which the electrode was prepared in three different ways: oxidized electrode surface, normal preparation, and reduced electrode surface. The oxygen content of the electrode surface determines the protic group concentration since the protic groups on the electrode surface are oxygen based, so by controlling the oxygen content we can also control the surface coverage of protic groups. In Figure 3.7b the normally polished electrode gives a CV of 0.040 mM DQ which does not include redox wave two (IIc/IIa, Figures 3.3 and 3.6), but does include redox wave three (IIIc/IIIa, Figures 3.3, 3.6, and 3.7). Figure 3.7a, in which the electrode has been oxidized, shows the same behavior as figure 3.7b with a change in the background subtraction which indicates that the charging current has changed, possibly due to a breakdown of the GC surface; this would be the case if the oxidation was extreme enough to cause patches of the GC surface to undergo irreversible reactions during CV scans, but not extreme enough to increase the number of protic groups to the point where they are near enough together to allowed a DQ molecule to interact with more than one of them at a time. Figure

3.7c, in which the electrode has been reduced (see Experimental section), shows that redox waves two and three are both present, indicating that whatever caused DQ to be reduced at redox wave three rather than wave two has decreased in concentration along with the decrease in the oxygen and therefore protic group content. Therefore, it can definitely be said that something about the oxidation state of the surface is responsible for the small size of the quinone wave two, and the most obvious factor is hydrogen bonding and protonation from the surface oxides.

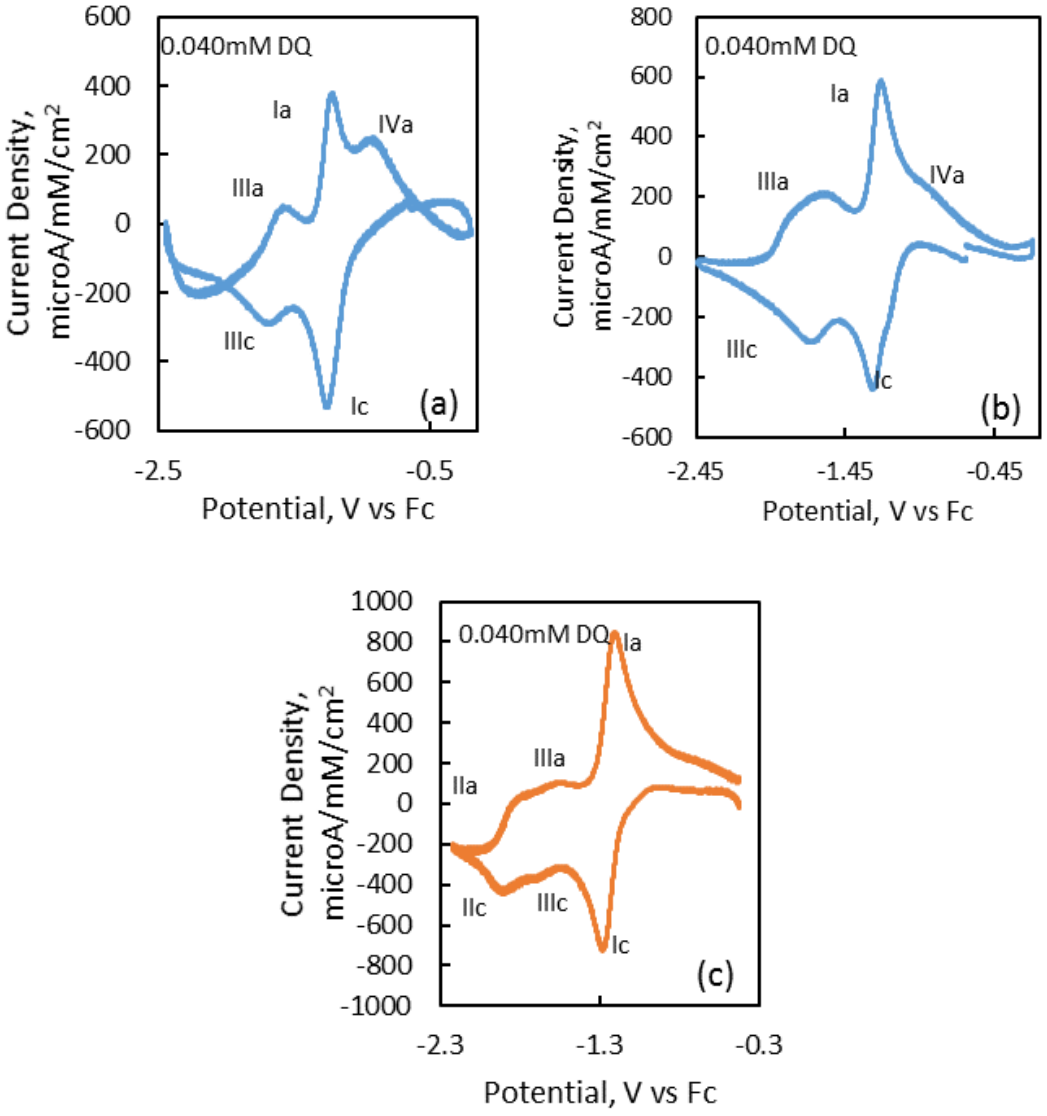

Figure 3.7. Background-subtracted CV's of 0.040 mM DQ with different amount of surface oxidation on the GC electrode: (a.) highly oxidized surface; (b.) normally polished surface; (c.) reduced GC surface. Scans were taken at 0.5 V/s in 0.1M NBu_4PF_6/MeCN. See Experimental section for electrode preparations.

The effect of water on the size of wave II. As noted in the previous chapter, CV's of the naphthoquinone vitamin K in ultra dry CH_2Cl_2 organic solvents have a chemically irreversible wave II, Figure 3.8. So far, the most general mechanisms to explain the unexpectedly small wave II are a radical dimer mechanism proposed by Macias-Ruvalcaba et al.[20] and a wedge scheme mechanism involving hydrogen bonding and proton transfer to the quinone radical anion from a phenolic group on the electrode surface proposed here. In the radical dimer mechanism, Scheme 3.2, it is proposed that the radical anion can dimerize and this dimer can be reduced by one electron slightly positive of the normal second reduction of the quinone. Since reduction of the dimer corresponds to 1 e^- per 2 quinones, this reduces the number of electrons transferred in the second wave resulting in a slightly smaller wave. In the proton transfer mechanism, we have suggested that phenol groups on the surface of the glassy carbon (GC) electrodes typically used for quinone voltammetric studies can hydrogen bond to the quinone radical anions, Scheme 3.3. Reduction of the H-bonded complex occurs at a potential positive of the normal second reduction and can lead to increased current between the waves and a decrease in the size of wave II. It is possible that both mechanisms are simultaneously operational, with the relative importance of each being weighted depending upon the identity and concentration of the quinone, the solvent and the condition of the GC electrode. It is, of course, also possible that neither mechanism is correct.

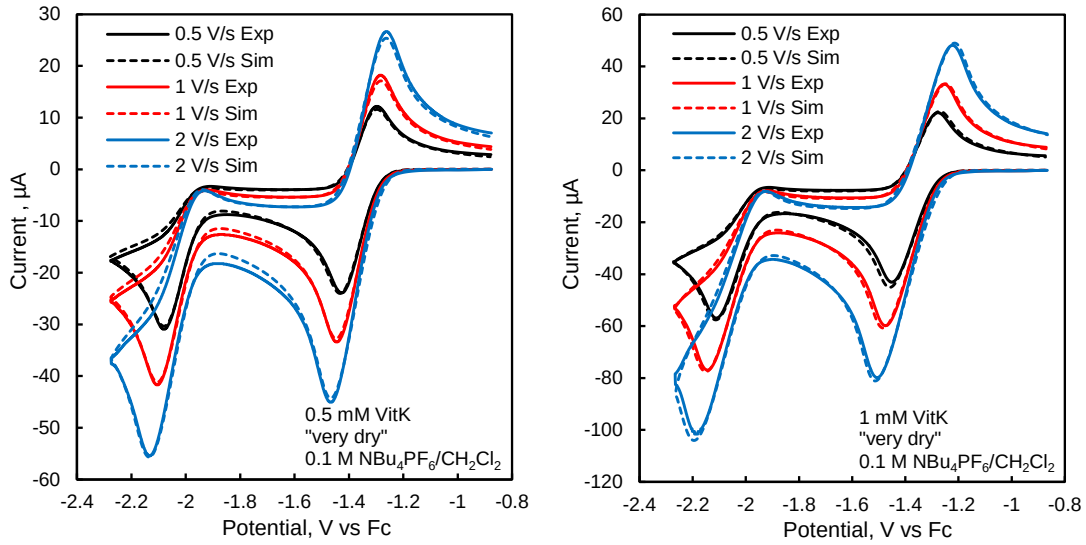

Figure 3.8. Background-subtracted experimental and simulated CVs of 0.5 mM (left) and1.0 mM (right) Vitamin K1 in "very dry" 0.1M NBu_4PF_6/CH_2Cl_2. Mechanism and parameters for the simulation are given in Table 3.1.

Table 3.1. Mechanism and Parameters used for Simulation in Figure 3.3 and Figure 3.8.[a]

Reaction	E° or K	k° or k_f	α	Species	D, cm^2/s
$Q + e = Q^-$	−1.351 V	0.050 cm/s	0.5	Q	1.59e−5
$Q^- + e = Q^{2-}$	−2.003 V	0.036 cm/s	0.5	Q^-	1.40e−5
$Q + Q^{2-} = 2\ Q^-$	1.05e11[b]	1.5e7 $M^{-1}s^{-1}$		Q^{2-}	1.40e−5
Q^{2-} = prod	6.55e10	34 s^{-1}		prod	1.00e−5

[a]Other parameters: Ru = 1350Ω, electrode area = $0.0706cm^2$.

[b]Thermodynamically redundant.

Given the above, another intriguing result from the water titration experiments starting from very dry CH_2Cl_2 that were discussed in Chapter 2 is that addition of a

small amount of water not only causes the peak potential of IIc to shift positive, it also reproducibly causes a decrease in peak current, Figure 2.5. The CV's shown in the Figures have been carefully background subtracted so this decrease is not due to a decrease in the background current at the slightly more positive potential. It is also observed with the other quinones that are reduced at different potentials, Figures 2.6 and 2.7. Along these lines, it is also interesting to note that the irreversible wave IIc observed in the absence of water is actually at the correct height for a full one electron reduction of the quinone radical anion, and, unlike the chemically reversible wave observed in the presence of excess water, Figure 3.2, can be nicely simulated by just using the irreversible SN_2 attack talked about in the previous chapter to modify the ideal mechanism of two electron transfer reactions. Good fits of the experimental CVs using the same mechanism and parameters are also found at different VitK concentrations and scan rates, Figure 3.8.

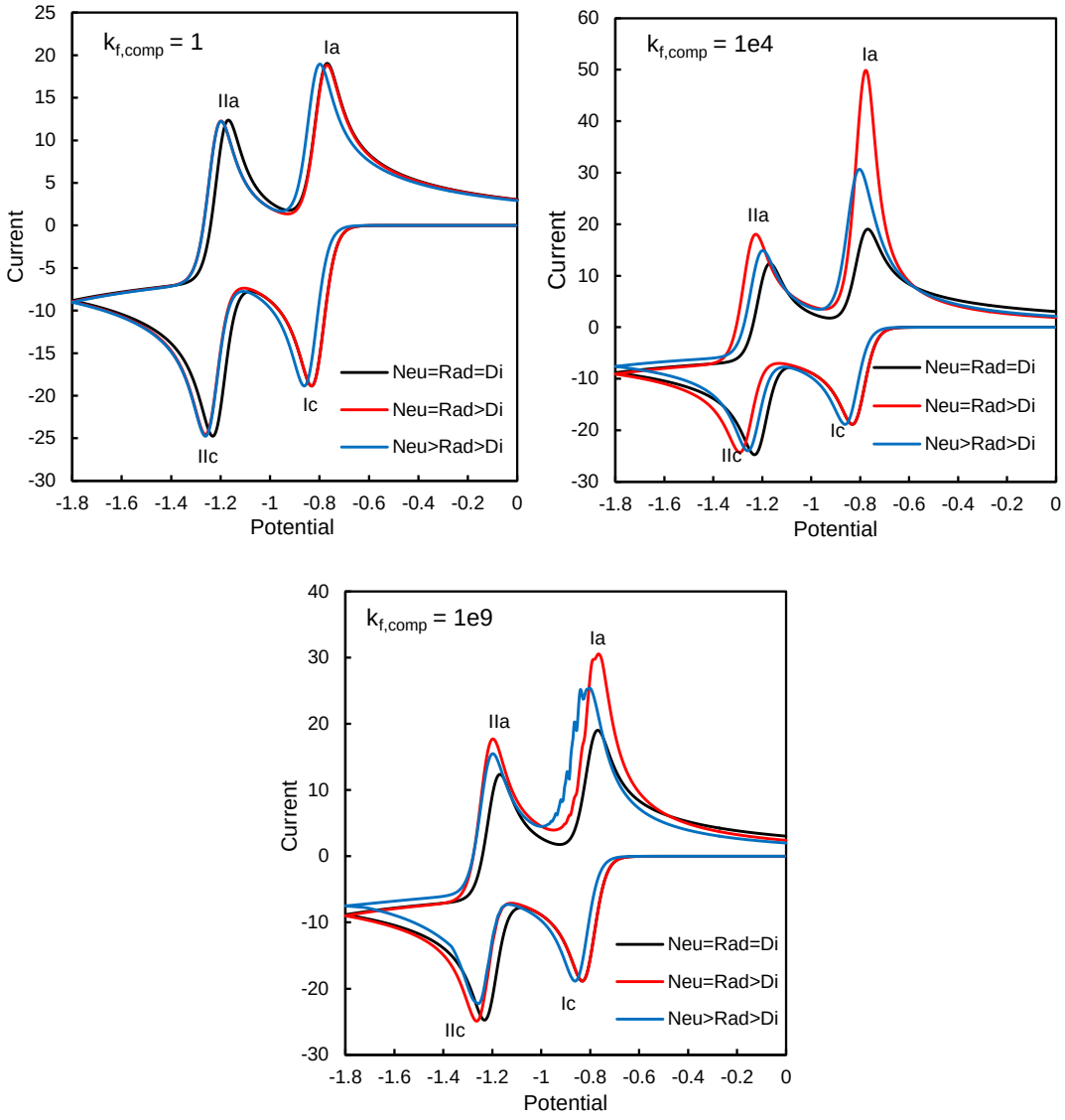

Figure 3.9. Simulated CVs (0.1 V/s) showing the effect of different diffusion coefficients with different k_f values for the comproportionation equilibria. The mechanism and parameters used are given in Table 3.2. Black: $D_{neu} = D_{rad} = D_{Di}$ = 1E−5 cm^2/s; Red: $D_{neu} = D_{rad}$ = 1E−5 cm^2/s, D_{Di} = 1E−6 cm^2/s; Blue: D_{neu} = 1E−5 cm^2/s, D_{rad} = 1E−6 cm^2/s, D_{Di} = 1E−7 cm^2/s.

Table 3.2. Mechanism and Parameters used for Simulations in Figure 3.9[a]

Reaction	E° or K	k° or k_f	α	Species	D, cm^2/s
neu + e = rad	−0.8 V	1e4 cm/s	0.5	Neu	1e−5
rad + e = di	−1.2 V	1e4 cm/s	0.5	Rad	varies
neu + di = 2 rad	5.76e6[b]	varies		Di	varies

[a]Other parameters: Ru = 135Ω, electrode area = 0.0706cm^2.

[b]Thermodynamically redundant.

The above observations indicate that there is no fundamental reason why the quinone radical anion cannot be reduced by a full one electron per quinone. They also hint that the explanation (or explanations) for the too small second wave involves water. One obvious effect that water could have would be to reduce the diffusion coefficients for the quinone dianion and to a lesser extent the radical anion, since strong hydrogen bonding between water molecules and the quinones in their reduced states will effectively increase their size. For electron transfer only, the different diffusion coefficients would not affect the voltammograms, however, if the comproportionation reaction in Scheme 3.2 was fast they could have an effect. This was explored using computer simulations by making very large changes (factor of 10) in the diffusion coefficients and noting the effect on the peak currents with different rates for the comproportionation step. These results are shown in Figure 3.9. With a slow comproportionation reaction there is no effect on the peak currents as expected, but with a fairly fast comproportionation there is an effect. However, the main effect, an increase in the height of the return peaks, is not what is observed experimentally.

While changing the diffusion coefficient of the quinone dianion would not be sufficient to explain the deviations from ideal behavior observed with quinones, there are other ways that H-bonding by water could have an effect. In the case of the two mechanisms discussed above, it is easy to see how the presence of water could facilitate both pathways. In the case of the radical anion dimerization, H-bonding of water could help hold together the dimer as well as ameliorate the electrostatic repulsion between radical anions. In the case of the surface phenol mechanism, water molecules hydrogen bonded to the surface phenols might facilitate proton transfer between phenol and radical anion on the forward scan, and between the phenolate and the monoprotonated hydroquinone on the return scan.

Conclusion

Oxygenated groups on the surface of glassy carbon electrodes can undergo proton transfer with electrogenerated species in solution. Unmanaged proton transfer from surface phenolic groups is a major contributor to the non-ideal character of para-quinone CV's. Concentration dependence studies at room temperature show that in polar, aprotic solvent para-quinone pi dimers are the exception rather than the rule, an idea that is reinforced by CV's comparing para-quinones with different amounts of steric hindrance. CV's of DQ with naphthol titrated in show that wave III, the wave that grows in at lower quinone concentrations, is at the right potential to be due to a PCET reaction involving phenols on the electrode surface. CV's in which the electrode has been oxidized or reduced in order to perturb the coverage of surface

oxygenated groups does definitely perturb wave III in the quinone CV's. Oxygenated groups affect para-quinone CV's through uncontrolled side reactions which need to be accounted for during analytical work.

REFERENCES

1. Astudillo, P. D.; Valencia, D. P.; Gonzàlez-Fuentes, M. A.; Dìaz-Sànchez, B. R.; Frontana, C.; and Gonzàlez, F. J. *Electrochim. Acta* **2012**, *81*, 197-204.

2. A. Guttler, T. Z., and J. Kuppers *Carbon* **2004**, *42*, 337-343.

3. Caesar Barbero, J. J. S., and Leonides Sereno *J. Electroanal. Chem.* **1988**, *248*, 321-340.

4. Chen, P.; Fryling, M. A.; McCreery, R. L. *Anal. Chem.* **1995**, *67*, 3115-3122.

5. Chen, P.; McCreery, R. L. *Anal. Chem.* **1996**, *68*, 3958-3965.

6. Dieker, W. E. v. d. L. a. J. W. *Anal. Chim. Acta.* **1980**, *119*, 1-24.

7. Du Pan, S. Y., Wu Ping, Lu Tianhong, and Cai Chenxin *Chin. J. Anal. Chem.* **2006**, *34*, 1688-1692.

8. DuVall, S. H.; McCreery, R. L. *Anal. Chem.* **1999**, *71*, 4594-4602.

9. DuVall, S. H.; McCreery, R. L. *J. Am. Chem. Soc.* **2000**, *122*, 6759-6764.

10. Esposti, M. D. *Biochim. Biophyl. Acta, Bioenerg.* **1998**, *1364*, 222-235.

11. Fleischer, N. A.; Office, U. S. P., Ed.; E.C.R.-Electro-Chemical Research Ltd.: Israel, 1996.

12. Gregory Pognon, T. B., Laurent Demarconnay, and Daniel Belanger *J. Power Sources* **2011**, *196*, 4117-4122.

13. Gupta, N.; Linschitz, H. *J. Am. Chem. Soc.* **1997**, *119*, 6384-6391.

14. Hong Liu, R. R., and Bruce E. Logan *Environ. Sci. Technol.* **2004**, *38*, 2281-2285.

15. Hui, Y.; Chng, E. L. K.; Chua, L. P.-L.; Liu, W. Z.; Webster, R. D. *Anal. Chem.*, **2010**, *82*, 1928-1934.

16. Joseph A. Letizia, S. C., Rocio Ponce Ortiz, Antonio Facchetti, Mark A. Ratner, and Tobin J. Marks *Chem. Eur. J.*, **2010**, *16*, 1911-1928.

17. Ken Nakai, Y. T., and Tsutomu Tsuchiya *Carbohydr. Res.* **1999**, *316*, 47-57.

18. Kuo, T.-C.; McCreery, R. L. *Anal. Chem.* **1999**, *71*, 1553-1560.

19. Macìas-Ruvalcaba, N. A.; Felton, G.A.N.; Evans, D. H. *J. Phys. Chem. C* **2009**, *111*, 338-345.

20. Macìas-Ruvalcabe, N.A.; Evans, D.H. *J. Phys. Chem. C* **2010**, *114*, 1285-1292.

21. Masashi Mamada, D. K., Jun-ichi Nishida, Shizuo Tokito, and Yoshiro Yamashita *ACS Appl. Mater. Interfaces* **2010**, *2*, 1303-1307.

22. McCreery, R. L. *Anal. Chem.* **2006**, *78*, 3490-3497.

23. McCreery, R. L. *Chem. Rev.* **2008**, *108*, 2646-2687.

24. Oana D. Jurchesco, M. P., Bart J. van Wees, and Thomas T. M. Palstra, *Adv. Mater.*, **2007**, *19*, 688-692.

25. Quan, M.; Sanchez, D.; Wasylkiw, M. F.; Smith, D. K. *J. Am. Chem. Soc.* **2007**, *129*, 12847-12856.

26. Ray, K.; McCreery, R. L. *Anal. Chem.* **1997**, *69*, 4680-4687.

27. Renè, A.; Evans, D. H. *J. Phys. Chem. C*, **2012**, *116*, 14454-14460.

28. Runnels, P. L.; Joseph, J. D.; Logman, M. J.; and Wightman, R. M. *Anal. Chem.* **1999**, *71*, 2782-2789.

29. Segal, A. R. C. a. A. W. *Biochim. Biophyl. Acta, Bioenerg.* **2004**, *1657*, 1-22.

30. Shearer, M. J. *Lancet* **1995**, *345*, 229-234.

31. Singer, A. P. a. M. *Critical Care* **2006**, *10*, 228-234.

32. Wang, S.; Singh, P. S.; Evans, D. H. *J. Phys. Chem. C* **2009**, *113*, 16686-16693.

33. Yanlan Hui, E. L. K. C., Cheryl Yi Lin Chng, Hwee Ling Poh, and Richard D. Webster *J. Am. Chem. Soc.* **2009**, *131*, 1523-1534.

34. Kottke, M. P. and Pullman, D. *Molec. Phys.* **2012**, *110*, 1953-1966.

35. Meunier, L; Seyewetz, A; and Haller, M. A. *Compt. Rend.* **1908**, *146*, 987-989.

36. Dowd, P.; Hershline, R.; Ham, S. W.; and Naganathan, S. *Science* **1995**, *269*, *5231*, 1684-1691.

Chapter 4. Duroquinone and 2-Naphthol: An Example of a Wedge Scheme Redox System

Abstract

Generalized reaction schemes can serve as powerful organizing tools that can be applied to many different chemical systems. The duroquinone (DQ) and 2-naphthol (NaphOH) system is presented as one that necessitates a 3-dimensional wedge scheme which includes e-transfer, H^+-transfer, and H-bonding reactions in order to explain its electrochemistry. Systems with DQ and the guests methanol and trifluoroacetic acid are presented as contrasting systems where either H^+-transfer or H-bonding with the guest may be ignored, respectively, and the CV's are shown to be qualitatively different from those of the DQ and NaphOH system. Literature pK_a values and DFT calculations to show that H^+-transfer must occur during the redox processes of the DQ and NaphOH system. The similarities between simulations of DQ and NaphOH CV's and experimental CV's are presented to show that the H^+-transfer must occur in a H-bonded complex between the DQ and the NaphOH. Finally, experimental CV's of the system are compared with simulations of different wedge schemes with the best fitting scheme having a slow-forming acid that is composed of 2 NaphOH molecules H-bonded together which takes advantage of the stability of the naphthol-naphthalate ($NaphO^-$--HONaph) H-bonded complex.

Introduction

The interface between proton transfer (H^+-transfer) reactions and electron transfer (e-transfer) reactions has been a popular area of research for several decades[1-9] and is particularly important in the field of artificial photosynthesis.[10-12] The interface between hydrogen bonded (H-bond) complexes and e-transfer reactions is a popular area of research for drug delivery,[13] materials design,[14] fundamental biology,[15, 16] and fundamental chemistry[17-20] and is related to the H^+-transfer e-transfer reactions.[21-23] Either set could be combined into "square" schemes wherein e-transfer reactions are placed along one cartesian axis and the H^+-transfer or H-bonding reactions are placed along the other—as shown in schemes 1 and 2—so that by changing the concentrations or identities of the chemical species, it is possible to explore different paths through the scheme.

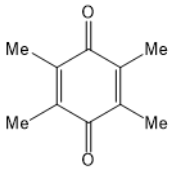

Duroquinone (DQ)

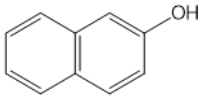

2-Naphthol (NaphOH)

Chart 4.1. Electroactive host and guest molecule used in this study in addition to the guests methanol (MeOH) and trifluoroacetic acid (CF_3COOH).

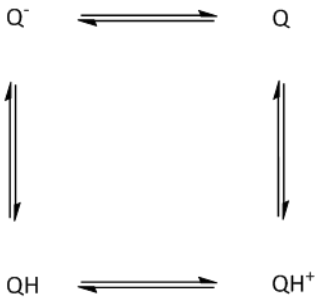

Scheme 4.1. H^+-transfer and e-transfer square scheme with one quinone (Q) and one proton.

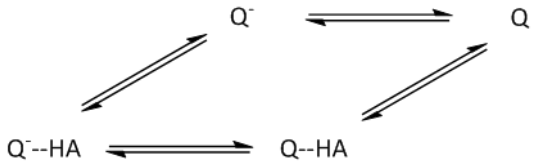

Scheme 4.2. H-bond and e-transfer square scheme with one quinone and one guest (HA).

Our group has combined these processes in the past[24, 25] with urea derivatives that contain both the electron donating and proton donating sides of the H-bonding complexes and the acids and bases in the H^+-transfer reactions. The combining of all three of these reaction types was referred to as a "cube" scheme and was then simplified to the "wedge" scheme by removing H^+-transfer reactions within the H-bond complex from the simulation and combining the thermodynamics of the e-transfer reaction pathways involving the H-bond complex so that it goes from the most stable protonation state on the oxidized side to the most stable protonation state on the reduced side, and vice versa, in one kinetic step. Our justification for simplifying the

cube scheme into the wedge scheme is that the e-transfer reaction is much slower than the H^+-transfer within the H-bond complex because the electron is transferring between the complex and the electrode, so it must tunnel through one or more layers of solvent molecules in order to reach its destination. The fact that the previous papers used electroactive ureas may give the false appearance that a three-dimensional reaction scheme is only necessary to describe electroactive molecules that can perform all three types of reactions through self-association. In the current chapter, it is shown that this is not the case and the system duroquinone (DQ) and 2-naphthol (NaphOH), chart 4.1, is presented as an example that requires both H^+-transfer and H-bond reactions to be considered in addition to e-transfer reactions in order to accurately describe the system's reactivity; examples of simple cube and wedge schemes for this are shown in schemes 3 and 4.

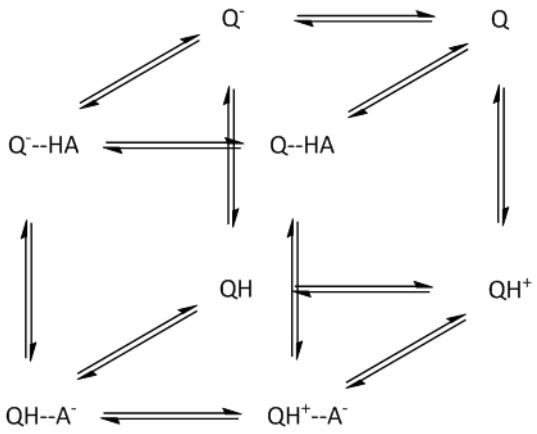

Scheme 4.3. Cube scheme with H^+-transfer, H-bonding, and e-transfer reactions together.

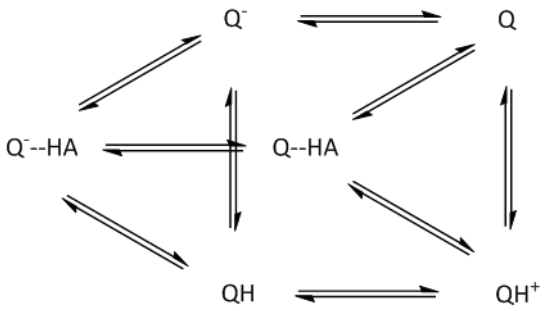

Scheme 4.4. Wedge scheme from removing the H^+-transfer within the H-bonding complex (front-most square on the cube).

Quinones have been the most common organic redox systems used throughout electrochemistry to test electrode materials[26, 27] and solvents[28-30] because they go through multiple, reversible redox reactions. Some of the most important steps in metabolism and photosynthesis use quinones to carry electrons from place to place, and these often use H-bonds to pre-bind the quinones in order to prepare for them to accept the electrons; because these H-bonds are often with phenolic functional groups,[31] having an accurate mechanism for the reduction and oxidation of quinones in the presence of phenols is a useful tool in its own right.

This chapter will show that the DQ NaphOH system undergoes H-bonding reactions and H^+-transfer reactions which affect the e-transfer reactions that it also undergoes. It will show that these occur in ways that are not explainable with square schemes that neglect either H-bonding or H^+-transfer. It will also show that the pure H^+-transfer square scheme is inaccurate even with the much more acidic trifluoro acetic acid (CF_3COOH) due to the existence of the quinhydrone complex and its associated wedge scheme. Further, it will show that a simple wedge scheme gives

much more accurate CV's than any of the square schemes, even those that allow H-bonding only in self association reactions to form a quinhydrone-like complex. Comparing different wedge schemes leads to the conclusion that in organic solvents the H-bonding complex between two NaphOH molecules and some water molecules is strong enough to measurably decrease the NaphOH's pK_a, which means that even in the pure H-bonding schemes, there may be some H^+-transfer reactions occurring. This last correction to the wedge scheme gives the most accurate simulations for this system yet.

Experimental

Chemicals. Duroquinone (DQ) and 2-naphthol (NaphOH) were obtained from Fisher Scientific and purified before use with sublimation. Tetrabutylammonium hexafluorophosphate was obtained from Fisher Scientific and purified by recrystallization three times from 95% ethanol in water followed by drying overnight in a vacuum oven at ~1 torr and 100 °C.

Acetonitrile was dried using the method of Grzeskowiak et al.[32] where the acetonitrile was refluxed with P_2O_5 and then fractionally distilled into a flame dried round bottom flask. This method has previously been used to dry acetonitrile to a water concentration of less than 1E-2 mM.

Cyclic Voltammograms. Cyclic voltammograms (CV's) were performed inside a dry box with a nitrogen atmosphere using a CHI 760C potentiostat/galvanostat with a 3 electrode setup. CV's were performed using a Pt wire

counter electrode, and a glassy carbon working electrode (3 mm diameter disk). The working electrode was cleaned in advance by manual polishing with 0.25 μm diamond paste and 0.05 μm alumina paste, followed by rinsing with water, then acetone, then soaking in iso-propanol with activated carbon for 15 min, followed by rinsing with water, then iso-propanol, then acetone again.

The water or deuterium oxide concentration was set by adding the appropriate amount of 18 MΩ H_2O or as-received D_2O. The concentration was set to 40 mM H_2O or 40 mM D_2O so that the 2-naphthol could be deuterated just through exchange with the D_2O in the water for a D/H ratio of 80/1 to allow kinetic isotope effect (KIE) measurements to be performed. DQ and NaphOH were added by adding known quantities of a dry stock electrolyte solution of ~0.02 M DQ or NaphOH via microliter syringe. Titrations of MeOH and CF_3COOH were performed through microliter syringe additions from the neat liquid.

A Ag wire quasi-reference electrode was used in situ and the system was re-referenced to ferrocene at the end of the experiment. Once in the electrolyte solution, the working electrode was cycled through the potential window a minimum of 2000 times at a scan rate of 20 V/s in order to ensure a reproducible background. The background was confirmed to be reproducible by comparing two scans at 0.1 V/s taken before and after 100 cycles at 20 V/s through the potential window. Any background water was added to the solution prior to the cycling to ensure that the presence of water also did not change the background through, for example, H-bonding to protic surface groups or groups with lone electron pairs.

Density Functional Theory Calculations. Density functional theory (DFT) calculations were performed using the rbdft method with the pVDZ basis functions. Gibbs free energy values were obtained through gas phase frequency calculations after optimization. The counterpoise correction was used to remove cross properties for frequency calculations involving two or more molecules. Except in calculations with the DQ radical anion, spin states were restricted.

Digital Simulations. Digital simulations of the CV's were performed with DigiSim 3.03 by BASi. Simulations with DQ were performed by fitting the two starting waves starting with the experimental $E_{1/2}$ values, then going to the rate constant, then iterating these two more times. Gibbs free energy predictions from the DFT calculations were used as starting points for the H-bond and H^+-transfer reactions. The values were then adjusted manually to arrive at simulated CV's that resembled the experimental CV's. Fittings for the total reaction were not performed due to interference from phenolic hydrogens on the glassy carbon surface as discussed in chapter 3,[33, 34] which the simulation software is unable to address. For quantitative purposes, these simulations should be considered only accurate to within at most 2 orders of magnitude.

Simulations for the H^+-transfer square scheme were performed by manually adjusting the H^+-transfer kinetic and thermodynamic coefficients to get the best fit to the data from the experiments where DQ:NaphOH = 1:0.5, while the redox potentials were fixed using either the experimentally determined potentials for DQ or the literature values for hydroduroquinone. Simulations for the H-bonded square scheme

were performed by fixing the redox potentials for DQ in the same way as above, assigning redox peaks to specific H-bond complexes, and then adjusting the kinetic and thermodynamic coefficients for the dimerization reactions to get the best fit for DQ:NaphOH = 1:0.5. H-bonded complexes were assigned in order of increasingly positive redox potential: $(NaphOH)DQ^{-}/(NaphOH)DQ^{2-}$, $(NaphOH)_2DQ^{-}/(NaphOH)_2DQ^{2-}$, $(NaphOH)DQ/(NaphOH)DQ^{-}$, $(NaphOH)_2DQ/(NaphOH)_2DQ^{-}$. Unless otherwise noted, the simulation parameters are given in the appendix.

Kinetic Isotope Effect. The kinetic isotope effect (KIE) was performed through the Nicholson method. Calculations were performed by comparing the peak to peak separation of a redox wave after correcting for IR drop by subtracting from the peak potential the product of the peak current in the raw data and the resistance of the solution. The resistance of the solution, 350 Ω, was determined by fitting CV's of only the first DQ redox wave. The corrected peak potentials are then subtracted from the $E_{1/2}$ value of the wave in order to get the difference (ΔE) and that is plugged into equation 4.2, along with the value of the diffusion coefficient (D^0) from fitted simulations, the temperature (T = 294.15K), the rate constant (ψ, which had to be determined by interpolation into the values of previously determined ψ vs ΔE table[35]), the value of the scan rate (ν = 0.1V/s, 0.5 V/s, 1.0 V/s, 2.0 V/s depending upon the specific scan), and the values from all the other constants (α = 0.5 because the oxidation and reduction peaks are equal in height; R = 8.31 J/molK; F = 96485 C/mol e^{-}), and the resulting heterogenous rate constants (k^0) for each CV scan were found.

The KIE is found by dividing the value from one scan with added H_2O by one with added D_2O, then the values from three different experiments at each scan rate are averaged together and the standard deviation is calculated and reported. Finding the kinetic parameters by fitting simulations would be convenient, but they are so close—and the redox peaks are so broad—that the fitting algorithm does not change anything when the value from the H_2O added experiments are used for the D_2O added experiments or vice versa.

$$\boldsymbol{\psi} = \frac{(\frac{\boldsymbol{D_O}}{\boldsymbol{D_R}})^{\alpha/2}\boldsymbol{k^0}}{(\boldsymbol{\pi D_O f \nu})^{1/2}}$$

Equation 4.1. Relationship between the dimensionless rate constant (ψ), the diffusion coefficients of the oxidized and reduced species (D_O and D_R), and the heterogenous rate constant (k^0).[35]

$$\boldsymbol{k^0} = \frac{(\boldsymbol{\pi D_O}\frac{\boldsymbol{F}}{\boldsymbol{RT}}\boldsymbol{\nu})^{1/2}\boldsymbol{\psi}}{(\frac{\boldsymbol{D_O}}{\boldsymbol{D_R}})^{\alpha/2}}$$

Equation 4.2. Same relationship as in equation 4.1, but rearranged to find k^0.

Results and Discussion

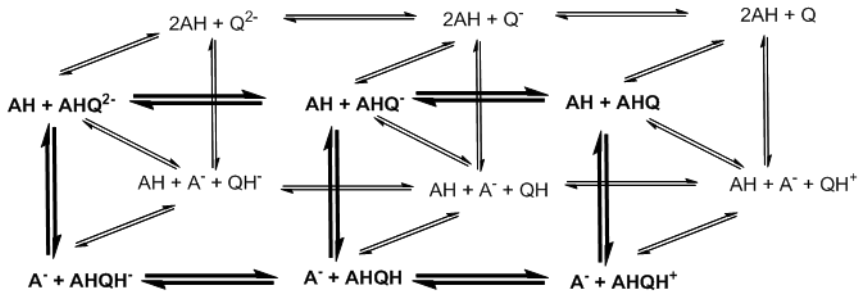

Scheme 4.5. A portion of the cube scheme for a quinone Q in the presence of a weak acid. Quinones can, in principle, have 3 oxidation states, 3 protonation states, and 7 H-bonded states.

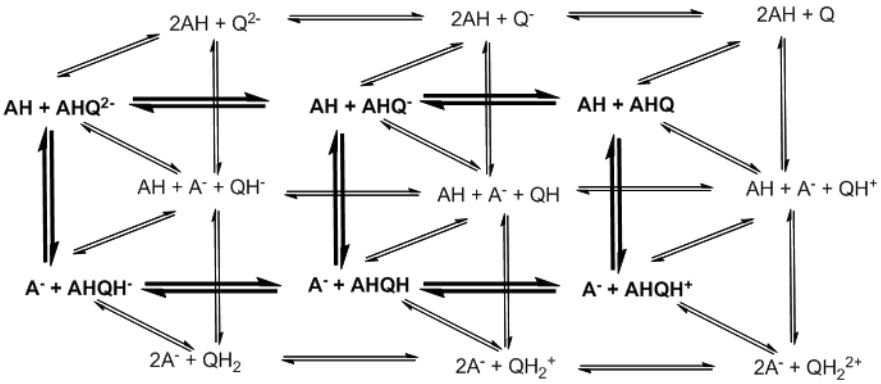

Scheme 4.6. The wedge scheme for arbitrary quinone with 3 oxidation states, 3 protonation states, and 2 H-bonded states.

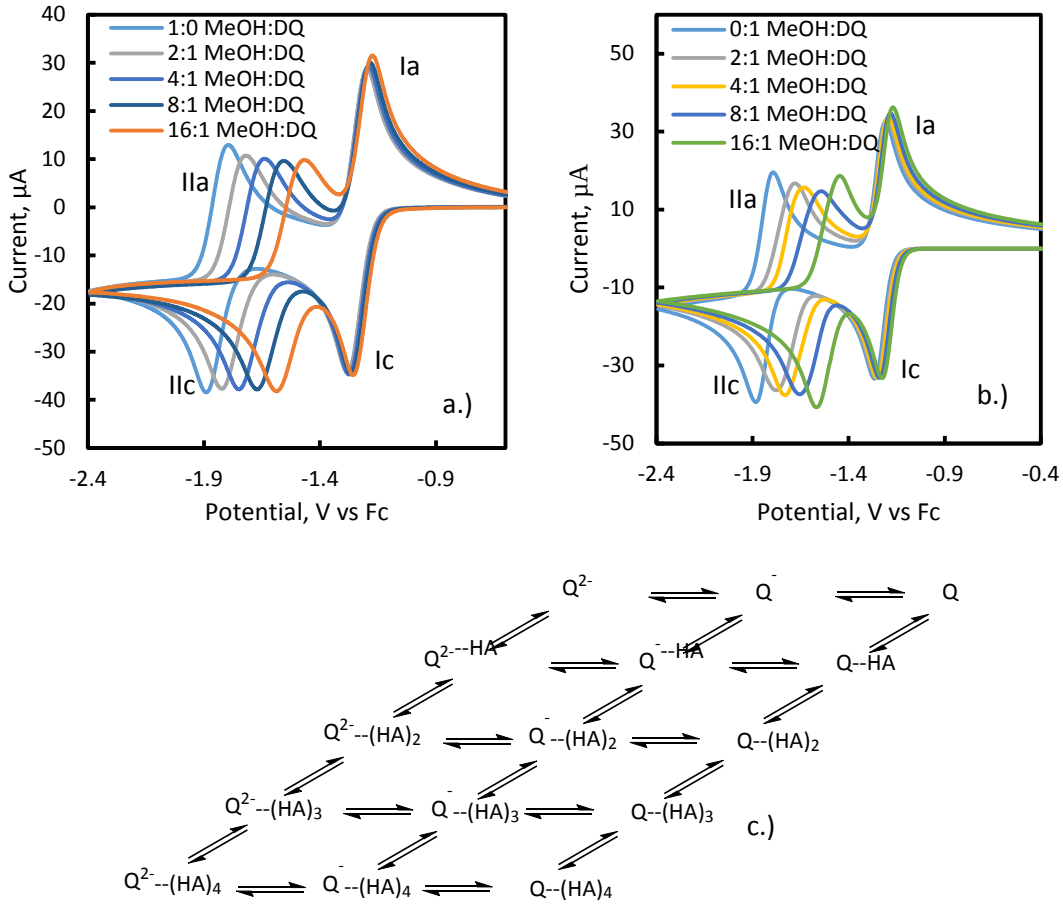

Figure 4.1. DQ in the presence of MeOH (a.) overlaid background-subtracted, experimental CV's taken at 0.5 V/s in MeCN with 0.001 M DQ and 0.1 M NBu_4PF_6, (b.) simulated CV's of the system, and (c.) scheme used for this simulation. The simulation parameters can be found in the appendix in table A.1.

Wedge scheme vs Square Schemes. Why Use Such Small Concentration Range. Since the square scheme is the basis of the wedge scheme, it is useful to examine in more detail two square schemes—H-bonding with e-transfer using DQ and

MeOH, and H^+-transfer with e-transfer using DQ and CF_3COOH—so that it is possible to make comparisons between their features and the features of the presumed wedge scheme in the DQ and NaphOH system. First there is figure 4.1a, which shows overlaid experimental CV's from a DQ solution into which MeOH was titrated. Very little changes with the addition of one equivalent of MeOH, but as the MeOH concentration increases wave II shifts positive gradually, with wave I shifting positive much less. The simulated CV's of this system—which are in figure 4.1b and use the scheme shown in figure 4.1c—show the same trend. The reason why the waves shift at all is because MeOH is donating the H to the H-bond, which can be thought of as adding a partial positive charge to the DQ, thus stabilizing the DQ^{-} relative to the DQ, and stabilizing the DQ^{2-} relative to the DQ^{-}. The reason why they only move slightly with each additional MeOH is that the Me group is a good electron donor to the OH group, which means that the H-bond only donates a very small partial positive charge to the DQ, which also makes the H-bond very weak in all three oxidation states. The reason why wave II moves more than wave I is that the electron-electron repulsion in the highest orbital of DQ2- pushes the energy level of the valence electrons much higher than in DQ-, thus making them much better at donating to a H-bond.

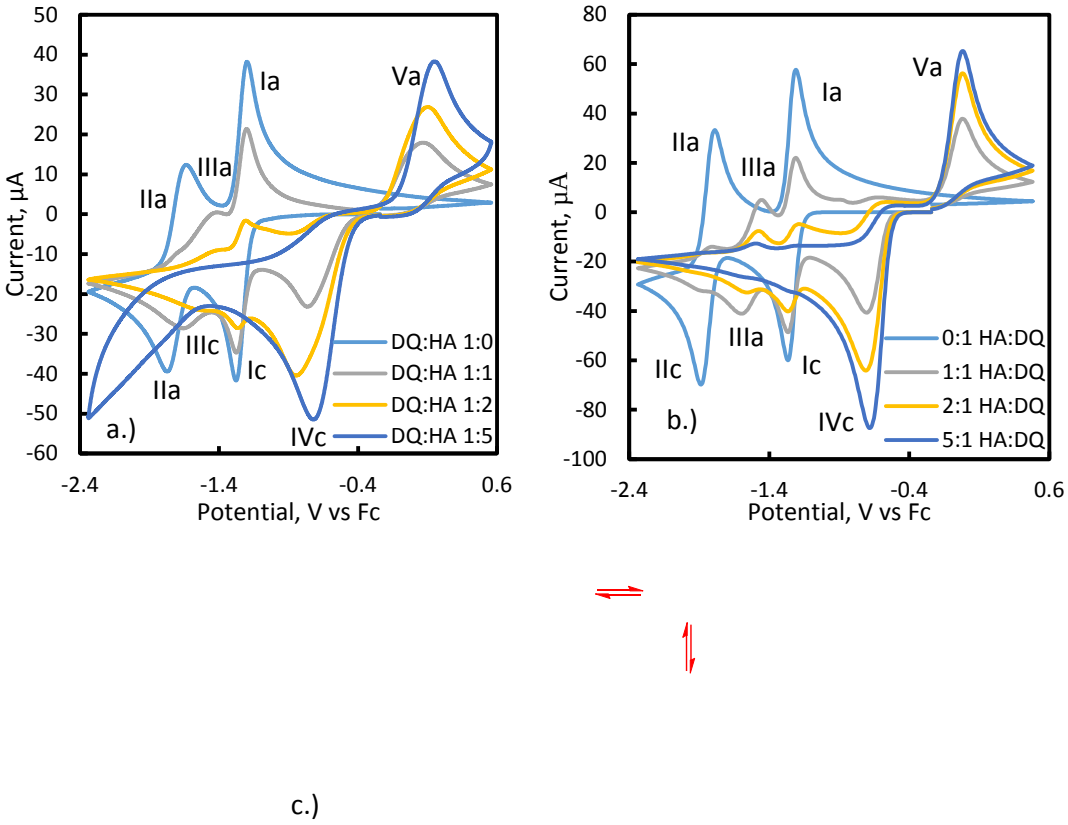

Figure 4.2. DQ in the presence of CF_3COOH (a.) overlaid background-subtracted experimental CV's at 0.5 V/s in MeCN with 0.001 M DQ and 0.1 M NBu_4PF_6, (b.) simulated CV's of the system, and (c.) scheme used for this simulation. The parameters can be found in the appendix in table A.2.

In figure 4.2a, there are experimental CV's of DQ in the presence of different concentrations of CF_3COOH, while in figure 4.2b there are simulations of this system that are based upon the mechanism in figure 4.2c. When CF_3COOH is added, there is an immediate disappearance of wave II, decrease in wave I, and two new waves appear labelled wave III and the irreversible wave with peaks labelled IVc and Va;

with increasing CF_3COOH concentration wave I eventually disappears altogether and so does wave III, leaving just peaks IVc and Va. Since the simulation shown in figure 4.2b and using the mechanism in 4.2c shows excellent qualitative agreement with the experiment, 4.2c can be used as a guide to see what is going on; although, wave III has enough complications according to this scheme that it shall be discussed on its own in the next paragraph. In every case, the electrochemical system starts out in the top right corner with DQ, and with no added CF_3COOH it stays along the top of the scheme, having two redox waves with nothing special. Because peak IVc is significantly positive of wave I, it can be said that adding CF_3COOH transfers H^+ to DQ, going directly down in the scheme, and that IVc is the result of the reduction of DQH^+, which takes the system left in the scheme to DQH. Due to electron donation to the carbonyl from the hydroxyl group, DQH is more basic than DQ, which means that once it is formed it will undergo H^+-transfer from CF_3COOH, taking the system down in the scheme again, and causing another potential inversion which results in e-transfer from the electrode, resulting in DQH_2. From here, it is necessary to talk about different paths through the scheme that occur simultaneously. If all of the CF_3COOH is used up protonating DQ during peak IVc, then the rest of the quinone will go through the regular path from DQ to DQ^-, thus giving us a smaller, but still present, wave I.

When quinones such as DQ and hydroquinones such as DQH_2 are present in the same solution some fraction of them will form dimers, tetramers, or higher order aggrigates that are held to gether by a combination of H-bonding between the OH groups of the hydroquinone and the CO groups of the quinone, and charge transfer

between the six-carbon rings at the core of the molecules.[36] When present as dimers, these are known as “quinhydrone” complexes. Formation of the quinhydrone complex—represented here as DQH_2DQ^x, where x is the net charge of the complex—is often favored by the presence of water, which adds the hydrophobicity of the six-carbon core as a factor in the complex’s formation. While formation of this complex is not as favorable in MeCN as it is in water, it does still happen, and once some quinone has reached DQ^- in the scheme shown in figure 4.2c, it becomes basic enough for the formation of the quinhydrone complex to be very favorable, meaning that—if DQH_2 is present as a product of peak IVc due to the presence of CF_3COOH at the start of the scan—the DQ^- moves diagonally to form DQH_2DQ^-. If the proportion of DQ to CF_3COOH is 1:1 at the start of the scan then by the time the scan is negative of wave I half of the quinone molecules near the electrode will be present as DQH_2 and the other half will be present as DQ^-, meaning that all or nearly all of the quinone will form DQH_2DQ^- if the dimerization constant is very favorable, which is is in the case of the simulations shown in figure 4.2b. Going directly left through the scheme, this is followed by e-transfer to the DQH_2DQ^- to form DQH_2DQ^{2-}, which happens in peak IIIc. Since both waves III and I are reversible, the system moves from DQH_2DQ^{2-} directly right to DQH_2DQ^- at peak IIIa, then diagonally up to DQ^- and at the potential of Ia, goes directly right to its starting point at DQ. The idea of a wave at the potential of III being due to a second e-transfer to a quinhydrone complex was first proposed by Gamboa-Valero et al.[36] who formed it in MeCN intentionally by mixing teogethere equal amounts of benzoquinone and benzohydroquinone just so they could measure its

redox potential. The only remaining peak is Va, which is positive of IVc, making it likely that this is the first oxidation of DQH_2 to DQH_2^+, with a possible overlapping e-transfer from DQH_2DQ to DQH_2DQ^+.

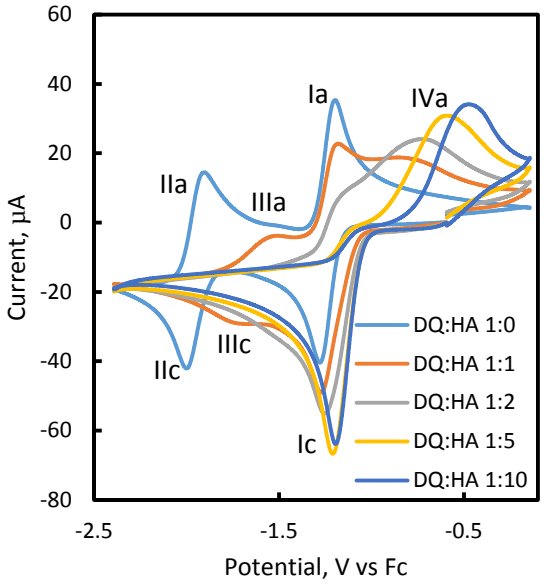

Figure 4.3. Overlaid background-substracted experimental CV's of 0.001 M DQ in the presence of increasing amounts of NaphOH in MeCN with 0.1M NBu_4PF_6 taken at 0.5 V/s.

Figure 4.3 displays overlayed CV's from an experiment wherein NaphOH was titrated into a DQ solution. With no NaphOH added, the DQ has its normal two redox waves that are close to ideal, and at high concentrations of NaphOH the two reversible redox waves have become one irreversible redox wave, peaks Ic/IVa, which is taken to indicate a H^+-transfer reaction just as when this was seen in figure 4.2. At a 1:1 ratio

the second wave has shifted significantly positive while remaining distinct from the first wave and remaining reversible. This is a behavior often seen with H-bonding systems such as figure 4.1, although the new oxidation peak that is positive of all of the pure DQ waves and that will grow into the oxidation side of the irreversible wave at high NaphOH concentrations indicates that H^+-transfer is still occurring at these lower concentrations. Before trying to fit this system with simulations, it is prudent to simplify the problem: since the full wedge scheme includes 5 H-bonded states for DQ, 6 for DQ^-, 7 for DQ^{2-}, and 3 protonation states for each, there are 54 different states that the quinone can be in, with all of the associated reactions going between the states. If the concentration of NaphOH is restricted to a maximum of 1.1 equivalents, then it is possible to restrict the H-bond states to 2 per quinone and the protonation states to just 2 for each oxidation state, which gives 12 states total, a much smaller theoretical space which is still adequate to tell the difference between wedge and square scheme mechanisms.

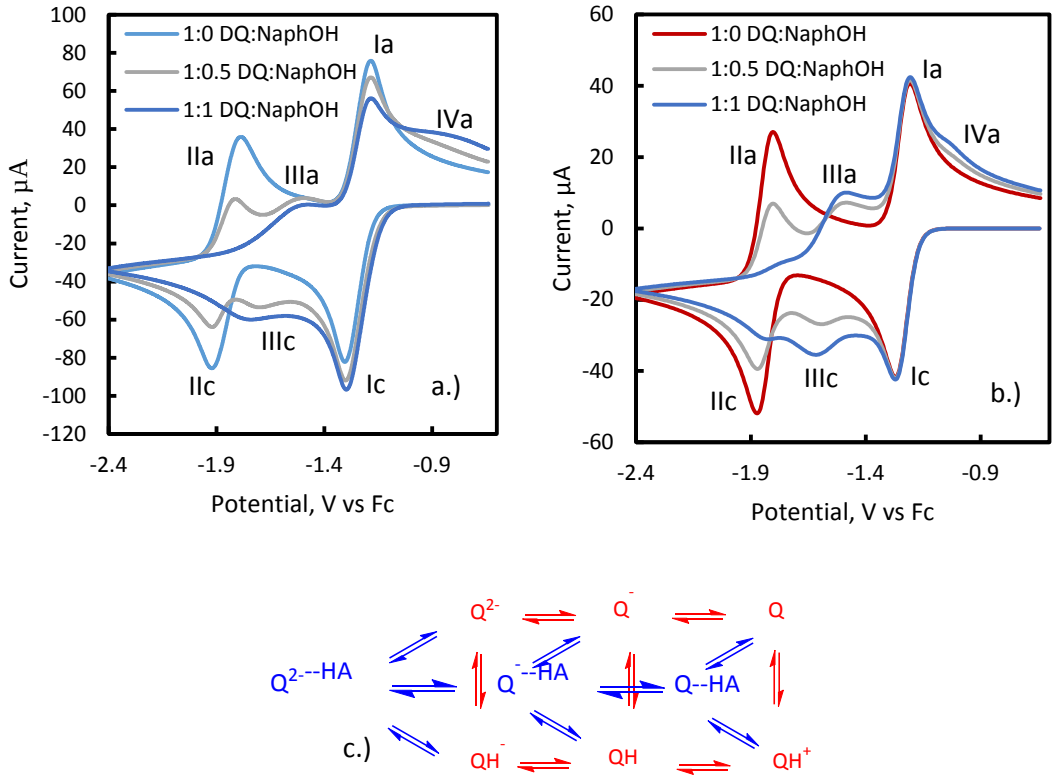

Figure 4.4. DQ in the presence of NaphOH (a.) overlaid background-subtracted experimental CV's at 0.5 V/s in MeCN with 0.001 M DQ and 0.1 M NBu_4PF_6, (b.) simulated CV's of the system, and (c.) scheme used for this simulation. The simulation parameters can be found in the appendix in table A.3.

Experimental CV's of DQ in the presence of 0 through 1.1 mM NaphOH are displayed in figure 4.4a, next to simulations which involve a wedge scheme with the H-bond complex between DQ and NaphOH in figure 4.4b, with the associated mechanism in figure 4.4c. With the addition of any NaphOH, wave II, which is a normal 2nd redox wave for quinones, decreases and wave III, which is proposed to be the H-bond complex between DQ and either one or two NaphOH molecules—appears

and then increases in current. Another oxidation peak, peak IVa, appears with the inclusion of any NaphOH and increases with addition of more NaphOH. The simulated wedge scheme, which assumes wave III is due to the reduction of a 1:1 DQ^{-}-NaphOH H-bond complex comes close to matching the experimental CV's in that wave II decreases in both cases, wave III appears and grows in both cases, and peak IVa also appears and then grows. The fact that wave II disappears in the experimental data at 0.8 equivalents of NaphOH rather than at 1.0 equivalents could be due to phenolic groups on the surface of the electrode which have been reported previously.[34] One of the things that the simulated CV's definitely do not get correct is that in the experimental data, as the concentration of NaphOH increases, the reduction side of wave I increases and the oxidation side decreases, whereas in the simulated CV's the reduction side remains constant.

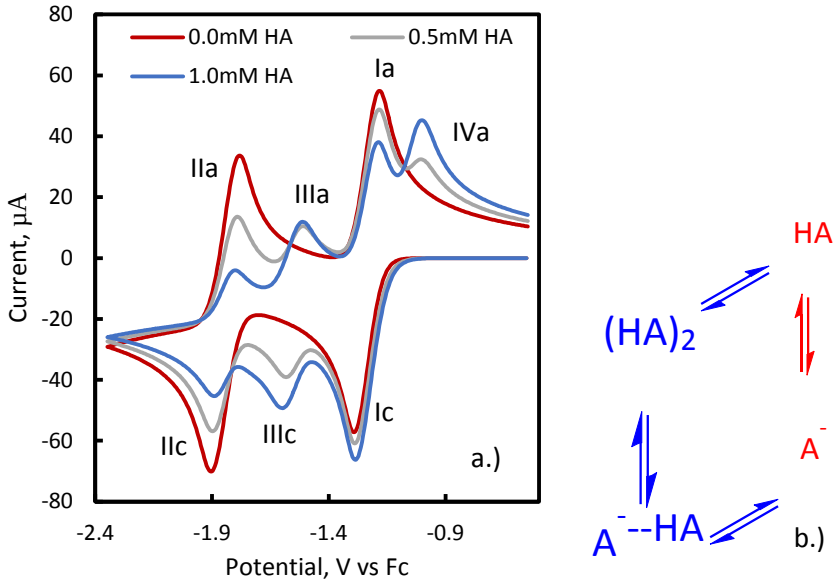

Figure 4.5. (a.) Simulations of the DQ and NaphOH system that includes (b.) an extra square scheme in which NaphOH molecules increase their acidity by H-bonding to each other. The simulation parameters can be found in the appendix in table A.5.

Modifying the wedge scheme slightly in figure 4.5a by pointing out that in MeCN there will be some concentration of a NaphOH-NaphOH H-bond complex, and that the NaphOH-NaphO$^-$ H-bond complex would be much more stable than a free floating NaphO$^-$, gives a low concentration acid that is a much stronger acid than free floating NaphOH. The square scheme corresponding to formation of this more acidic species is shown in figure 4.5b. Since this complex would be much more stable with the inclusion of a cluster of water molecules, it likely forms slowly on the time scale of the experiment similar to other phenolic H-bond structures that have been observed.[37] The inclusion of a square scheme between this stronger acid and DQ

results in simulated CV's that are more accurate than with the wedge scheme alone and raises the question of whether pure square schemes would be better at describing the electrochemistry of the DQ and NaphOH system. This is similar to another system in which a fraction of CF_3CH_2OH apparently becomes much more acidic than the rest when it is allowed to affect the electrochemistry of an ortho-quinone.[38] In that case, the proposed explanation was that once 3 acid molecules H-bond to the same quinone they become more acidic, but here the requirement that the stronger acid be used up early in the scan, which will be discussed later, means that it makes more sense to have the NaphOH preform the acid.

Table 4.1. The pK_a's and adjusted pK_a's of the relevant acids.

Acid	pK_a (H_2O)	pK_a (MeCN)
DQH^+	−1[39]	9.3
DQH	5.1[40]	19.53
DQH^-	>11.4[39]	>28.65
NaphOH	9.51[41]	19.81

DQH^- is estimated based upon BQH^-, and the assumption that DQ will be more basic due to the electron donation from its methyl groups. pK_a for MeCN adjusted from H_2O values using Barrette, Johnson, and Sawyer's method.[42]

Table 4.1 shows, on the left, literature values and estimates for the pK_a of NaphOH and protonated DQ in its different oxidation states, and on the right, those

same values adjusted to what they should be in MeCN.[42] From this table it can be clearly seen that in either solvent DQH^+ and DQH are both more acidic than NaphOH, whereas DQH^- is less acidic than NaphOH. From this, it can be concluded that H^+-transfer from NaphOH to DQ and DQ^- is unfavorable and that H^+-transfer from NaphOH to DQ^{2-} is favorable in both solvents. Moreover, this must be the case for all circumstances unless the values here turn out to be off by several orders of magnitude, with NaphOH and DQ^- in MeCN being the one exception. One of the assumptions made by a H-bonding only square scheme is that there is no H^+-transfer, which cannot be the case in a system that has the pK_a values shown above.

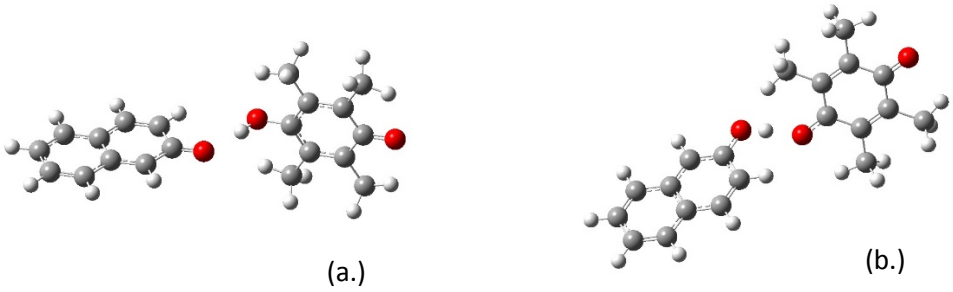

Figure 4.6. a.) DFT calculated structure for the H-bonded complex of NaphOH and DQ^{2-}. Free energy of association are: −42.67 kcal/mol to $NaphO^-$ and DQH^-, and 56.54 kcal/mol to NaphOH and DQ^{2-}. Total energy difference NaphOH + DQ^{2-} <=> $NaphO^-$ + DQH^- is −99.21 kcal/mol. The complex between NaphOH and DQ^{2-} is unstable in the NaphOH form and must have the proton on the DQ^{2-} instead. b.) DFT calculated structure for the H-bonded complex between NaphOH and DQ^-. The complex is stable in the NaphOH form.

Figure 4.6a shows a DFT calculated structure for a H-bonded DQ/NaphOH dimer in which DQ is in its doubly reduced oxidation state and has the proton bonded to it; the frequency calculation in which the H is on the $NaphO^-$ did not converge. This is in contrast to the H-bond complex between NaphOH and DQ in its singly reduced state, figure 4.6b, which optimized to the proton on the NaphOH as the most stable form. Comparing the H-bonded structure in the doubly reduced state to the two possible monomeric forms, NaphOH and DQ^{2-} vs $NaphO^-$ and DQH^-, it can be seen that the H-bonded structure is more stable than the independent molecules when the proton is on the DQH^-, but less stable than the independent molecules when the proton is on the NaphOH, for a total difference of −99.21 kcal/mol in favor of the proton being on DQH^-. Furthermore, the optimization calculation for the H-bonding complex in figure 4.6b started out with the molecules closer together by almost 1 Å; which means that the potential energy surface calculated by Gaussian favored distancing the two molecules rather than elongating the O-H bond in order to move the H closer to the $NaphO^-$. Combined with the literature pK_a values of the respective acids, these DFT calculations should make it clear that H^+-transfer must happen in this system when DQ reaches its doubly reduced state.

Table 4.2. DFT calculated Strengths of H-Bonded Complexes in the DQ/NaphOH system

Complex	Gas Phase ΔG (kcal/mol)	Solvent Correction (kcal/mol)	Solution delG (kcal/mol)	Keq
DQ-NaphOH	5.892	−5.553	0.338	0.565
DQ^{-}-NaphOH	−8.047	−40.091	−48.138	2.02×10^{35}
DQH^{-}-$NaphO^{-}$	42.671	−183.982	−141.311	4.30×10^{103}

Table 4.2 holds the results of DFT frequency calculations followed by COSMO Therm to determine the stability of the three most important H-bonded complexes. DFT is known to overestimate H-bonding strengths,[43] but even assuming an overestimate of well over an order of magnitude would still mean that the H-bond complex is strong enough to move the 2nd reduction wave far enough to be wave III. Since it is unrealistic for a single H-bond to affect a redox potential more than a H^{+}-transfer, the actual ratio of the equilibria for the DQ^{-}-NaphOH complex and the DQH—NaphO` complex is probably something like 1E7 rather than what is shown here.

Figure 4.3 shows CV's in which DQ is being reduced and re-oxidized in the presence of equal or excess of NaphOH. The CV's at higher NaphOH concentrations show a single, sharp, two electron reduction that occurs very close to the potential of a normal first reduction, and a single, broad, two electron oxidation which is much broader than the reduction. Similar behavior was observed by Astudillo et al. 2007 to

occur in MeCN when an excess of CH_3COOH was added to a solution of BQ;[44] there, the explanation was that the acid protonated both the singly reduced and doubly reduced quinone and formed a H-bonded complex between the protonated quinone and the conjugate acid. The acid present here is much weaker and present at a much lower concentration than in Astudillo et al., but there is enough NaphOH so that an H-bond complex can form between the NaphOH and the $NaphO^-$ after one H^+ is transfered to the quinone, thus promoting the H^+-transfer reaction. What is important to note here, however, is that oxidation peak IVa is present in CV's in figure 4.2 where the concentration of NaphOH is lower than that of DQ. It can be determined from this that H^+-transfer is likely occurring at concentrations of NaphOH which are equal to or greater than DQ, and in some cases where NaphOH is present at a lower concentration.

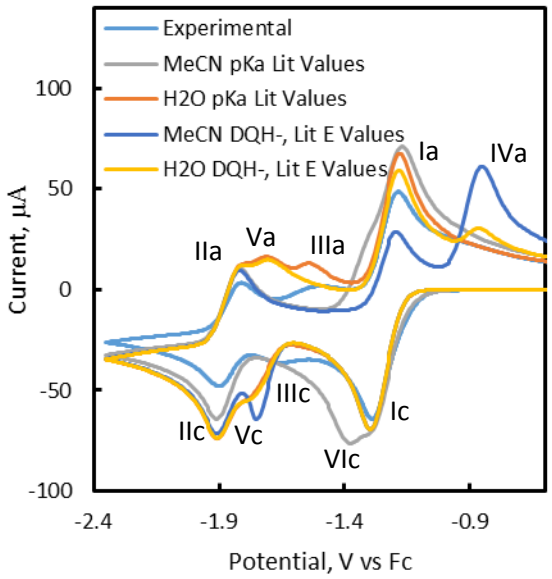

Figure 4.7. Overlay of experimental CV for 1 mM DQ and 0.5 mM NaphOH in 0.10 M NBu_4PF_6/MeCN at 0.5 V/s and digital simulations of CV's using H^+-transfer only scheme with either the pK_a values from table 4.1 or the literature redox potential, -0.811V vs Fc, for the DQH/DQH^- couple,[39, 45] the difference between that and the DQH^+/DQH couple found in simulations used for figure 4.2, and the DQH^- pK_a values from table 4.1. The rest of the parameters can be found in the appendix in table A.2, except for the quinhydrone formation constants which were set to 0 so that this set of simulations would look at only e-transfer and H^+-transfer reactions.

Figure 4.7 shows five overlaid CV's where one of them is from an experiment with a 1:0.5 ratio of DQ to NaphOH, two are simulations of H^+-transfer square schemes using different pK_a values, and the remaining two use literature values for the redox potential of the DQH/DQH^- couple[39, 45], the difference between that and the DQH^+/DQH couple used for figure 4.2 and only vary by using the pK_a values for

DQH^- from table 4.1. The experimental wave III appears as a broad, reversible wave roughly evenly between waves I and II. Wave III in the simulation using MeCN pK_a values gives a reversible wave which is shifted positive by several hundred millivolts from where it is in the experiment and is labelled as peak VIc on the reduction side and is a shoulder of peak Ia on the oxidation side. The simulation that uses water pK_a values has an irreversible oxidation with no reduction at the potential of the experimental wave III, and a reversible wave, labelled V, just positive of the normal wave II. The separation of wave III in the simulation using the water pK_a values into wave V and peak IIIa can be explained by recognizing that the H^+-transfer itself is very unfavorable (by five orders of magnitude) and therefore is only going to occur when the free quinone starts to be reduced to DQ^{2-} which gives us a single reduction peak that is close to, but positive of wave II (peak Vc). Because the K_{eq} of the H^+-transfer reaction of DQ^{2-} and NaphOH is within two orders of magnitude of one, some of the $NaphO^-$ will be able to take back their protons when all of the NaphOH is in the $NaphO^-$ form, thus giving peak Va, but once a sufficient number of $NaphO^-$ has been converted to NaphOH, the back reaction where NaphOH protonates DQ^{2-} will compete with the electron transfer and the rest of the $NaphO^-$ will have to wait to reclaim their protons until the electric potential is sufficient to oxidize DQH^- directly, closer to −1.5V, which gives us peak IIIa. This discrepancy between the simulated and experimental data is very easily explained by pointing out that systems in which an organic acid and organic base react in an aprotic solvent have been observed to result in an H-bonded complex between the conjugate base and acid,[25, 44] which is not a

consideration in a H^+-transfer only square scheme. An H-bonding complex between $NaphO^-$ and DQH/DQH^- would result in electron density being donated from the $NaphO^-$ to the quinone which would contribute to stabilizing the DQH and destabilizing the DQH^-. This would shift the potential of that species negative, exactly as observed here in wave V. Meanwhile, using the literature DQH reduction potential—which must be negative of that for DQ because it and DQH have the same charge and structure but DQ is not a radical—gives us an irreversible oxidation peak positive of wave I which is labelled peak IVa and the reduction peak Vc, with no wave III at all. The H^+-transfer equilibrium constant only determines the size of these waves. From comparing figures 4.4 and 4.7, it can be concluded that any mechanism to explain this system which does not include H-bonding complexes is very likely to be wrong provided that the K_a values from the literature and the DFT calculations are accurate to within a few orders of magnitude.

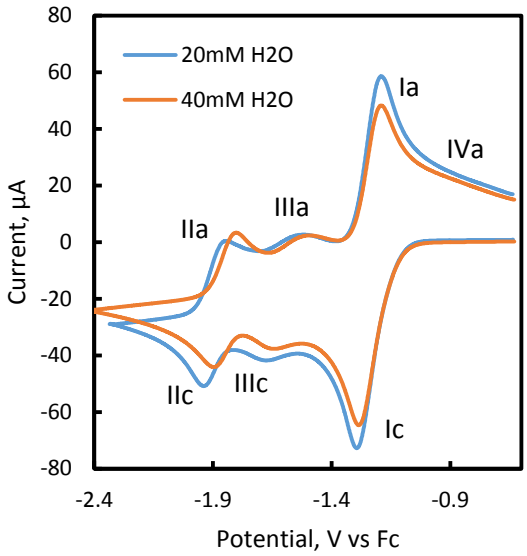

Figure 4.8. Overlaid background-subtracted CV's of 1.0 mM DQ and 0.5 mM NaphOH in 0.1M NBu_4PF_6/MeCN taken at 0.5 V/s in the presence of different amounts of water. Blue: 20 mM H_2O. Red: 40 mM H_2O. Wave III is shifted 0.2945V positive of wave II with 20 mM H_2O present and 0.282 V with 40 mM H_2O present.

From the preceding discussion, NaphOH should be able to protonate DQ^{2-} to generate DQH^-, but it is highly unlikely that wave III in the CV's of DQ with NaphOH could be simply due to the DQH/DQH^- transition. As noted earlier, a much more likely possibility is that this wave is due to the reduction of the NaphOH/DQ^- H-bond complex. Some indirect evidence for this is found in the data in figure 4.8, which shows overlapping CV's of 0.5:1 NaphOH:DQ mixtures that were performed with differing concentrations of water in the MeCN. Wave I is hardly affected, which has been observed before[33] and should be the case given the small water concentrations involved in both of them. Also, both waves II and III have moved to

more positive potentials with increasing water concentrations, which makes sense because both of these correspond to the second reduction of a quinone molecule which has been observed to be affected much more dramatically by H-bonding.[33, 46] The amount to which the presence of NaphOH has shifted the second reduction potential of some of the DQ—from wave II to wave III—is 294.5mV for the 20 mM H_2O solution and 282 mV for the 40 mM H_2O solution, which means that the shift in the wave is 12.5 mV greater in the less polar solution. An explanation for this is that wave III corresponds to a H-bonding complex between NaphOH and DQ^{-}/DQ^{2-}, and that the shift is the result of water stabilizing the separated molecules as compared to the dimerized molecules by means of H-bonding. The greater the stability of the H-bonding complex, the further positive it will shift the reduction potential. Adding water will stabilize to the separated molecules through water H-bonds, and this destabilizes the NaphOH/DQ-complex, resulting in a smaller potential shift.

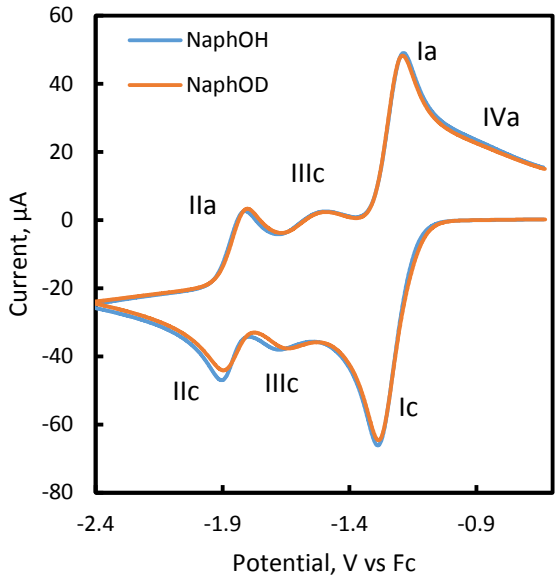

Figure 4.9. Overlaid CV's of a kinetic isotope effect (KIE) study. The scans pictured here were taken at 0.5 V/s with 1.0 mM DQ and 0.5 mM NaphOH/NaphOD in MeCN with 0.1 M NBu_4PF_6 and 40 mM H_2O/D_2O. The actual data for the calculation also included CV's at 1.0 V/s and 2.0 V/s, and contain 3 different runs at each of the three scan rates.

Table 4.3. The KIE values of wave III determined at different scan rates for the system 1.0 mM DQ in the presence of 0.5 mM NaphOH and 40 mM H_2O or D_2O in MeCN with 0.1 M NBu_4PF_6.

Scan Rate	Average KIE (H/D)	Number of Scans Considered
0.5V/s	1.013	3
1.0V/s	1.067	3
2.0V/s	1.039	3
Combined	1.040	9

In figure 4.9 there are overlapping CV's from a KIE study taken in MeCN which shows that exchanging NaphOH for NaphOD in this system does nothing to the electrochemistry. The actual calculated KIE is 1.040, shown in table 4.3, which is very close to having no KIE at all. This suggests that the H^+-transfer is not in concert with the e-transfer in this system, but the H^+-transfer within the H-bonded complex is still not ruled out. Since the position of the H^+ or D^+ nucleus in the H-bonded complex can be modeled as the nucleus vibrating from one oxygen to the other, and the IR absorption energy is 3,400cm^{-1} and 2,500cm^{-1} for H and D respectively,[47] the frequency of the vibration is somewhere near 1E14 Hz, which means that the kinetic constants for both of these transfer reactions should also be on the order of 1E14 s^{-1} within an H-bonded complex and therefore would not be likely to show up in a KIE experiment with the scan rates used here, which still leaves open the possibility of a concerted H^+-transfer and e-transfer that is simply too difficult to measure with this experimental setup.

Comparing Different Wedge Schemes. Looking back onto figure 4.4, it can be seen that a simple wedge scheme with the only H-bond complex being between one NaphOH and one DQ, DQ^-, or DQ^{2-}, and that while this does have redox waves and peaks at the right potentials, it does not accurately reflect the fact that wave I increases its reductive current and decreases its oxidative current in the experimental data. The solution to this presented in figure 4.5 was a slow forming, moderately strong acid made from an H-bonding complex of NaphOH. The reason why it has to be a moderately strong acid is because the only way to increase the size of the first

reduction peak and the size of peak IVa at the same rate is to have a potential inversion, for which H^+-transfer would be the most obvious answer; the reason why it must be a NaphOH H-bond complex is because both peaks increase with increasing NaphOH concentration and the NaphOH was thoroughly purified via sublimation, thus ruling out contamination; the reason why it must be slow forming is because a fast forming acid would also be a fast degrading acid, which means that the H^+-transfer would happen all through the CV, rather than just at the beginning, thus resulting in peak IVa increasing while the wave I reduction peak does not increase. It is now important to examine other possibilities.

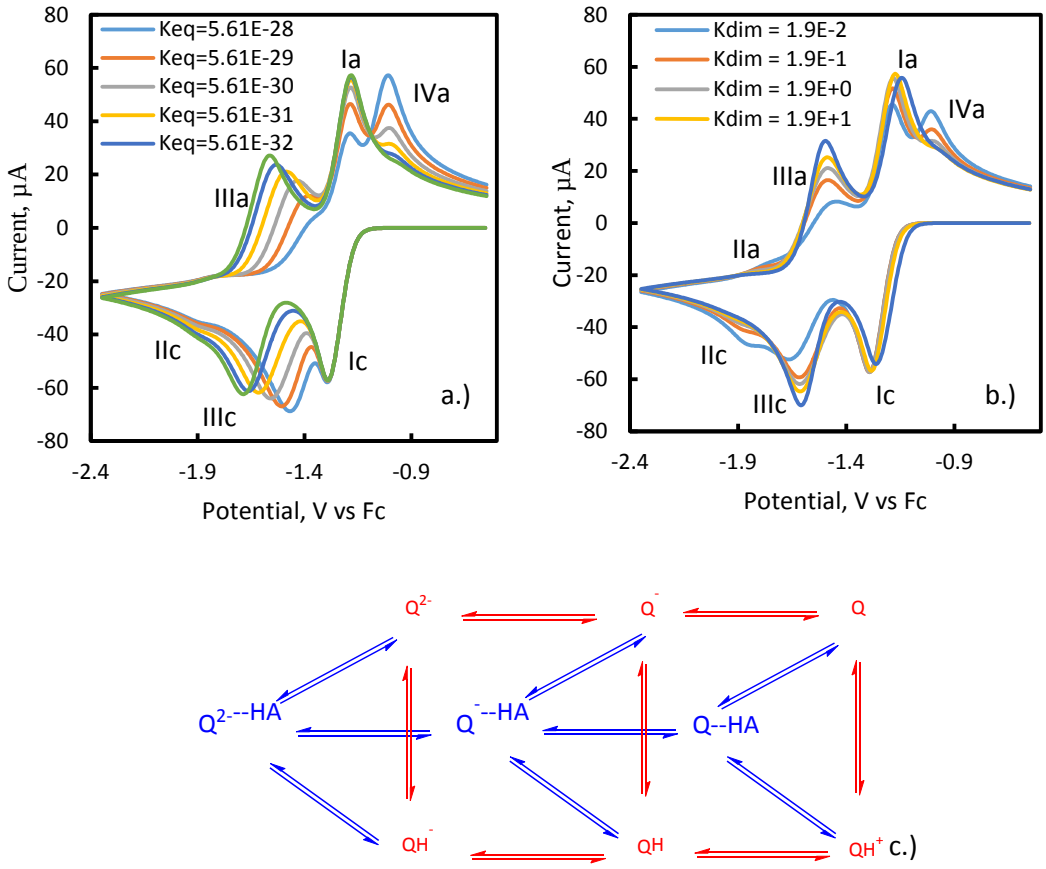

Figure 4.10. Overlaid, simulated CV's of the simple wedge scheme, 1.0 mM DQ with 1.0 mM NaphOH in 0.1 M NBu_4PF_6/MeCN taken at 1.0 V/s (a.) changing K_{eq} of the DQ + NaphOH H^+-transfer reaction, (b.) changing the K_{dim} of the DQ + NaphOH reaction, and (c.) the scheme used for the simulations. The parameters not listed here can be found in the appendix in table A.3.

Starting with the wedge scheme used to make figure 4.4, it is possible to change the K_{eq} of the H^+-transfer reaction, as in figure 4.10a, or the K_{dim} of the H-bond complex, as in figure 4.10b, between the NaphOH and the DQ in different oxidation states: making the first of these more favorable might cause peaks Ic and IVa to

increase at the expense of peak Ia because a larger proportion of the DQ will be reduced in a two electron step at the potential of Ic which can only be reversed at the potential of IVa because of the H^+-transfer; at the same time, changing the K_{dim} may give us the desired result because the H^+-transfer must happen through the H-bonded complex, so that increasing the strength of this complex would give more opportunity for the H^+-transfer reaction, and thus the irreversible two electron step. Displayed in figures 10a and 10b are overlays of simulations of these mechanisms using a DQ:NaphOH ratio of 1:1, where any increase peak Ic would be obvious since because peak Ic for $K_{eq} = -31$ and $K_{dim} = 1.9E+0$ has the same height as the simulation with no NaphOH present. What is shown here is that in every case, the peak height of Ic does not change, thus ruling out this mechanism to solve this problem. It may be argued that continuing to make K_{eq} more favorable would cause peak Ic to grow because wave III would start to overlap with it even more, but that would require wave III to shift so far positive that it would no longer match up even slightly to the wave III in the experimental data.

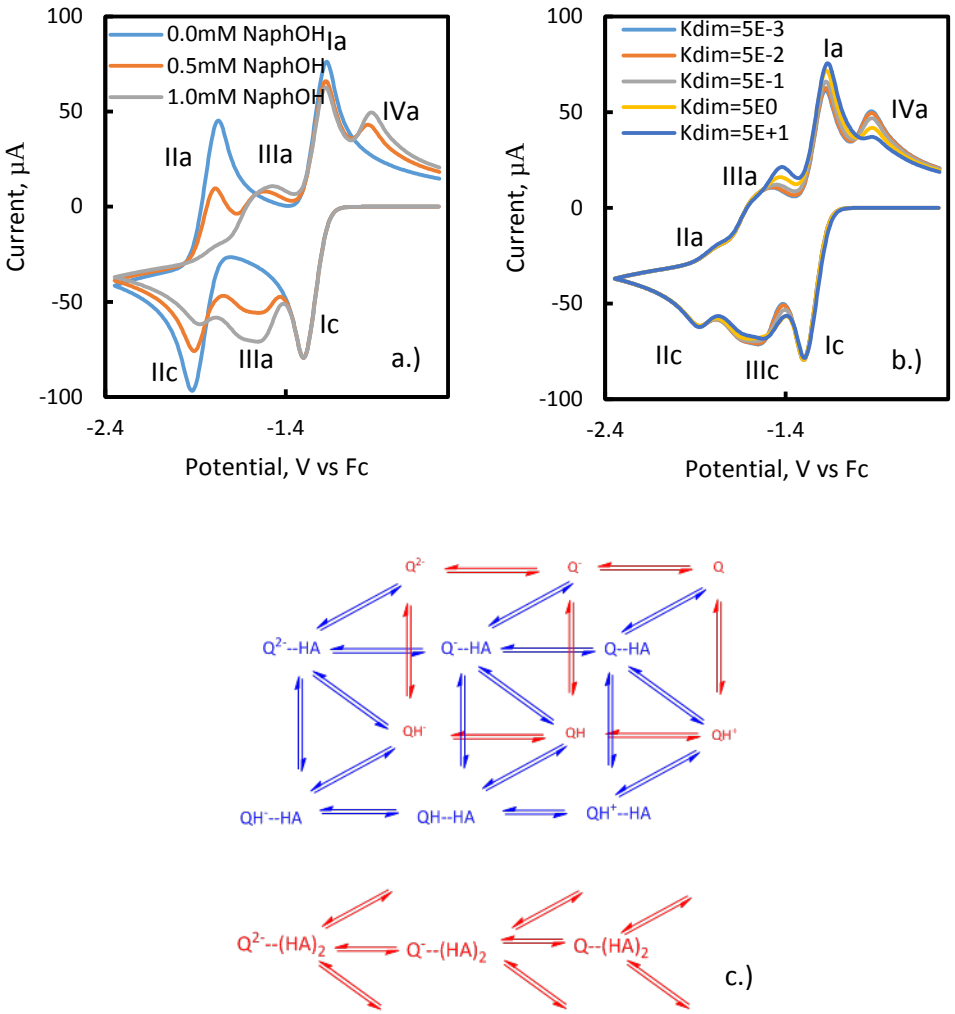

Figure 4.11. Overlaid simulated CV's of the DQ + NaphOH wedge scheme which includes H-bond complexes that include one or two NaphOH molecules per DQ, rather than just one NaphOH per DQ. (a.) Overlaid CV's with different NaphOH concentrations, (b.) overlaid CV's with 1:1 DQ:NaphOH ratio, changing the strength of the H-bonding complex between one DQ and two NaphOH molecules, and (c.) the scheme used in the simulations. The simulated conditions are 1.0 mM DQ in 0.1 M NBu_4PF_6/MeCN taken at 1.0 V/s. The parameters not listed here can be found in the appendix in table A.4.

In figure 4.11 there are overlays of a set of CV's comparing different possible parameters for a wedge scheme that includes two H-bonding steps. In figure 4.11a the simulations of the two H-bond wedge scheme show that the reduction peak for wave I does not change in height with increasing NaphOH concentration. Note that in figure 4.11b, the height of the reduction peak of wave I does not change as the strength of the DQ and two NaphOH H-bond complex changes until wave III has shifted so far positive that it has become a set of shoulders for wave I, which is not the potential at which it appears in the experimental data. Note also how the reduction side of wave I does increase with increasing NaphOH concentration in figures 4.4 and 4.5.

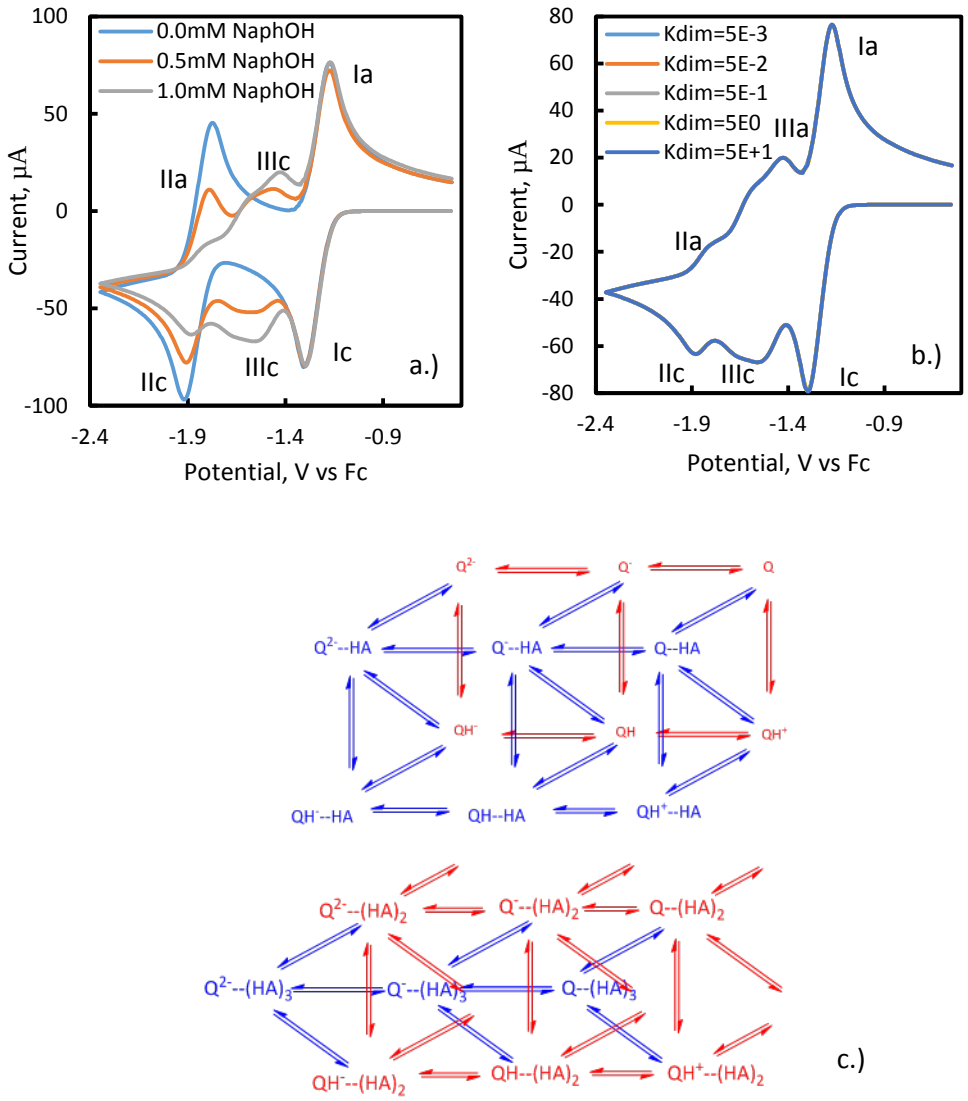

Figure 4.12. (a.) Overlaid CV's with different NaphOH concentrations with three NaphOH per DQ maximum, (b.) overlaid CV's with 1:1 DQ:NaphOH ratio, changing the strength of the H-bonding complex between one DQ and three NaphOH molecules, and (c.) the scheme used in the simulations. Simulations use 1.0mM DQ in 0.1M NBu_4PF_6/MeCN at 1.0 V/s. The parameters not listed here can be found in the appendix in table A.6.

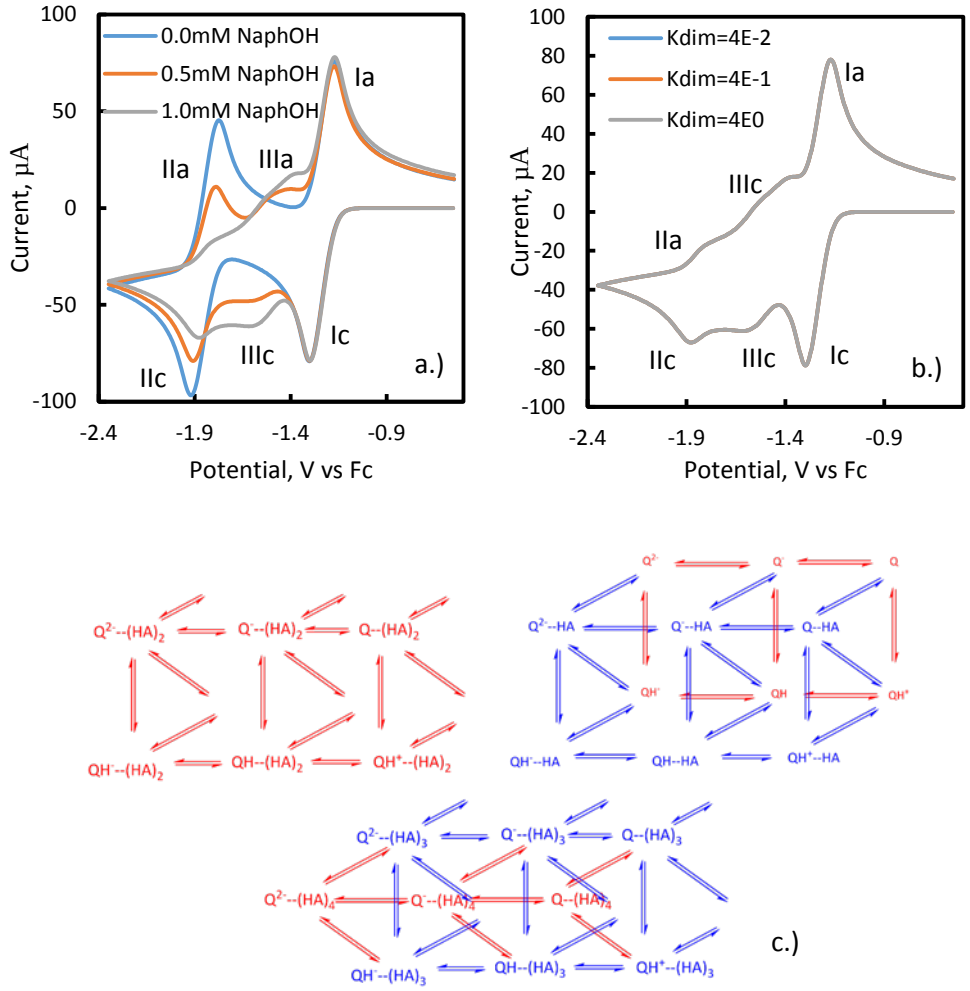

Figure 4.13. Overlaid simulated CV's of the DQ + NaphOH wedge scheme which includes H-bond complexes that have four NaphOH molecules per DQ, rather than just one NaphOH per DQ. (a.) Overlaid CV's with different NaphOH concentrations with four NaphOH per DQ maximum, (b.) overlaid CV's with 1:1 DQ:NaphOH ratio, changing the strength of the H-bonding complex between one DQ and four NaphOH molecules; (c.) scheme used for simulations. These are simulated CV's of 1.0 mM DQ in NBu_4PF_6/MeCN at 1.0V/s. The parameters not listed here can be found in the appendix in table A.7.

Figures 4.12 and 4.13 show CV's from simulations that start with the two NaphOH H-bond scheme from figure 4.11 that came the closest to reproducing the experimental data, and expand that to either the three NaphOH per DQ H-bond complexes or the four NaphOH per DQ H-bond complexes. In figure 4.12a, there are see overlaid scans for the three H-bond scheme that go from 0 equivalents of NaphOH to 1 equivalent of NaphOH, which show that there is no increase in wave I's reduction peak; comparing that to figure 4.12b, it can be seen that changing the H-bonding strength of the third NaphOH H-bond does not change the CV at all. This is because the concentration of NaphOH is such that the concentration of NaphOH available to be the third H-bond donor is insignificant by the time there are quinones that have two H-bonds already. Unsurprisingly, figures 4.13a and 4.13b—which are the NaphOH dependence overlays and the H-bonding strength overlays for the four H-bond wedge scheme—show the same lack of change for the same reason.

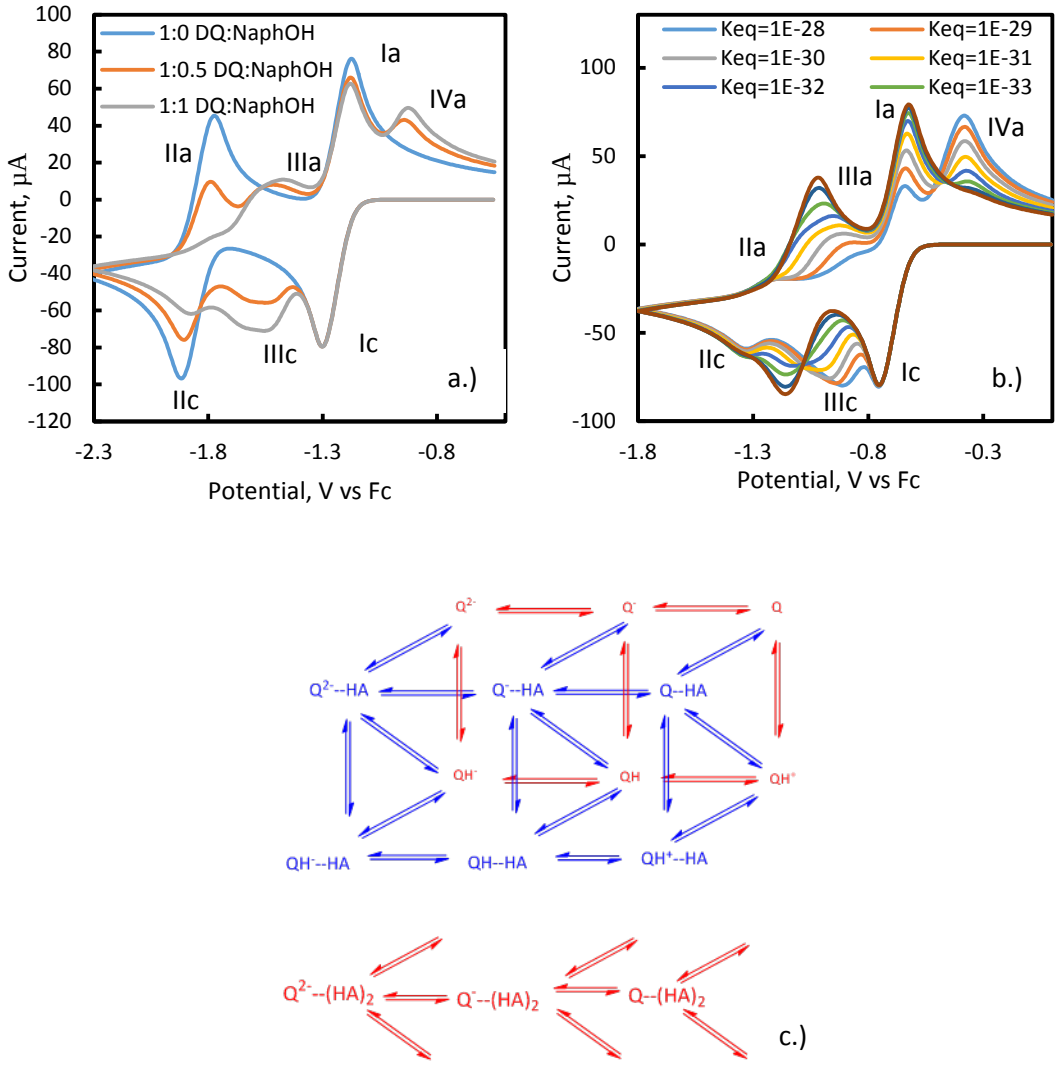

Figure 4.14. Simulations of the DQ and NaphOH system using the wedge scheme with two NaphOH per DQ maximum in each H-bond complex with (a.) changing NaphOH concentration, (b.) keeping 1:1 DQ:NaphOH concentration while changing the K_{eq} of the DQ + NaphOH H-transfer reaction, and (c.) the scheme used for the simulations. Simulations had used 1.0 mM DQ in 0.1 M NBu_4PF_6/MeCN at 1.0V/s. The parameters not listed here can be found in the appendix in table A.4.

Shown in figure 4.14 are CV's of the wedge scheme with different values for the pK_a of NaphOH, where 4.14a shows overlaid scans for different concentrations of NaphOH, and figure 4.14b shows simulated scans in which the equilibrium constant for the H^+-transfer is changed while the NaphOH is present at 1 equivalent. The difference between this data and the data in figure 4.10a is that the simulation is now allowing two NaphOH molecules to H-bond to each quinone at once, thus allowing part of wave III to shift into wave I without the whole thing going. In figure 4.14a it can be seen that the height of the reduction side of wave I is the same in all cases, regardless of NaphOH concentration, and in figure 4.14b it is possible to see that wave III still has to shift significantly positive in order for the reduction side of wave I to grow in. Figures 4.15a and 4.15b are the same in every way except that the H^+-transfer now requires a free-floating NaphOH to impact the H-bond complex, resulting in the NaphOH-$NaphO^-$ H-bond complex. There actually is an increase in peak Ic along with the decrease in peak Ia and with wave III staying put, but now peak IVa has turned into a full wave with shoulders, which is not even close to the irreversible peak that is shown in the experimental data.

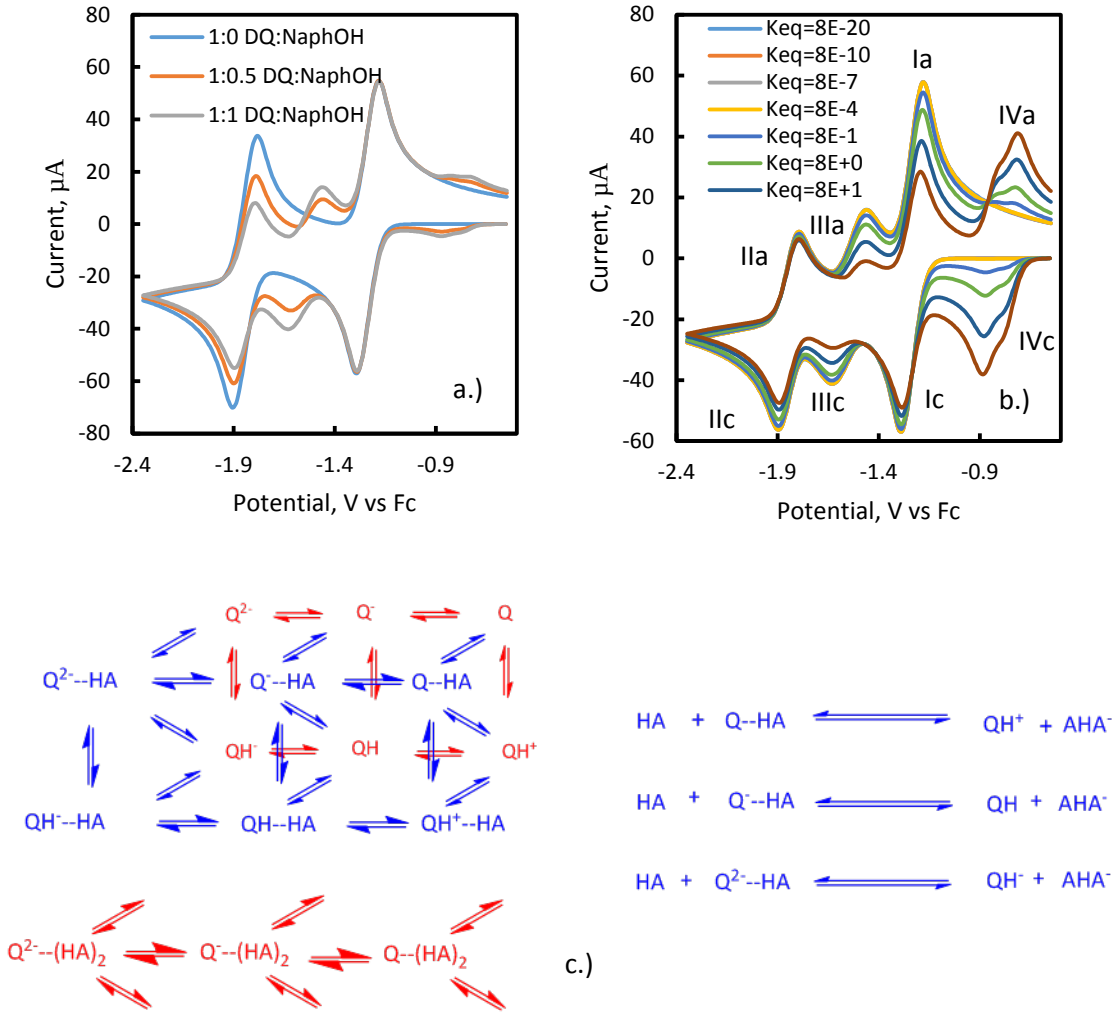

Figure 4.15. Simulations of the DQ and NaphOH system using the wedge scheme and requiring one NaphOH to impact the DQ and NaphOH H-bond complex in order to transfer the proton. (a.) Changing the NaphOH concentration; (b.) staying at 1:1 DQ:NaphOH concentration ratio while changing the K_{eq} of the DQ + NaphOH H^+-transfer reaction, and (c.) the scheme used for the simulations. Simulations used 1.0 mM DQ in 0.1 M NBu_4PF_6/MeCN and were taken at 1.0 V/s. The parameters not listed here can be found in the appendix in table A.8.

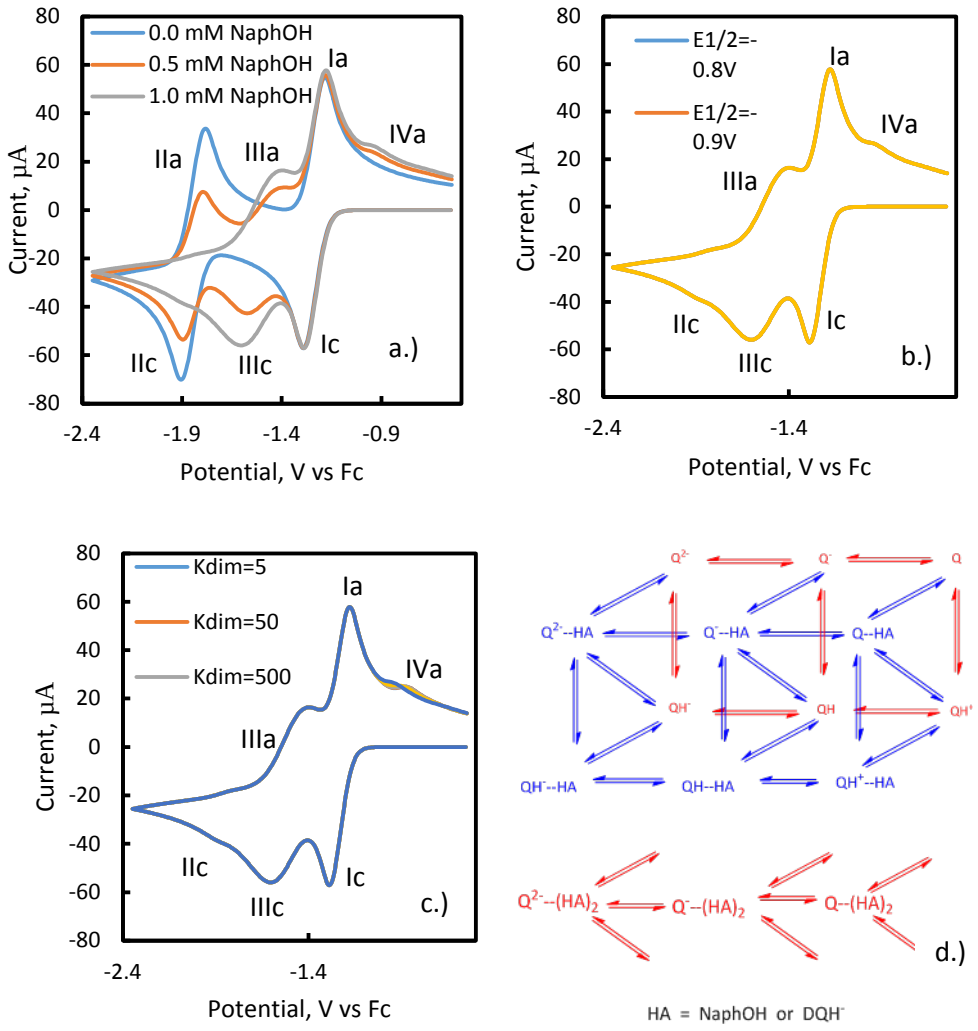

Figure 4.16. Simulated CV's of the DQ and NaphOH system using the simple wedge scheme while including an additional H-bond dimerization between protonated and non-protonated DQ molecules. (a.) Changing NaphOH concentration; (b.) keeping the DQ:NaphOH concentration at 1:1 while changing the E° value of reduction of $[DQHDQ]^{2-}$; (c.) changing the K_{dim} of the DQH^{-} and DQ dimer; (d.) the scheme used for the simulations. The simulations use 1.0 mM DQ in 0.1 M NBu_4PF_6/MeCN at 1.0 V/s. The parameters not given here can be found in the appendix in table A.9.

Looking back on the scheme for the strong acid and DQ, which includes a H-bonding scheme between the protonated, reduced DQ species and either DQ^{-} or DQ^{2-}, Figure 4.16 has a CV's from a mechanism where the quinones can H-bond to either NaphOH or the protonated DQ species, with the mechanism appearing next to the CV's. Because there is a whole new H-bonding scheme here, both the dimerization constant between the DQH^{-} and DQ needs to be fit as well as the redox potential of the most relevant new e-transfer, from $[DQHDQ]^{2-}$ to $[DQHDQ]^{3-}$. In figure 4.16a there is the overlay of CV's with different concentrations of NaphOH at the most generous possible parameters: K_{dim}=50000 and $E° = -0.8$, which shows that the reduction side of wave I still does not increase with increasing NaphOH concentration. In figures 4.16b and 4.16c there are overlaid CV's with the NaphOH:DQ ratio at 1:1 and with changing the redox potential or the dimerization coefficient, respectively. Note that not only does the reduction side of wave I not change in 4.16b or 4.16c, but the only change is to peak IVa as the dimerization constant changes, with no change due to changes in the redox potential. The doubly protonated quinone was not included here because the low concentrations of NaphOH used here coupled with its weakly acidic character would have made the doubly protonated DQ concentration in any oxidation state small enough to be undetectable by these methods.

Conclusion

A three dimensional redox scheme involving e-transfer, H^+-transfer, and H-bonding reactions is required to accurately simulate the DQ and NaphOH chemical system. H-bonding reactions are known to shift the potentials of the redox waves gradually with respect to the guest concentration; H^+-transfer reactions are known to shift the potential of redox waves radically while making them irreversible. CV's of the DQ and NaphOH system have both of those characteristics, where a 1:1 DQ:NaphOH mixture shows the first redox wave gaining a new oxidation peak that is irreversible just like with H^+-transfer, while the second normal redox wave disappears in favor of a new wave at intermediate potentials which shows no kinetic isotope effect which would be the case with a strong H-bond complex. This data cannot be simulated and fitted with a normal square scheme which includes only e-transfer and H-bonding or only e-transfer and H^+-transfer. Wedge schemes which do not include a NaphOH-NaphOH H-bond complex fit most of the experimental data's characteristics fairly well, but not all of them. Adding the NaphOH-NaphOH H-bond complex as a slow forming acid gives simulated CV's of the DQ and NaphOH system that accurately reproduce the experimental data.

References

1. Cukler, R. I. *Journal of Physical Chemistry* **1994**, *98*, 9, 2377-2381.

2. DiLabio, G. A.; Johnson, E. R. *Journal of the American Chemical Society* **2007**, *129*, 19, 6199-6203.

3. Nassar, A.-E. F.; Zhang, Z.; Hu, N.; Rusling, J. F. *Journal of Physical Chemistry B* **1997**, *101*, 12, 2224-2231.

4. Odom, J. M.; H. D. Peck, J. *Annyal Review of Microbiology* **1984**, *38*, 551-592.

5. Schrauben, J. N.; Hayoun, R.; Valdez, C. N.; Braten, M.; Fridley, L.; Mayer, J. M. *Science* **2012**, *336*, 6086, 1298-1301.

6. Stiefel, E. I. *Proceedings of the National Academy of Sciences* **1973**, *70*, 4, 988-992.

7. Weatherly, S. C.; Yang, I. V.; Thorp, H. H. *Journal of the American Chemical Society* **2001**, *123*, 6, 1236-1237.

8. Wikstrom, M. *Nature* **1989**, *338*, 776-778.

9. Wikstrom, M. K. F. *Nature* **1977**, *266*, 271-273.

10. Hammarstrom, L.; Styring, S. *Energy and Environmental Science* **2011**, *4*, 2379-2388.

11. Meyer, T. J.; Huynh, M. H. V.; Thorp, H. H. *Angewante Chimie* **2007**, *46*, 28, 5284-5304.

12. Sjodin, M.; Styring, S.; Akermark, B.; Sun, L.; Hammarstrom, L. *Journal of the American Chemical Society* **2000**, *122*, 16, 3832-3936.

13. Saito, G.; Swanson, J. A.; Lee, K.-D. *Advanced Drug Delivery Reviews* **2003**, *55*, 2, 199-215.

14. Ahn, S.-k.; Kasi, R. M.; Kim, S.-C.; Sharma, N.; Zhou, Y. *Soft Matter* **2008**, *4*, 1151-1157.

15. Berthomieu, C.; Hienerwadel, R.; Boussac, A.; Breton, J.; Diner, B. A. *Biochemistry* **1998**, *37*, 30, 10547-10554.

16. Caffrey, M. S.; Daldal, F.; Holden, H. M.; Cusanovich, M. A. *Biochemistry* **1991**, *30*, 17, 4119-4125.

17. Doyle, A. G.; Jacobsen, E. N. *Chemical Reviews* **2007**, *107*, 12, 5713-5743.

18. Ge, Y.; Lilienthal, R. R.; Smith, D. K. *Journal of the American Chemical Society* **1996**, *118*, 16, 3976-3977.

19. Kar, H.; Molla, M. R.; Ghosh, S. *Chemical Communications* **2013**, 49, 4220-4222.

20. Osuka, A.; Yoneshima, R.; Shiratori, H.; Osuka, A.; Okada, T.; Taniquchi, S.; Mataga, M. *Chemical Communications* **1998**, 15, 1567-1568.

21. Huynh, M. H. V.; Meyer, T. J. *Chemical Reviews* **2007**, *107*, 11, 5004-5064.

22. Murata, T.; Morita, Y.; Yakiyama, Y.; Fukui, K.; Yamochi, H.; Saito, G.; Nakasuji, K. *Journal of the American Chemical Society* **2007**, *129*, 35, 10837-10846.

23. Rhile, I. J.; Mayer, J. M. *Journal of the American Chemical Society* **2004**, *126*, 40, 12718-12719.

24. Clare, L. A.; Pham, A. T.; Magdaleno, F.; Acosta, J.; Woods, J. E.; Cooksy, A. L.; Smith, D. K. *Journal of the American Chemical Society* **2013**, *135*, 50, 18930-18941.

25. Tamashiro, B. T.; Cedano, M. R.; Pham, A. T.; Smith, D. K. *Journal of Physical Chemistry C* **2015**, *119*, 23, 12865-12874.

26. Lindquist, J. *Journal of Electroanalytical Chemistry and Interfacial Electrochemistry* **1974**, *52*, 1, 37-46.

27. Samuelsson, R.; Sharp, M. *Electrochimica Acta* **1978**, *23*, 4, 315-317.

28. Arshid, F. M.; Giles, C. H.; Jain, S. K. *Journal of the Chemical Society* **1956**, 559-569.

29. Cheek, G. T. *Electrochemical Society Transactions* **2015**, *64*, 34, 1-6.

30. Tessensohn, M. E.; Hirao, H.; Webster, R. D. *Journal of Physical Chemistry C* **2012**, *117*, 1081-1090.

31. Guskov, A.; Kern, J.; Gabdulkhakov, A.; Broser, M.; Zouni, A.; Saenger, W. *Nature Structural and Molecular Biology* **2009**, *16*, 334-342.

32. Grzeskowiak, I.; Galezowski, W.; Jarczewski, A. *Canadian Journal of Chemistry* **2001**, *79*, 1128-1134.

33. Staley, P. A.; Lopez, E. M.; Clare, L. A.; Smith, D. K. *Journal of Physical Chemistry C* **2015**, *119*, 35, 20319-20327.

34. Staley, P. A.; Newell, C. M.; Pullman, D. P.; Smith, D. K. *Analytical Chemistry* **2014**, *86*, 21, 10917-10924.

35. Bard, A. J.; Faulkner, L. R. *Electrochemical Methods: Fundamentals and Applications*, 2nd ed.; Wiley: Hoboken, NJ, 2004, pp 242-243.

36. Gamboa-Valero, N.; Astudillo, P. D.; Gonzalez-Fuentes, M. A.; Leyva, M. A.; Rosales-Hoz, M. d. J.; Gonzalez, F. J. *Electrochimica Acta* **2016**, *188*, 602-610.

37. Zhang, Q.; Tiefenbacher, K. *Journal of the American Chemical Society* **2013**, *135*, 43, 16213-16219.

38. Macias-Ruvalcaba, N. A.; Okamura, N.; Evans, D. H. *Journal of Physical Chemistry B* **2006**, *110*, 43, 22043-22047.

39. Eggins, B. R.; Chambers, J. Q. *Journal of the Electrochemical Society* **1970**, *117*, 2, 186192.

40. Dixon, W. T.; Murphy, D. *Journal of the Chemical Society, Faraday Transactions 2* **1976**, *72*, 1221-1230.

41. Bhattacharyya, D.; Jr., C. E. H.; Northey, R. P. *Hazardous Waste and Hazardous Materials* **1986**, *3*, 4, 405-429.

42. Hr., W. C. B.; Jr., H. W. J.; Sawyer, D. T. *Analytical Chemistry* **1984**, *56*, 1890-1898.

43. Barich, D. H.; Nicholas, J. B.; Haw, J. F. *Journal of Physical Chemistry A* **2001**, *105*, 4708-4715.

44. Astudillo, P. D.; Tiburcio, J.; Gonzalez, F. J. *Journal of Electroanalytical Chemistry* **2007**, *604*, 1, 57-64.

45. Gupta, N.; Linschitz, H. *Journal of the American Chemical Society* **1997**, *119*, 27, 6384-6391.

46. Quan, M.; Sanchez, D.; Wasylkiw, M. F.; Smith, D. K. *Journal of the American Chemical Society* **2007**, *129*, 42, 12847-12856.

47. Corcelli, S. A.; Lawrence, C. P.; Skinner, J. L. *Journal of Chemical Physics* **2004**, *120*, 17, 8107-8117.

Appendix

Table A.1		
Simulation Parameters for DQ and MeOH used in figure 4.1b		
Terms	Thermodynamic Parameter	Forward Kinetic Constant
charge transfer reactions:		
reaction[1]: DQ + e = DQ-	E0[1] (V): -1.39393	ks[1] (cm/s): 10000
reaction[2]: DQ- + e = DQ2-	E0[2] (V): -1.9935	ks[2] (cm/s): 0.014318
reaction[3]: MeOHDQ + e = MeOHDQ-	E0[3] (V): -1.3533	ks[3] (cm/s): 10000
reaction[4]: MeOHDQ- + e = MeOHDQ2-	E0[4] (V): -1.8842	ks[4] (cm/s): 5
reaction[5]: MeOH2DQ + e = MeOH2DQ-	E0[5] (V): -1.328	ks[5] (cm/s): 10000
reaction[6]: MeOH2DQ- + e = MeOH2DQ2-	E0[6] (V): -1.788	ks[6] (cm/s): 0.2
reaction[7]: MeOH3DQ + e = MeOH3DQ-	E0[7] (V): -1.308	ks[7] (cm/s): 10000
reaction[8]: MeOH3DQ- + e = MeOH3DQ2-	E0[8] (V): -1.738	ks[8] (cm/s): 1.1728
reaction[9]: MeOH4DQ + e = MeOH4DQ-	E0[9] (V): -1.258	ks[9] (cm/s): 10000
reaction[10]: MeOH4DQ- + e = MeOH4DQ2-	E0[10] (V): -1.708	ks[10] (cm/s): 1.608
reaction[11]: MeOH5DQ- + e = MeOH5DQ2-	E0[11] (V): -1.41508	ks[11] (cm/s): 2
homogeneous chemical reactions:		
reaction[1]: MeOH + DQ = MeOHDQ	Keq[1]: 50	kf[1]: 1E+009
reaction[2]: MeOH + DQ- = MeOHDQ-	Keq[2]: 243.01 (TSR)	kf[2]: 1E+009

reaction[3]: MeOH + DQ2- = MeOHDQ2-	Keq[3]: 17094 (TSR)	kf[3]: 1E+009
reaction[4]: MeOH + MeOHDQ = MeOH2DQ	Keq[4]: 38.2	kf[4]: 1E+009
reaction[5]: MeOH + MeOHDQ- = MeOH2DQ-	Keq[5]: 102.25 (TSR)	kf[5]: 1E+009
reaction[6]: MeOH + MeOHDQ2- = MeOH2DQ2-	Keq[6]: 4319.8 (TSR)	kf[6]: 1E+009
reaction[7]: MeOH + MeOH2DQ = MeOH3DQ	Keq[7]: 1.2124	kf[7]: 1E+009
reaction[8]: MeOH + MeOH2DQ- = MeOH3DQ-	Keq[8]: 2.6403 (TSR)	kf[8]: 1E+009
reaction[9]: MeOH + MeOH2DQ2- = MeOH3DQ2-	Keq[9]: 18.479 (TSR)	kf[9]: 1E+009
reaction[10]: MeOH + MeOH3DQ = MeOH4DQ	Keq[10]: 0.65606	kf[10]: 1E+008
reaction[11]: MeOH + MeOH3DQ- = MeOH4DQ-	Keq[11]: 4.5916 (TSR)	kf[11]: 1E+009
reaction[12]: MeOH + MeOH3DQ2- = MeOH4DQ2-	Keq[12]: 14.756 (TSR)	kf[12]: 1E+009
reaction[13]: MeOH + MeOH4DQ- = MeOH5DQ-	Keq[13]: 4	kf[13]: 1E+009
reaction[14]: MeOH + MeOH5DQ2- = MeOH6DQ2-	Keq[14]: 20	kf[14]: 1E+009
	DQ starting concentration (mol/L)	0.001
	Diffusion Coefficient (everything, cm^2/s)	1.552E-5
	Resistance (Ohms)	350

	Electrode area (cm^2)	0.0706
	Temperature (K)	298.2

Table A.2		
Simulation Parameters for DQ and CF_3COOH used in figure 4.2b and 4.7		
Terms	Thermodynamic Parameter	Forward Kinetic Constant
charge transfer reactions:	charge transfer parameters:	
reaction[1]: DQ + e = DQ-	E0[1] (V): -1.248	ks[1] (cm/s): 10000
reaction[2]: DQ- + e = DQ2-	E0[2] (V): -1.848	ks[2] (cm/s): 0.02
reaction[3]: DQH+ + e = DQH	E0[3] (V): -0.748	ks[3] (cm/s): 0.5
reaction[4]: DQH + e = DQH-	E0[4] (V): -0.848	ks[4] (cm/s): 0.02
reaction[5]: DQH2+ + e = DQH2	E0[5] (V): -0.048	ks[5] (cm/s): 0.02
reaction[6]: DQH2DQ+ + e = DQH2DQ	E0[6] (V): 0.052	ks[6] (cm/s): 0.02
reaction[7]: DQH2DQ + e = DQH2DQ-	E0[7] (V): -1.198	ks[7] (cm/s): 0.02
reaction[8]: DQH2DQ- + e = DQH2DQ2-	E0[8] (V): -1.448	ks[8] (cm/s): 0.05
homogeneous chemical reactions:		
reaction[1]: AcH + DQ = DQH+ + Ac-	Keq[1]: 0.1	kf[1]: 1E+006
reaction[2]: AcH + DQ- = DQH + Ac-	Keq[2]: 2.8196E+007 (TSR)	kf[2]: 1E+005
reaction[3]: AcH + DQ2- = DQH- + Ac-	Keq[3]: 2.2417E+024 (TSR)	kf[3]: 1E+005
reaction[4]: AcH + DQH = DQH2+ + Ac-	Keq[4]: 1	kf[4]: 1E+009
reaction[5]: AcH + DQH- = DQH2 + Ac-	Keq[5]: 3.3137E+013 (TSR)	kf[5]: 1E+009
reaction[6]: DQH2 + DQ = DQH2DQ	Keq[6]: 10	kf[6]: 1E+008

reaction[7]: DQH2 + DQ- = DQH2DQ-	Keq[7]: 69.987 (TSR)	kf[7]: 1E+008
reaction[8]: DQH2 + DQ2- = DQH2DQ2-	Keq[8]: 4.0288E+008 (TSR)	kf[8]: 1E+008
	DQ starting concentration (mol/L)	0.001
	Diffusion Coefficient (everything, cm^2/s)	1E-5
	Resistance (Ohms)	350
	Electrode area (cm^2)	0.0706
	Temperature (K)	298.2

Table A.3		
Simulation Parameters for DQ and NaphOH using Wedge Scheme with 1 NaphOH per DQ maximum for the H-bond Complex used in figures 4.4b, figure 4.10 and figure 4.14		
Terms	Thermodynamic Parameter	Forward Kinetic Constant
charge transfer reactions:		
reaction[1]: DQ + e = DQ-	E0[1] (V): -1.237	ks[1] (cm/s): 10000
reaction[2]: DQ- + e = DQ2-	E0[2] (V): -1.837	ks[2] (cm/s): 0.05
reaction[3]: DQH+ + e = DQH	E0[3] (V): -0.04899 (TSR)	ks[3] (cm/s): 10
reaction[4]: DQH + e = DQH-	E0[4] (V): -0.94225 (TSR)	ks[4] (cm/s): 10
reaction[5]: NaphOHDQ + e = NaphOHDQ-	E0[5] (V): -1.148	ks[5] (cm/s): 10
reaction[6]: NaphOHDQ- + e = NaphOHDQ2-	E0[6] (V): -1.548	ks[6] (cm/s): 10
homogeneous chemical reactions:		
reaction[1]: NaphOH + DQ = NaphO- + DQH+	Keq[1]: 5.61E-032	kf[1]: 0
reaction[2]: NaphOH + DQ- = NaphO- + DQH	Keq[2]: 6.71E-012	kf[2]: 0
reaction[3]: NaphOH + DQ2- = NaphO- + DQH-	Keq[3]: 8880	kf[3]: 0
reaction[4]: NaphOH + DQ = NaphOHDQ	Keq[4]: 1.9	kf[4]: 1E+009
reaction[5]: NaphOH + DQ- = NaphOHDQ-	Keq[5]: 60.658 (TSR)	kf[5]: 1E+009
reaction[6]: NaphOH + DQ2- = NaphOHDQ2-	Keq[6]: 4.6462E+006 (TSR)	kf[6]: 1E+009

reaction[7]: NaphO- + DQH+ = NaphOHDQ	Keq[7]: 3.3868E+031 (TSR)	kf[7]: 1E+009
reaction[8]: NaphO- + DQH = NaphOHDQ-	Keq[8]: 9.0399E+012 (TSR)	kf[8]: 1E+009
reaction[9]: NaphO- + DQH- = NaphOHDQ2-	Keq[9]: 523.22 (TSR)	kf[9]: 1E+008
reaction[10]: NaphOH + NaphO- = NaphOHONaph-	Keq[10]: 1	kf[10]: 1E+009
	DQ starting concentration (mol/L)	0.001
	Diffusion Coefficient (everything, cm^2/s)	1E-5
	Resistance (Ohms)	350
	Electrode area (cm^2)	0.0706
	Temperature (K)	298.2

Table A.4		
Simulation Parameters for DQ and NaphOH using Wedge Scheme with 2 NaphOH per DQ maximum for the H-bond Complex used in figure 4.11		
Terms	Thermodynamic Parameter	Forward Kinetic Constant
charge transfer reactions:		
reaction[1]: DQ + e = DQ-	E0[1] (V): -1.237	ks[1] (cm/s): 10000
reaction[2]: DQ- + e = DQ2-	E0[2] (V): -1.837	ks[2] (cm/s): 0.05
reaction[3]: DQH+ + e = DQH	E0[3] (V): -0.04899 (TSR)	ks[3] (cm/s): 10
reaction[4]: DQH + e = DQH-	E0[4] (V): -0.94225 (TSR)	ks[4] (cm/s): 10
reaction[5]: NaphOHDQH+ + e = NaphOHDQH	E0[5] (V): -0.01916 (TSR)	ks[5] (cm/s): 10
reaction[6]: NaphOHDQH + e = NaphOHDQH-	E0[6] (V): -0.68215 (TSR)	ks[6] (cm/s): 10
reaction[7]: NaphOHDQ + e = NaphOHDQ-	E0[7] (V): -1.148	ks[7] (cm/s): 10
reaction[8]: NaphOHDQ- + e = NaphOHDQ2-	E0[8] (V): -1.548	ks[8] (cm/s): 10
reaction[9]: NaphOHDQHONaph + e = NaphOHDQHONaph-	E0[9] (V): -1.01484 (TSR)	ks[9] (cm/s): 10
reaction[10]: NaphOHDQHONaph- + e = NaphOHDQHONaph2-	E0[10] (V): -1.46466 (TSR)	ks[10] (cm/s): 10
homogeneous chemical reactions:		
reaction[1]: NaphOH + DQ = NaphO- + DQH+	Keq[1]: 5.61E-031	kf[1]: 0
reaction[2]: NaphOH + DQ- = NaphO- + DQH	Keq[2]: 6.71E-011	kf[2]: 0
reaction[3]: NaphOH + DQ2- = NaphO- + DQH-	Keq[3]: 88800	kf[3]: 0
reaction[4]: NaphOH + DQ = NaphOHDQ	Keq[4]: 1.9	kf[4]: 1E+009
reaction[5]: NaphOH + DQ- = NaphOHDQ-	Keq[5]: 60.658 (TSR)	kf[5]: 1E+009

reaction[6]: NaphOH + DQ2- = NaphOHDQ2-	Keq[6]: 4.6462E+006 (TSR)	kf[6]: 1E+009
reaction[7]: NaphO- + DQH+ = NaphOHDQ	Keq[7]: 3.3868E+030 (TSR)	kf[7]: 1E+009
reaction[8]: NaphO- + DQH = NaphOHDQ-	Keq[8]: 9.0399E+011 (TSR)	kf[8]: 1E+009
reaction[9]: NaphO- + DQH- = NaphOHDQ2-	Keq[9]: 52.322 (TSR)	kf[9]: 1E+008
reaction[10]: NaphOH + DQH+ = NaphOHDQH+	Keq[10]: 0.18966 (TSR)	kf[10]: 1E+008
reaction[11]: NaphOH + DQH = NaphOHDQH	Keq[11]: 0.60568 (TSR)	kf[11]: 1E+008
reaction[12]: NaphOH + DQH- = NaphOHDQH-	Keq[12]: 15064 (TSR)	kf[12]: 1E+009
reaction[13]: NaphOH + NaphOHDQ = NaphOHDQH+ + NaphO-	Keq[13]: 5.6E-032	kf[13]: 0
reaction[14]: NaphOH + NaphOHDQ- = NaphOHDQH + NaphO-	Keq[14]: 6.7E-013	kf[14]: 0
reaction[15]: NaphOH + NaphOHDQ2- = NaphOHDQH- + NaphO-	Keq[15]: 287.9	kf[15]: 0
reaction[16]: NaphOH + NaphOHDQ = NaphOHDQHONaph	Keq[16]: 0.5	kf[16]: 1E+008
reaction[17]: NaphOH + NaphOHDQ- = NaphOHDQHONaph-	Keq[17]: 89	kf[17]: 1E+009
reaction[18]: NaphOH + NaphOHDQ2- = NaphOHDQHONaph2-	Keq[18]: 2280	kf[18]: 1E+009
reaction[19]: NaphO- + NaphOHDQH+ = NaphOHDQHONaph	Keq[19]: 8.9286E+030 (TSR)	kf[19]: 1E+009
reaction[20]: NaphO- + NaphOHDQH = NaphOHDQHONaph-	Keq[20]: 1.3284E+014 (TSR)	kf[20]: 1E+009
reaction[21]: NaphO- + NaphOHDQH- = NaphOHDQHONaph2-	Keq[21]: 7.9194 (TSR)	kf[21]: 1E+007

reaction[22]: NaphOH + NaphO- = NaphOHONaph-	Keq[22]: 1	kf[22]: 1E+009
	DQ starting concentration (mol/L)	0.001
	Diffusion Coefficient (everything, cm^2/s)	1E-5
	Resistance (Ohms)	350
	Electrode area (cm^2)	0.0706
	Temperature (K)	298.2

Table A.5		
Simulation Parameters for DQ and NaphOH using Wedge Scheme with Stronger Acid from NaphOH H-bond Complex used in figure 4.5		
Terms	Thermodynamic Parameter	Forward Kinetic Constant
charge transfer reactions:		
reaction[1]: DQ + e = DQ-	E0[1] (V): -1.237	ks[1] (cm/s): 10000
reaction[2]: DQ- + e = DQ2-	E0[2] (V): -1.837	ks[2] (cm/s): 0.05
reaction[3]: DQH+ + e = DQH	E0[3] (V): -0.748	ks[3] (cm/s): 10000
reaction[4]: DQH + e = DQH-	E0[4] (V): -0.848	ks[4] (cm/s): 10000
reaction[5]: NaphOHDQ + e = NaphOHDQ-	E0[5] (V): -1.168	ks[5] (cm/s): 10000
reaction[6]: NaphOHDQ- + e = NaphOHDQ2-	E0[6] (V): -1.498	ks[6] (cm/s): 10000
homogeneous chemical reactions:		
reaction[1]: NaphOH + DQ = NaphO- + DQH+	Keq[1]: 5.6E-024	kf[1]: 0
reaction[2]: NaphOH + DQ- = NaphO- + DQH	Keq[2]: 1.0291E-015 (TSR)	kf[2]: 0
reaction[3]: NaphOH + DQ2- = NaphO- + DQH-	Keq[3]: 53.329 (TSR)	kf[3]: 0
reaction[4]: NaphOH + DQ = NaphOHDQ	Keq[4]: 19	kf[4]: 1E+009
reaction[5]: NaphOH + DQ- = NaphOHDQ-	Keq[5]: 278.54 (TSR)	kf[5]: 1E+009
reaction[6]: NaphOH + DQ2- = NaphOHDQ2-	Keq[6]: 1.4932E+008 (TSR)	kf[6]: 1E+009
reaction[7]: NaphO- + DQH+ = NaphOHDQ	Keq[7]: 3.3929E+024 (TSR)	kf[7]: 1E+009
reaction[8]: NaphO- + DQH = NaphOHDQ-	Keq[8]: 2.7065E+017 (TSR)	kf[8]: 1E+009
reaction[9]: NaphO- + DQH- = NaphOHDQ2-	Keq[9]: 2.8E+006 (TSR)	kf[9]: 1E+009
reaction[10]: NaphOH + NaphOH = NaphOH2	Keq[10]: 1500	kf[10]: 100
reaction[11]: NaphOH + NaphO- = NaphOH2-	Keq[11]: 2.6786E+014 (TSR)	kf[11]: 1000
reaction[12]: NaphOH2 + DQ = DQH+ + NaphOH2-	Keq[12]: 1E-012	kf[12]: 1000

reaction[13]: NaphOH2 + DQ- = DQH + NaphOH2-	Keq[13]: 0.00018378 (TSR)	kf[13]: 1E+008
reaction[14]: NaphOH2 + DQ2- = DQH- + NaphOH2-	Keq[14]: 9.523E+012 (TSR)	kf[14]: 1E+009
	DQ starting concentration (mol/L)	0.001
	Diffusion Coefficient (everything, cm^2/s)	1E-5
	Resistance (Ohms)	350
	Electrode area (cm^2)	0.0706
	Temperature (K)	298.2

Table A.6		
Simulation Parameters for DQ and NaphOH using Wedge Scheme with 3 NaphOH per DQ maximum for the H-bond Complex used in figure 4.12		
Terms	Thermodynamic Parameter	Forward Kinetic Constant
charge transfer reactions:		
reaction[1]: DQ + e = DQ-	E0[1] (V): -1.237	ks[1] (cm/s): 10000
reaction[2]: DQ- + e = DQ2-	E0[2] (V): -1.837	ks[2] (cm/s): 0.05
reaction[3]: NaphOHDQ + e = NaphOHDQ-	E0[3] (V): -1.168	ks[3] (cm/s): 10
reaction[4]: NaphOHDQ- + e = NaphOHDQ2-	E0[4] (V): -1.498	ks[4] (cm/s): 0.2
reaction[5]: NaphOH2DQ + e = NaphOH2DQ-	E0[5] (V): -1.098	ks[5] (cm/s): 10
reaction[6]: NaphOH2DQ- + e = NaphOH2DQ2-	E0[6] (V): -1.348	ks[6] (cm/s): 0.2
reaction[7]: NaphOH3DQ + e = NaphOH3DQ-	E0[7] (V): -1.128	ks[7] (cm/s): 10
reaction[8]: NaphOH3DQ- + e = NaphOH3DQ2-	E0[8] (V): -1.448	ks[8] (cm/s): 0.2
reaction[9]: DQH+ + e = DQH	E0[9] (V): -0.748	ks[9] (cm/s): 10
reaction[10]: DQH + e = DQH-	E0[10] (V): -0.848	ks[10] (cm/s): 0.2
reaction[11]: NaphOHDQH+ + e = NaphOHDQH	E0[11] (V): -0.698	ks[11] (cm/s): 10
reaction[12]: NaphOHDQH + e = NaphOHDQH-	E0[12] (V): -0.748	ks[12] (cm/s): 0.2
reaction[13]: NaphOH2DQH+ + e = NaphOH2DQH	E0[13] (V): -0.628	ks[13] (cm/s): 10
reaction[14]: NaphOH2DQH + e = NaphOH2DQH-	E0[14] (V): -0.688	ks[14] (cm/s): 0.2
homogeneous chemical reactions:		
reaction[1]: NaphOH + DQ = NaphO- + DQH+	Keq[1]: 5.6E-024	kf[1]: 0

reaction[2]: NaphOH + DQ- = NaphO- + DQH	Keq[2]: 1.0291E-015 (TSR)	kf[2]: 0
reaction[3]: NaphOH + DQ2- = NaphO- + DQH-	Keq[3]: 53.329 (TSR)	kf[3]: 0
reaction[4]: NaphOH + DQ = NaphOHDQ	Keq[4]: 19	kf[4]: 1E+009
reaction[5]: NaphOH + DQ- = NaphOHDQ-	Keq[5]: 278.54 (TSR)	kf[5]: 1E+009
reaction[6]: NaphOH + DQ2- = NaphOHDQ2-	Keq[6]: 1.4932E+008 (TSR)	kf[6]: 1E+009
reaction[7]: NaphO- + DQH+ = NaphOHDQ	Keq[7]: 3.3929E+024 (TSR)	kf[7]: 1E+009
reaction[8]: NaphO- + DQH = NaphOHDQ-	Keq[8]: 2.7065E+017 (TSR)	kf[8]: 1E+009
reaction[9]: NaphO- + DQH- = NaphOHDQ2-	Keq[9]: 2.8E+006 (TSR)	kf[9]: 1E+007
reaction[10]: NaphOH + DQH+ = NaphOHDQH+	Keq[10]: 1.9E-007 (TSR)	kf[10]: 1E+007
reaction[11]: NaphOH + DQH = NaphOHDQH	Keq[11]: 1.3298E-006 (TSR)	kf[11]: 1E+009
reaction[12]: NaphOH + DQH- = NaphOHDQH-	Keq[12]: 6.5135E-005 (TSR)	kf[12]: 1E+009
reaction[13]: NaphOH + NaphOHDQ = NaphOHDQH+ + NaphO-	Keq[13]: 5.6E-032	kf[13]: 0
reaction[14]: NaphOH + NaphOHDQ- = NaphOHDQH + NaphO-	Keq[14]: 4.9133E-024 (TSR)	kf[14]: 0
reaction[15]: NaphOH + NaphOHDQ2- = NaphOHDQH- + NaphO-	Keq[15]: 2.3263E-011 (TSR)	kf[15]: 0
reaction[16]: NaphOH + NaphOHDQ = NaphOH2DQ	Keq[16]: 5	kf[16]: 1E+008
reaction[17]: NaphOH + NaphOHDQ- = NaphOH2DQ-	Keq[17]: 76.207 (TSR)	kf[17]: 1E+009

reaction[18]: NaphOH + NaphOHDQ2- = NaphOH2DQ2-	Keq[18]: 26125 (TSR)	kf[18]: 1E+009
reaction[19]: NaphO- + NaphOHDQH+ = NaphOH2DQ	Keq[19]: 8.9286E+031 (TSR)	kf[19]: 1E+009
reaction[20]: NaphO- + NaphOHDQH = NaphOH2DQ-	Keq[20]: 1.5511E+025 (TSR)	kf[20]: 1E+009
reaction[21]: NaphO- + NaphOHDQH- = NaphOH2DQ2-	Keq[21]: 1.123E+015 (TSR)	kf[21]: 1E+008
reaction[22]: NaphOH + NaphOHDQH+ = NaphOH2DQH+	Keq[22]: 0.89286 (TSR)	kf[22]: 1E+009
reaction[23]: NaphOH + NaphOHDQH = NaphOH2DQH	Keq[23]: 13.608 (TSR)	kf[23]: 1E+009
reaction[24]: NaphOH + NaphOHDQH- = NaphOH2DQH-	Keq[24]: 140.55 (TSR)	kf[24]: 1E+009
reaction[25]: NaphOH + NaphOH2DQ = NaphOH2DQH+ + NaphO-	Keq[25]: 1E-032	kf[25]: 0
reaction[26]: NaphOH + NaphOH2DQ- = NaphOH2DQH + NaphO-	Keq[26]: 8.7737E-025 (TSR)	kf[26]: 0
reaction[27]: NaphOH + NaphOH2DQ2- = NaphOH2DQH- + NaphO-	Keq[27]: 1.2515E-013 (TSR)	kf[27]: 0
reaction[28]: NaphOH + NaphOH2DQ = NaphOH3DQ	Keq[28]: 0.2	kf[28]: 1E+009
reaction[29]: NaphOH + NaphOH2DQ- = NaphOH3DQ-	Keq[29]: 0.062233 (TSR)	kf[29]: 1E+009
reaction[30]: NaphOH + NaphOH2DQ2- = NaphOH3DQ2-	Keq[30]: 0.0012705 (TSR)	kf[30]: 1E+009
reaction[31]: NaphO- + NaphOH2DQH+ = NaphOH3DQ	Keq[31]: 2E+031 (TSR)	kf[31]: 1E+009

reaction[32]: NaphO- + NaphOH2DQH = NaphOH3DQ-	Keq[32]: 7.0931E+022 (TSR)	kf[32]: 1E+009
reaction[33]: NaphO- + NaphOH2DQH- = NaphOH3DQ2-	Keq[33]: 1.0152E+010 (TSR)	kf[33]: 1E+009
reaction[34]: NaphOH + NaphO- = NaphOHONaph-	Keq[34]: 1500	kf[34]: 1E+009
	DQ starting concentration (mol/L)	0.001
	Diffusion Coefficient (everything, cm^2/s)	1E-5
	Resistance (Ohms)	350
	Electrode area (cm^2)	0.0706
	Temperature (K)	298.2

Table A.7		
Simulation Parameters for DQ and NaphOH using Wedge Scheme with 4 NaphOH per DQ maximum for the H-bond Complex used in figure 4.13		
Terms	Thermodynamic Parameter	Forward Kinetic Constant
charge transfer reactions:		
reaction[1]: DQ + e = DQ-	E0[1] (V): -1.237	ks[1] (cm/s): 10000
reaction[2]: DQ- + e = DQ2-	E0[2] (V): -1.837	ks[2] (cm/s): 0.05
reaction[3]: NaphOHDQ + e = NaphOHDQ-	E0[3] (V): -1.168	ks[3] (cm/s): 10
reaction[4]: NaphOHDQ- + e = NaphOHDQ2-	E0[4] (V): -1.498	ks[4] (cm/s): 0.2
reaction[5]: NaphOH2DQ + e = NaphOH2DQ-	E0[5] (V): -1.098	ks[5] (cm/s): 10
reaction[6]: NaphOH2DQ- + e = NaphOH2DQ2-	E0[6] (V): -1.348	ks[6] (cm/s): 0.2
reaction[7]: NaphOH3DQ + e = NaphOH3DQ-	E0[7] (V): -1.128	ks[7] (cm/s): 10
reaction[8]: NaphOH3DQ- + e = NaphOH3DQ2-	E0[8] (V): -1.448	ks[8] (cm/s): 0.2
reaction[9]: NaphOH4DQ + e = NaphOH4DQ-	E0[9] (V): -1.198	ks[9] (cm/s): 0.2
reaction[10]: NaphOH4DQ- + e = NaphOH4DQ2-	E0[10] (V): -1.598	ks[10] (cm/s): 0.02
reaction[11]: DQH+ + e = DQH	E0[11] (V): -0.748	ks[11] (cm/s): 10
reaction[12]: DQH + e = DQH-	E0[12] (V): -0.848	ks[12] (cm/s): 0.2
reaction[13]: NaphOHDQH+ + e = NaphOHDQH	E0[13] (V): -0.698	ks[13] (cm/s): 10
reaction[14]: NaphOHDQH + e = NaphOHDQH-	E0[14] (V): -0.748	ks[14] (cm/s): 0.2
reaction[15]: NaphOH2DQH+ + e = NaphOH2DQH	E0[15] (V): -0.628	ks[15] (cm/s): 10
reaction[16]: NaphOH2DQH + e = NaphOH2DQH-	E0[16] (V): -0.688	ks[16] (cm/s): 0.2

reaction[17]: NaphOH3DQH+ + e = NaphOH3DQH	E0[17] (V): -0.568	ks[17] (cm/s): 0.2
reaction[18]: NaphOH3DQH + e = NaphOH3DQH-	E0[18] (V): -0.608	ks[18] (cm/s): 0.02
homogeneous chemical reactions:		
reaction[1]: NaphOH + DQ = NaphO- + DQH+	Keq[1]: 5.6E-024	kf[1]: 0
reaction[2]: NaphOH + DQ- = NaphO- + DQH	Keq[2]: 1.0291E-015 (TSR)	kf[2]: 0
reaction[3]: NaphOH + DQ2- = NaphO- + DQH-	Keq[3]: 53.329 (TSR)	kf[3]: 0
reaction[4]: NaphOH + DQ = NaphOHDQ	Keq[4]: 19	kf[4]: 1E+009
reaction[5]: NaphOH + DQ- = NaphOHDQ-	Keq[5]: 278.54 (TSR)	kf[5]: 1E+009
reaction[6]: NaphOH + DQ2- = NaphOHDQ2-	Keq[6]: 1.4932E+008 (TSR)	kf[6]: 1E+009
reaction[7]: NaphO- + DQH+ = NaphOHDQ	Keq[7]: 3.3929E+024 (TSR)	kf[7]: 1E+009
reaction[8]: NaphO- + DQH = NaphOHDQ-	Keq[8]: 2.7065E+017 (TSR)	kf[8]: 1E+009
reaction[9]: NaphO- + DQH- = NaphOHDQ2-	Keq[9]: 2.8E+006 (TSR)	kf[9]: 1E+007
reaction[10]: NaphOH + DQH+ = NaphOHDQH+	Keq[10]: 1.9E-007 (TSR)	kf[10]: 1E+007
reaction[11]: NaphOH + DQH = NaphOHDQH	Keq[11]: 1.3298E-006 (TSR)	kf[11]: 1E+009
reaction[12]: NaphOH + DQH- = NaphOHDQH-	Keq[12]: 6.5135E-005 (TSR)	kf[12]: 1E+009
reaction[13]: NaphOH + NaphOHDQ = NaphOHDQH+ + NaphO-	Keq[13]: 5.6E-032	kf[13]: 0
reaction[14]: NaphOH + NaphOHDQ- = NaphOHDQH + NaphO-	Keq[14]: 4.9133E-024 (TSR)	kf[14]: 0

reaction[15]: NaphOH + NaphOHDQ2- = NaphOHDQH- + NaphO-	Keq[15]: 2.3263E-011 (TSR)	kf[15]: 0
reaction[16]: NaphOH + NaphOHDQ = NaphOH2DQ	Keq[16]: 5	kf[16]: 1E+008
reaction[17]: NaphOH + NaphOHDQ- = NaphOH2DQ-	Keq[17]: 76.207 (TSR)	kf[17]: 1E+009
reaction[18]: NaphOH + NaphOHDQ2- = NaphOH2DQ2-	Keq[18]: 26125 (TSR)	kf[18]: 1E+009
reaction[19]: NaphO- + NaphOHDQH+ = NaphOH2DQ	Keq[19]: 8.9286E+031 (TSR)	kf[19]: 1E+009
reaction[20]: NaphO- + NaphOHDQH = NaphOH2DQ-	Keq[20]: 1.5511E+025 (TSR)	kf[20]: 1E+009
reaction[21]: NaphO- + NaphOHDQH- = NaphOH2DQ2-	Keq[21]: 1.123E+015 (TSR)	kf[21]: 1E+008
reaction[22]: NaphOH + NaphOHDQH+ = NaphOH2DQH+	Keq[22]: 0.89286 (TSR)	kf[22]: 1E+009
reaction[23]: NaphOH + NaphOHDQH = NaphOH2DQH	Keq[23]: 13.608 (TSR)	kf[23]: 1E+009
reaction[24]: NaphOH + NaphOHDQH- = NaphOH2DQH-	Keq[24]: 140.55 (TSR)	kf[24]: 1E+009
reaction[25]: NaphOH + NaphOH2DQ = NaphOH2DQH+ + NaphO-	Keq[25]: 1E-032	kf[25]: 0
reaction[26]: NaphOH + NaphOH2DQ- = NaphOH2DQH + NaphO-	Keq[26]: 8.7737E-025 (TSR)	kf[26]: 0
reaction[27]: NaphOH + NaphOH2DQ2- = NaphOH2DQH- + NaphO-	Keq[27]: 1.2515E-013 (TSR)	kf[27]: 0
reaction[28]: NaphOH + NaphOH2DQ = NaphOH3DQ	Keq[28]: 2	kf[28]: 1E+009

reaction[29]: NaphOH + NaphOH2DQ- = NaphOH3DQ-	Keq[29]: 0.62233 (TSR)	kf[29]: 1E+009
reaction[30]: NaphOH + NaphOH2DQ2- = NaphOH3DQ2-	Keq[30]: 0.012705 (TSR)	kf[30]: 1E+009
reaction[31]: NaphO- + NaphOH2DQH+ = NaphOH3DQ	Keq[31]: 2E+032 (TSR)	kf[31]: 1E+009
reaction[32]: NaphO- + NaphOH2DQH = NaphOH3DQ-	Keq[32]: 7.0931E+023 (TSR)	kf[32]: 1E+009
reaction[33]: NaphO- + NaphOH2DQH- = NaphOH3DQ2-	Keq[33]: 1.0152E+011 (TSR)	kf[33]: 1E+009
reaction[43]: NaphOH + NaphO- = NaphOHONaph-	Keq[34]: 1E-036	kf[34]: 0
	DQ starting concentration (mol/L)	0.001
	Diffusion Coefficient (everything, cm^2/s)	1E-5
	Resistance (Ohms)	350
	Electrode area (cm^2)	0.0706
	Temperature (K)	298.2

Table A.8		
Simulation Parameters for DQ and NaphOH using Wedge Scheme with 1 NaphOH per DQ maximum for the H-bond Complex, NaphOH impact required for H^+-transfer used in figure 4.15		
Terms	Thermodynamic Parameter	Forward Kinetic Constant
charge transfer reactions:		
reaction[1]: DQ + e = DQ-	E0[1] (V): -1.237	ks[1] (cm/s): 1
reaction[2]: DQ- + e = DQ2-	E0[2] (V): -1.837	ks[2] (cm/s): 0.05
reaction[3]: DQH+ + e = DQH	E0[3] (V): -0.748	ks[3] (cm/s): 0.5
reaction[4]: DQH + e = DQH-	E0[4] (V): -0.848	ks[4] (cm/s): 0.2
reaction[5]: NaphOHDQH+ + e = NaphOHDQH	E0[5] (V): -0.698	ks[5] (cm/s): 0.2
reaction[6]: NaphOHDQH + e = NaphOHDQH-	E0[6] (V): -0.748	ks[6] (cm/s): 0.02
reaction[7]: NaphOHDQ + e = NaphOHDQ-	E0[7] (V): -1.168	ks[7] (cm/s): 0.2
reaction[8]: NaphOHDQ- + e = NaphOHDQ2-	E0[8] (V): -1.498	ks[8] (cm/s): 0.02
reaction[9]: NaphOH2DQ + e = NaphOH2DQ-	E0[9] (V): -1.09401 (TSR)	ks[9] (cm/s): 10000
reaction[10]: NaphOH2DQ- + e = NaphOH2DQ2-	E0[10] (V): -1.41466 (TSR)	ks[10] (cm/s): 10000
homogeneous chemical reactions:		
reaction[1]: NaphOH + DQ = NaphO- + DQH+	Keq[1]: 5.6E-024	kf[1]: 0
reaction[2]: NaphOH + DQ- = NaphO- + DQH	Keq[2]: 1.0291E-015 (TSR)	kf[2]: 0
reaction[3]: NaphOH + DQ2- = NaphO- + DQH-	Keq[3]: 53.329 (TSR)	kf[3]: 0
reaction[4]: NaphOH + DQ = NaphOHDQ	Keq[4]: 19	kf[4]: 1E+009
reaction[5]: NaphOH + DQ- = NaphOHDQ-	Keq[5]: 278.54 (TSR)	kf[5]: 1E+009
reaction[6]: NaphOH + DQ2- = NaphOHDQ2-	Keq[6]: 1.4932E+008 (TSR)	kf[6]: 1E+009
reaction[7]: NaphOH + NaphOHDQ = DQH+ + NaphOH2-	Keq[7]: 0.7896	kf[7]: 100

reaction[8]: NaphOH + NaphOHDQ- = DQH + NaphOH2-	Keq[8]: 9.8985E+006 (TSR)	kf[8]: 100
reaction[9]: NaphOH + NaphOHDQ2- = DQH- + NaphOH2-	Keq[9]: 9.568E+017 (TSR)	kf[9]: 100
reaction[10]: NaphOH + DQH+ = NaphOHDQH+	Keq[10]: 1.9E-006 (TSR)	kf[10]: 0
reaction[11]: NaphOH + DQH = NaphOHDQH	Keq[11]: 1.3298E-005 (TSR)	kf[11]: 0
reaction[12]: NaphOH + DQH- = NaphOHDQH-	Keq[12]: 0.00065135 (TSR)	kf[12]: 0
reaction[13]: NaphOH + NaphOHDQ = NaphOHDQH+ + NaphO-	Keq[13]: 5.6E-031	kf[13]: 0
reaction[14]: NaphOH + NaphOHDQ- = NaphOHDQH + NaphO-	Keq[14]: 4.9133E-023 (TSR)	kf[14]: 0
reaction[15]: NaphOH + NaphOHDQ2- = NaphOHDQH- + NaphO-	Keq[15]: 2.3263E-010 (TSR)	kf[15]: 0
reaction[16]: NaphOH + NaphOHDQ = NaphOH2DQ	Keq[16]: 0.5	kf[16]: 0
reaction[17]: NaphOH + NaphOHDQ- = NaphOH2DQ-	Keq[17]: 8.9	kf[17]: 0
reaction[18]: NaphOH + NaphOHDQ2- = NaphOH2DQ2-	Keq[18]: 228	kf[18]: 0
reaction[19]: NaphOH + NaphOH2DQ = NaphOHDQH+ + NaphOH2-	Keq[19]: 3.0005E-006 (TSR)	kf[19]: 0
reaction[20]: NaphOH + NaphOH2DQ- = NaphOHDQH + NaphOH2-	Keq[20]: 14.789 (TSR)	kf[20]: 0
reaction[21]: NaphOH + NaphOH2DQ2- = NaphOHDQH- + NaphOH2-	Keq[21]: 2.7334E+012 (TSR)	kf[21]: 0
reaction[22]: NaphOH + NaphOH = NaphOH2	Keq[22]: 1500	kf[22]: 100

reaction[23]: NaphOH + NaphO- = NaphOH2-	Keq[23]: 2.679E+024 (TSR)	kf[23]: 1E+009
	DQ starting concentration (mol/L)	0.001
	Diffusion Coefficient (everything, cm^2/s)	1E-5
	Resistance (Ohms)	350
	Electrode area (cm^2)	0.0706
	Temperature (K)	298.2

Table A.9		
Simulation Parameters for DQ and NaphOH using Wedge Scheme with 2 NaphOH per DQ maximum for the H-bond Complex, H-bond possible for protonated and unprotonated DQ molecules used in figure 4.16		
Terms	Thermodynamic Parameter	Forward Kinetic Constant
charge transfer reactions:		
reaction[1]: DQ + e = DQ-	E0[1] (V): -1.237	ks[1] (cm/s): 1
reaction[2]: DQ- + e = DQ2-	E0[2] (V): -1.837	ks[2] (cm/s): 0.05
reaction[3]: NaphOHDQ + e = NaphOHDQ-	E0[3] (V): -1.168	ks[3] (cm/s): 0.5
reaction[4]: NaphOHDQ- + e = NaphOHDQ2-	E0[4] (V): -1.548	ks[4] (cm/s): 0.2
reaction[5]: DQH+ + e = DQH	E0[5] (V): -0.748	ks[5] (cm/s): 0.5
reaction[6]: DQH + e = DQH-	E0[6] (V): -0.848	ks[6] (cm/s): 0.2
reaction[7]: DQHDQ + e = DQHDQ-	E0[7] (V): -1.128	ks[7] (cm/s): 10000
reaction[8]: DQHDQ- + e = DQHDQ2-	E0[8] (V): -1.648	ks[8] (cm/s): 10000
reaction[9]: DQHDQ2- + e = DQHDQ3-	E0[9] (V): -1.948	ks[9] (cm/s): 10000
homogeneous chemical reactions:		
reaction[1]: NaphOH + DQ = NaphO- + DQH+	Keq[1]: 5.6E-020	kf[1]: 0
reaction[2]: NaphOH + DQ- = NaphO- + DQH	Keq[2]: 1.0291E-011 (TSR)	kf[2]: 0
reaction[3]: NaphOH + DQ2- = NaphO- + DQH-	Keq[3]: 5.3329E+005 (TSR)	kf[3]: 0
reaction[4]: NaphOH + DQ = NaphOHDQ	Keq[4]: 19	kf[4]: 1E+009
reaction[5]: NaphOH + DQ- = NaphOHDQ-	Keq[5]: 278.54 (TSR)	kf[5]: 1E+009
reaction[6]: NaphOH + DQ2- = NaphOHDQ2-	Keq[6]: 2.1335E+007 (TSR)	kf[6]: 1E+009

reaction[7]: NaphO- + DQH+ = NaphOHDQ	Keq[7]: 3.3929E+020 (TSR)	kf[7]: 1E+009
reaction[8]: NaphO- + DQH = NaphOHDQ-	Keq[8]: 2.7065E+013 (TSR)	kf[8]: 1E+009
reaction[9]: NaphO- + DQH- = NaphOHDQ2-	Keq[9]: 40.007 (TSR)	kf[9]: 1E+009
reaction[10]: DQH+ + DQ- = DQ + DQH	Keq[10]: 1.8378E+008 (TSR)	kf[10]: 0
reaction[11]: DQH+ + DQ2- = DQ + DQH-	Keq[11]: 9.523E+024 (TSR)	kf[11]: 0
reaction[12]: DQH + DQ2- = DQ- + DQH-	Keq[12]: 5.1818E+016 (TSR)	kf[12]: 0
reaction[13]: DQH+ + DQ = DQHDQ+	Keq[13]: 6.5	kf[13]: 1E+009
reaction[14]: DQH+ + DQ- = DQHDQ	Keq[14]: 9.1888E+008 (TSR)	kf[14]: 1E+009
reaction[15]: DQH + DQ = DQHDQ	Keq[15]: 5	kf[15]: 1E+009
reaction[16]: DQH+ + DQ2- = DQHDQ-	Keq[16]: 8.8234E+020 (TSR)	kf[16]: 1E+009
reaction[17]: DQH + DQ- = DQHDQ-	Keq[17]: 347.63 (TSR)	kf[17]: 1E+009
reaction[18]: DQH- + DQ = DQHDQ-	Keq[18]: 9.2653E-005 (TSR)	kf[18]: 1E+009
reaction[19]: DQH- + DQ- = DQHDQ2-	Keq[19]: 1.0491E-011 (TSR)	kf[19]: 1E+009
reaction[20]: DQH + DQ2- = DQHDQ2-	Keq[20]: 5.4361E+005 (TSR)	kf[20]: 1E+009
reaction[21]: DQH- + DQ2- = DQHDQ3-	Keq[21]: 1.3959E-013 (TSR)	kf[21]: 1E+009
reaction[22]: NaphOH + NaphO- = NaphOH2-	Keq[22]: 1500	kf[22]: 1E+009

	DQ starting concentration (mol/L)	0.001
	Diffusion Coefficient (everything, cm^2/s)	1E-5
	Resistance (Ohms)	350
	Electrode area (cm^2)	0.0706
	Temperature (K)	298.2